Republic of Iraq
Ministry of Higher Education and Scientific Research
University of Misan/College of Engineering
Civil Engineering Department

NONLINEAR ANALYSIS OF SIMPLY SUPPORTED COMPOSITE STEEL-CONCRETE SECTIONS WITH DIFFERENT GEOMETRIC CONFIGURATIONS

BY

Burer Mohammed Abdulwahid

B.Sc. Civil Engineering, 2016

A THESIS

Submitted in partial fulfillment of

The requirements for the degree of

Master of Science / Master of Structural Engineering

(In civil engineering)

The University of Missan

August 2022

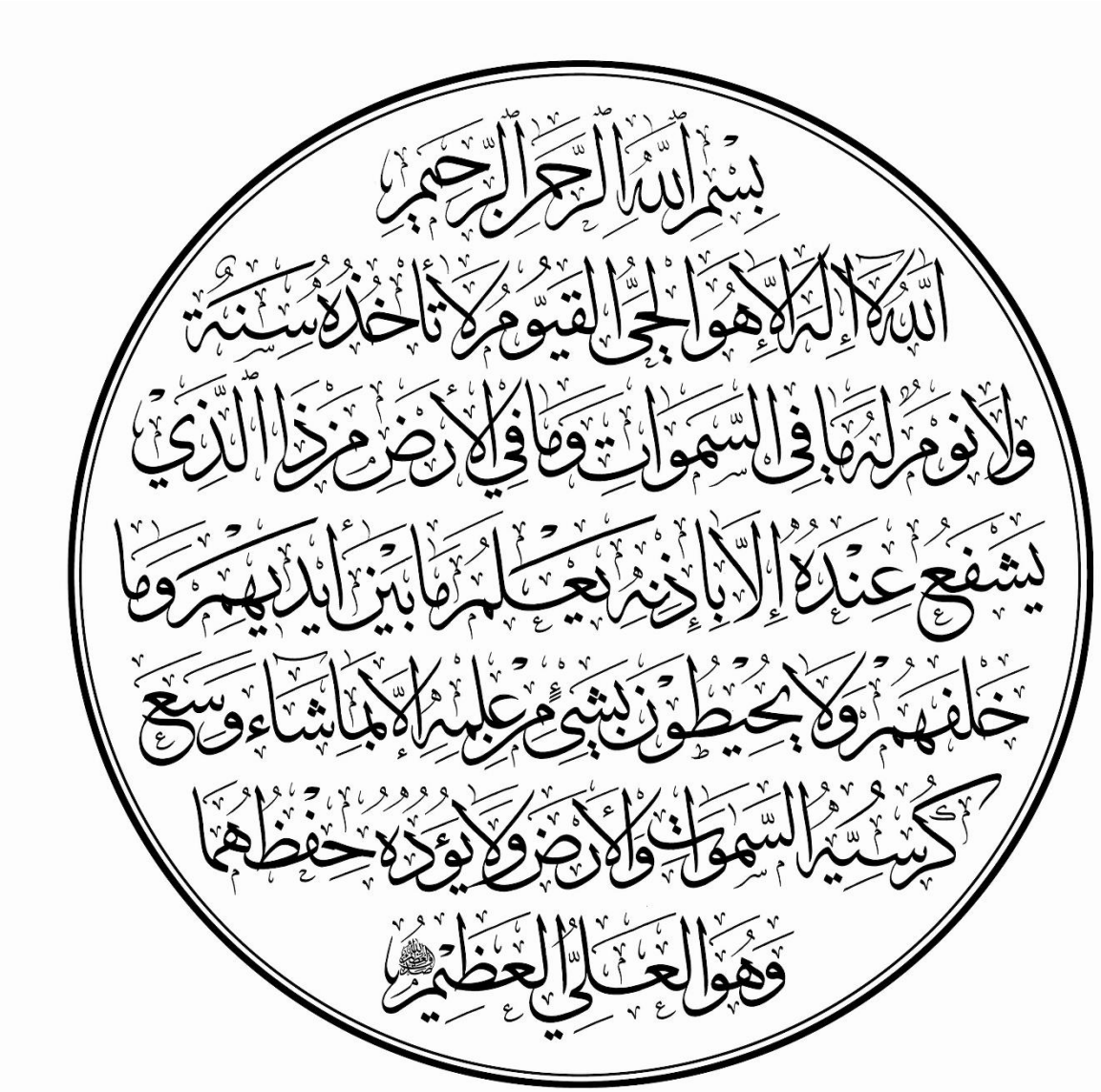

سورة البقرة (255)

Dedication

- To whom stood beside me and took care of me over the years, to my wife, daughter, family and close friend.

- To all those who supported and helped me, made the difficult easy, especially to my supervisor Prof. Dr. Saad F. Resan.

I present my effort to them with all of my respect and appreciation.

ACKNOWLEDGEMENTS

First of all, all my thanks for **Allah** who led me during my way to complete this work.

I would like to express my cordial thanks and deepest gratitude to my supervisor **Prof. Dr. Saad F. Resan**, whom I had the honor of being under his supervision, for his advice, help, and encouragement during the course of this study.

I would like to extend my thanks to **Prof. Dr. Abbas O. Dawood** Dean of the college of engineering, and **Asst. Prof. Dr. Samir M. Chassib**, the Head of Civil Engineering Department.

Special thanks go to **my mother and father** for thier great efforts. Also, thanks go to **my brothers** and **my close friend**.

Special thanks also go to **Asst. Lec. Ali W Abdulghani,** for his effort in helping me in ANSYS program.

Burer Mohammed Abdulwahid

2022

SUPERVISOR CERTIFCATION

I certify that the thesis titled " **Nonlinear Analysis of Simply Supported Composite Steel-Concrete Sections with Different Geometric Configurations**" which is being submitted by **Burer Mohammed Abdulwahid** and prepared under my supervision at the University of Misan, Department of Civil Engineering, in partial fulfillment of the requirements for the Degree of Master of Science in Civil Engineering (Structures).

Signature:
Prof. Dr. Saad F. Resan
Date:

In view of the available recommendations, I forward this thesis for discussion by the examining committee.

Signature:
Assist. Prof. Dr. Samir M. Chassib
(Head of Civil Eng. Department)
Date:

EXAMINING COMMITTTEE'S REPORT

We certify that we have read this thesis titled **" Nonlinear Analysis of Simply Supported Composite Steel-Concrete Sections with Different Geometric Configurations"** which is being submitted by **Burer Mohammed Abdulwahid**, and as Examining Committee, examined the student in its contents. In our opinion, the thesis is adequate for award of degree of Master of Science in Civil Engineering.

Signature:
Name:. Prof. Dr. Saad F. Resan
(Supervisor)
Date: / /

Signature:
Name:
(Member)
Date: / /

Signature:
Name:
(Member)
Date: / /

Signature:
Name:
(Chairman)
Date: / /

Approval of the College of Engineering

Signature:
Name: Prof. Dr. Abbas O. Dawood
Dean, College of Engineering
Date: / /

ABSTRACT

The thesis deals with various composite mode of concrete-built up steel section composite beams using many proposed composite configuration modes such as traditional composite beam, merged sections beside the plated sections. The first side of the study included investigation of the composite beam numerically. Three modes were suggested with smart distribution of the materials beside investigating the effect of variation of dimensions and properties on the ultimate load carrying capacity of such beams to satisfy the design requirements according to the provisions of the American Standard (ACI and AISC for concrete and steel respectively). Various materials could be arranged in an multi configuration according to the optimum design procedure, which the optimization tends to utilize and employee the materials in a perfect position. The main variable in this study is the performing of three modes which were the traditional composite, merging both of the concrete and steel in the compression region, and utilizing of multi flanged U- shape steel section instead of the I-shaped steel section.

The results revealed that the selection of optimum material distribution within composite section depends on the adopted shape configuration of used built up steel section while for intermediate length of plate, where the compression force located in deck, the stresses contributed significantly in resisting the applied forces. proper dimension selection and section configuration affected the moment capacity of the section beside its domination on the failure mode. The best improving technique associated with yield parameters that relate to bottom flange likewise strength, thickness, and widths while the effect of concrete deck limited to width, besides; the webs' geometrical and material characteristics have slightly affected on the obtained tension flange yield moment capacities. For merged compressive region introduced composite mode, always there are a domain of cover plate thickness that compatible

with main design criteria which maintain optimum section of compatible tension and compression forces. For combined compressive region introduced composite mode, the variation of thickness corresponding with significantly improving in composite section tension flange yielding, and the improving rates ranged between 1 to 2 as the thickness changed from 8mm to 30 mm. For composite section of multi flanges number (Mode III), for specific flange number, the determined moment capacity increased as flange thickness increased, the assigned strength is extremely improved as flange number increase for a certain limit of provide the tension area In current case study, two flanges of various flange thickness are proper for compactable design (the improving rates are 2.16 and 2.73) while the three-flange conditioned by lower flange thickness (10mm) (the improving rates is 1.82).

The second part included analysis of the composite beam by use of finite element analysis by use of ANSYS software. The parameters of the finite element analysis were the location of the steel section which placed under the concrete section and inside the concrete section (at the compression zone). The third model included use of steel plate in form of U-shape grooved inside the concrete section. The model with separated mode (the steel under the concrete section) revealed higher ultimate load carrying capacity than the other models which the both sections resisted the applied forced otherwise the other model which the steel section contributed to enhancing the compression zone more than the tension one.

Table of Contents

List of Figure

List of Table

NOMENCLATURE

Symbol	Description	Unit
A	Cross-sectional area	mm^2
b	Beam width	mm
d	Effective depth.	mm
E	Modulus of elasticity	MPa
Ec	Modulus of elasticity of concrete	MPa
Es	Modulus of elasticity of reinforcing bars	MPa
E_T	Strain hardening modulus	
F	Function of principal state $(\sigma_{xp}, \sigma_{yp}, \sigma_{zp})$	
f_t	Ultimate uniaxial tensile strength of concrete	MPa
f_r	Modulus of rupture of concrete	MPa
fcb	Ultimate biaxial compressive strength	MPa
f_1	Ultimate compressive strength for a state of biaxial compression superimposed on hydrostatic stress state	MPa
$fc´$	Compressive strength of concrete cylinder	MPa
fy	Yielding stress of steel reinforcement	MPa
f_2	Ultimate compressive strength for a state of uniaxial compression superimposed on hydrostatic stress state	MPa
$f'c$	Concrete ultimate uniaxial compressive strength	MPa
f_y	Steel yield strength and	MPa
f_u	Steel ultimate tensile strength	MPa
f_{cr}, ε_{cr}	Cracking stress and strain	MPa
h	Height of the cross section	mm

Symbol	Description	Unit
L	Span length of the beam	mm
Le	Effective length	mm
P *and* V	Any applied force on the structure	kN
Pcr	Cracking load	kN
Pu	Ultimate load	kN
u,v,w	Displacement components in x,y and z coordinates	mm
W_{ext} ,W_{int}	External and internal work	
x,y,z	Global coordinate	
α	Haunch angle with horizontal line	Degree
β	Shear transfer coefficient	
B_t , β_c	Opened and closed shear transfer coefficient	
γ,	shear strain	
ε	Strain	
ε_o	Strain at ultimate compressive stress $f'c$	
ε_u	Ultimate strain	
ζ , η	Local coordinates	
σ	Stress	MPa
σ_h^a	Ambient hydrostatic stress state	MPa
σxp	Principal stress in the x – direction.	MPa
σyp	Principal stress in the y – direction.	MPa
σzp	Principal stress in the z – direction.	MPa
σh	Hydrostatic stress.	MPa
τ	Shear stress	MPa

ν	Poisson's ratio	
ACI	American Concrete Institute	
ANSYS	(ANalysis SYStem) Computer Program	
APDL	Ansys Parametric Design Language	
BS	British Standards (BSI: British Standards Institute)	
EC	Euro Code	
FE	Finite Element	
FEA	Finite Element Analysis	
FEM	Finite Element Method	
HSC	High Strength Concrete	
NSC	Normal Strength Concrete	
RC	Reinforced Concrete	

CHAPTER ONE: INTRODUCTION

1.1 General

The composite action in members built up of different materials results in savings in construction cost. These savings can be further advanced by employing optimization techniques in the design of composite members. There are many kinds of composite beam including: the steel-timber, timber-concrete, plastic concrete and the most important and most frequently encountered combination of construction materials is that of steel and concrete. In common practice, composite plate girders are designed by a trail and-error approach due to the complexity of the design rules. The design of a composite girder is a tedious and time-consuming job for the designer. The two complementary materials, structural steel and reinforced concrete are introduced and it is shown how composite action is achieved in the case of composite slabs, beams and columns. The use of composite construction for buildings and bridges is outlined and illustrated by several typical examples; its main advantages are also illustrated by comparison with structures of steel and concrete used independently. Attention is drawn to the effect of this form of construction on other more general problems such as: fire resistance rating, speed of construction, flexibility and final fitting out. The most important and most frequently encountered combination of construction materials is that of steel and concrete, with applications in multi- story commercial buildings and factories, as well as in bridges as shown in Figure 1.1. It should be added that the combination of concrete cores, steel frame and composite floor construction has become the standard construction method for multi-story commercial buildings in several countries. Much progress has been made, for example in Japan, where the structural steel/reinforced concrete frame is the standard

system for tall buildings. The main reason for this preference is that the sections and members are best suited to resist repeated earthquake loadings, which require a high amount of resistance and ductility [1].

Figure 1.1 The combination of concrete cores, steel frame and composite floor construction [1].

Single composite elements, such as isolated beams, columns and slabs Figure 1.1, whilst they are of high quality and resistance, they are also, in many cases, expensive. This is the case particularly for buildings with small column spacing's, floor beam spans well below 9 m and low loadings. On the other hand, composite floor construction is highly competitive if spans are increased to 12, 15 or even 20

m. There is, of course, a demand for larger column-free spans in buildings to facilitate open planning or greater flexibility in office layout [2].

Figure 1.2 shows several composite beam cross-sections in which the wet concrete has been cast in situ on timber shuttering. For single span beams, sagging bending moments, due to applied vertical loads, cause tensile forces in the steel section and compression in the concrete deck thereby making optimum use of each material. Therefore, composite beams, even with small steel sections, have high stiffness and can carry heavy loads on long spans. [2].

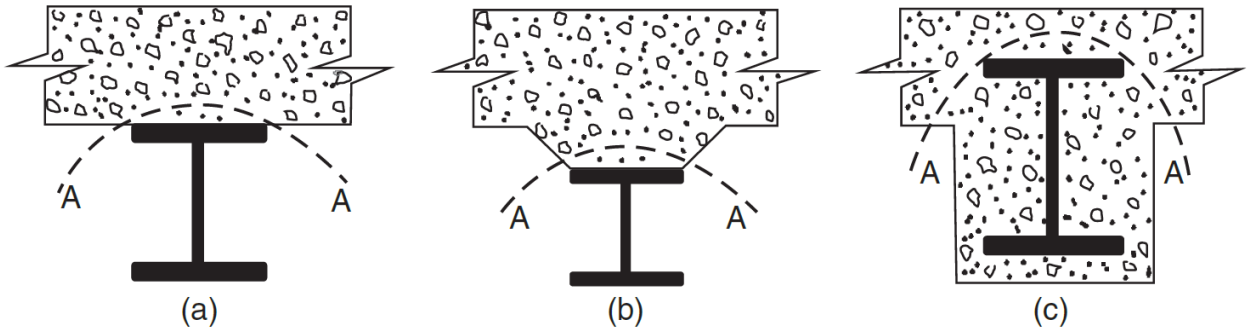

Figure 1.2 Composite Structural Elements in Buildings [2].

1.2 Composite Action in Beams

Composite steel-concrete beams are ubiquitous structural elements in which a steel beam and a solid or composite slab are interconnected by shear connection to act together to resist action effects as a single structural member. Generally, this connection is achieved through headed shear connectors welded to the top flange of the steel beam. The studs resist longitudinal slip and the vertical separation between the two elements. In continuous or semi-continuous structures, members are subject to either positive (sagging) or negative (hogging) bending moments. The most efficient use of the materials' strengths occurs when the beam is subjected to positive

bending at the mid-span. In this case, the steel component is subjected to tensile forces and the concrete component primarily in compression, thus utilizing the best attributes of each material [2]. If slip is free to occur at the interface between the steel section and the concrete slab, each component will act independently, as shown in Figure (1.3). If slip at the interface is eliminated, or at least reduced, the slab and the steel member will act together as a composite unit. The resulting increase in resistance will depend on the extent to which slip is prevented. It should be noted that Figure (1.4) refers to the use of headed stud shear connectors. The degree of interaction depends mainly on the degree of shear connection used [1]. Instead of an in situ concrete slab, precast concrete floor or deck units can be used. Careful detailing and construction practice are needed to ensure adequate containment for the connectors. Regarding the large prefabricated deck elements with longitudinal joints, the gaps between the units would be filled with mortar in the final structure, thereby giving composite action with the beams. Such structural systems were introduced during the early 1960's. In Germany more than 100 car parks, university, school and office buildings (see Figure (1.5)) have been built in this way. The use of precast deck units reduces on-site construction operations and avoids wet trades. The units themselves are cast on steel formwork in a shop to ensure high quality and small (strict) tolerances [2].

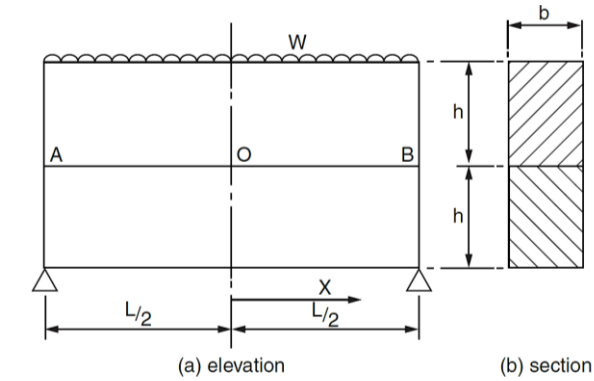

Figure 1.3 Composite Steel Beam-Concrete Slab Interaction [2]

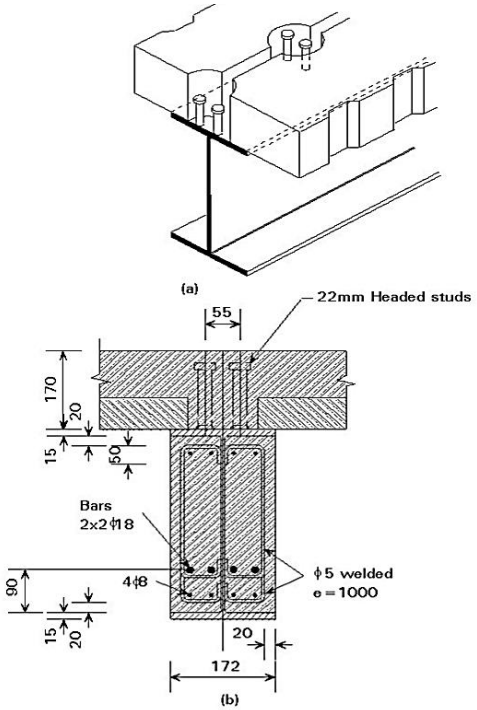

Figure 1.4 Instead of an in situ concrete slab, precast concrete floor or deck units can be used [2].

Figure 1.5 Use of Precast Concrete Floor Units [2].

1.3 Behavior of Composite Beams

The difference between Composite and non-composite beams under equal distributed loads were shown in the Figure (1.4) [3]. The concrete slab is not connected to the steel section and therefore behaves independently. As it is weak in longitudinal bending, it deforms to the curvature of the steel section and has its own neutral axis. The bottom surface of the concrete slab is free to slide over the top flange of the steel section and the slip will occurs. The bending resistance of the slab is often so small that it is ignored Figure (1.5) [4]. In this case, the concrete slab is connected to the steel section and both acts together in carrying the load. Slip between the slab and steel section is now prevented and the connection resists a longitudinal shear force similar in distribution to the vertical shear force shown in Figure (1.6) [4].

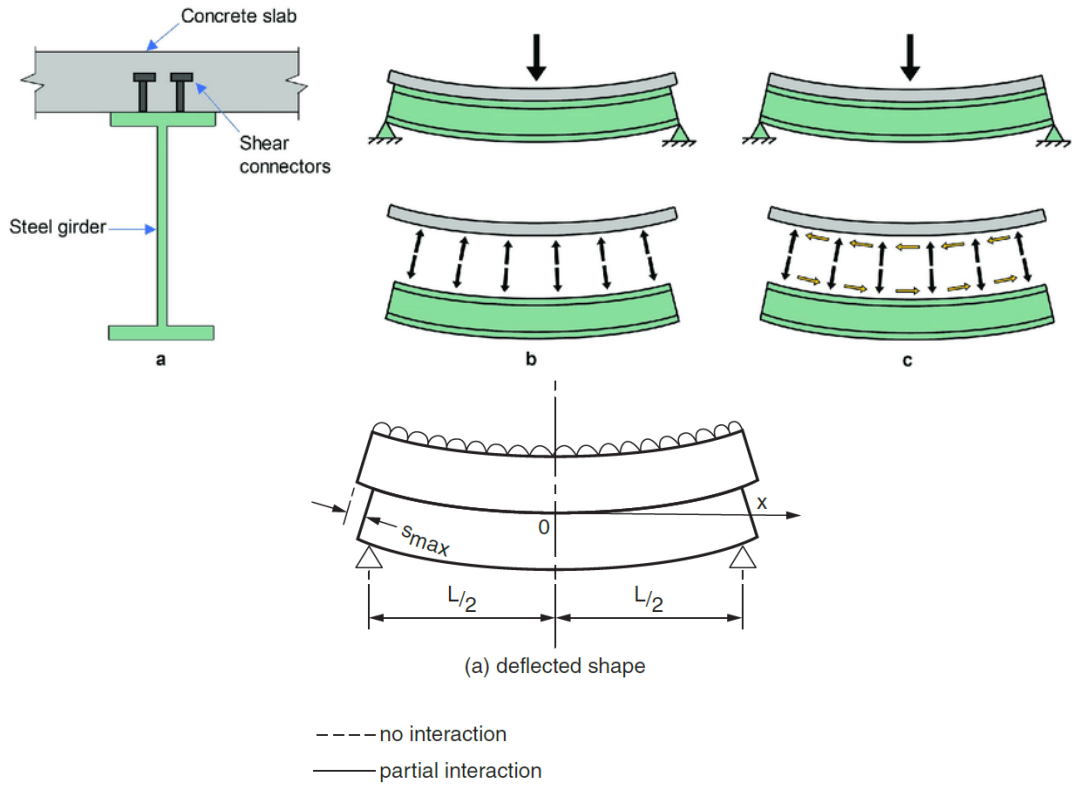

Figure 1.6 Composite and non-composite beams under equal distributed loads [4].

1.4 Buckling

In science, buckling is a mathematical instability, leading to a failure mode. Theoretically, buckling is caused by a bifurcation in the solution to the equations of static equilibrium. Buckling is characterized by a sudden sideways failure of a structural member subjected to high compressive stress, where the compressive stress at the point of failure is less than the ultimate compressive stress that the material is capable of withstanding. Mathematical analysis of buckling often makes use of an "artificial" axial load eccentricity that introduces a secondary bending moment that is not a part of the primary applied forces being studied. As an applied load is increased on a member, such as a column, it will ultimately become large enough to cause the member to become unstable and is said to have buckled. Further load will cause significant and somewhat unpredictable deformations, possibly

leading to complete loss of the member's load-carrying capacity. If the deformations that follow buckling are not catastrophic the member will continue to carry the load that caused it to buckle. If the buckled member is part of a larger assemblage of components such as a building, any load applied to the structure beyond that which caused the member to buckle will be redistributed within the structure [5]. Usually, three types of basic buckling phenomena; local, distortional and global buckling.

1.4.1 Local Buckling

Local buckling is normally defined as the mode which involves plate-like deformations alone, without the translation of the intersection lines of the adjacent plate elements. Another important feature of local buckling is that the associated buckling length is the smallest among the three modes, and typically less than the width of any plate that construct the cross section [6] as revealed in Figure (1.7 a).

1.4.2 Distortional buckling

It is seeming to be the most problematic mode. As far as the associated buckling length is concerned it is typically in between the lengths of local and global modes, while the transverse deformations involve both plate-like deformations and the translation of one or multiple intersection lines of adjacent plate elements [6] as revealed in Figure (1.7 b).

1.4.3 Global Buckling

Global buckling can be considered as the simplest and clearest case: global buckling is a buckling mode where the member deforms with no deformation in its cross-sectional shape. Thus, the deformations can be characterized by the displacement and torsion of the system line of the member. Depending on the deformations and the type of loading, further subclasses can be defined such as:

flexural buckling, torsional buckling, flexural-torsional buckling and lateral-torsional buckling [6] as revealed in Figure (1.7 c).

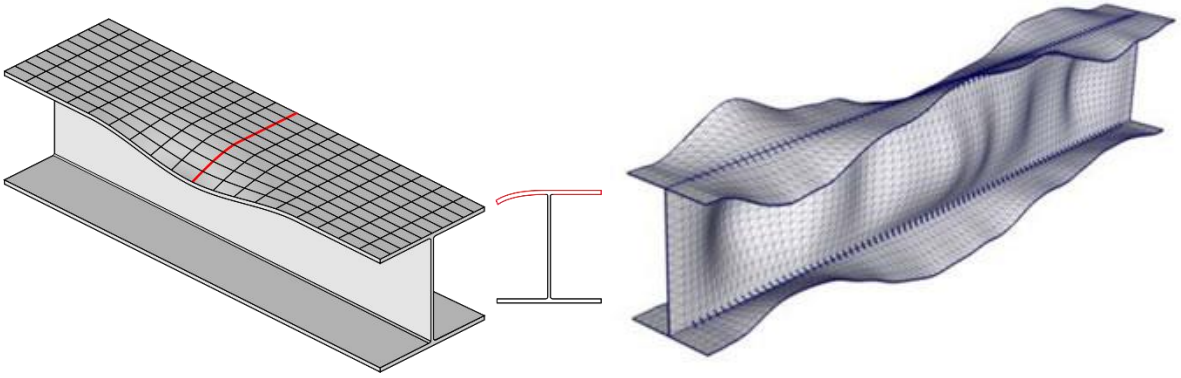

(a) Local buckling **(b) Distortional buckling**

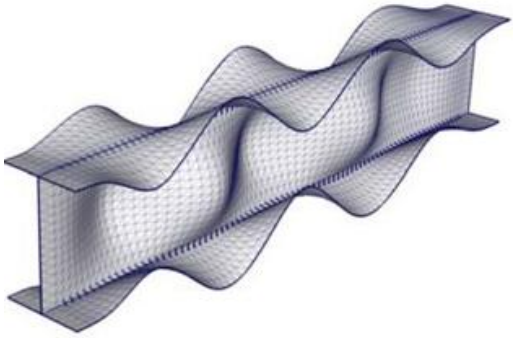

(c) **Global buckling**

Figure 1.7 Buckling types in steel beams [6].

1.5 Shear Connectors

the total shear force at the interface between a concrete slab and steel beam is approximately eight times the total load carried by the beam. Therefore, mechanical shear connectors are required at the steel-concrete interface. These connectors are designed to (a) transmit longitudinal shear along the interface, and (b) Prevent separation of steel beam and concrete slab at the interface [7].

1.5.1 Types of shear connectors

A. Rigid

As the name implies, these connectors are very stiff and they sustain only a small deformation while resisting the shear force. They derive their resistance from bearing pressure on the concrete, and fail due to crushing of concrete. Short bars, angles, T-sections are common examples of this type of connectors. Also anchorage devices like hooped bars are attached with these connectors to prevent vertical separation. This type of connectors is shown in Fig (1.8) [7].

b-Flexible

Headed studs, channels come under this category. These connectors are welded to the top flange of the steel beam. They derive their stress resistance through bending and undergo large deformation before failure. Typical flexible connectors are shown in Fig (1.9) [7]. The stud connectors are the types used extensively. The shank and the weld collar adjacent to steel beam resist the shear loads whereas the head resists the uplift.

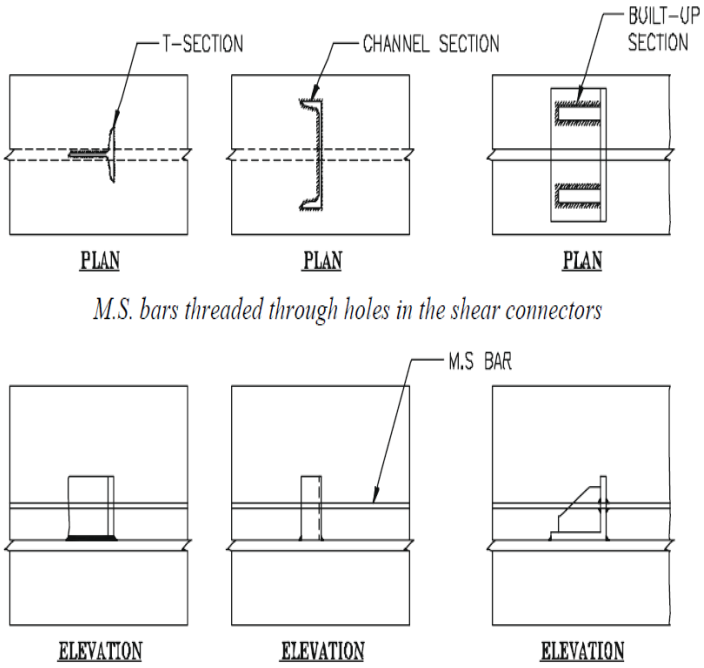

Figure 1.8 rigid connectors as slab uplift preventor [7].

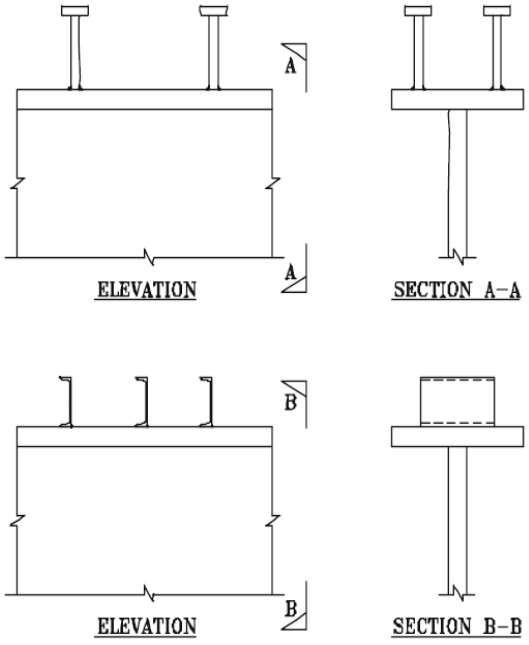

Figure 1.9 composite beams flexible connectors [7].

c-Bond or anchorage

These connectors derive their resistance through bond and anchorage action. These are shown in figure (1.10) [7].

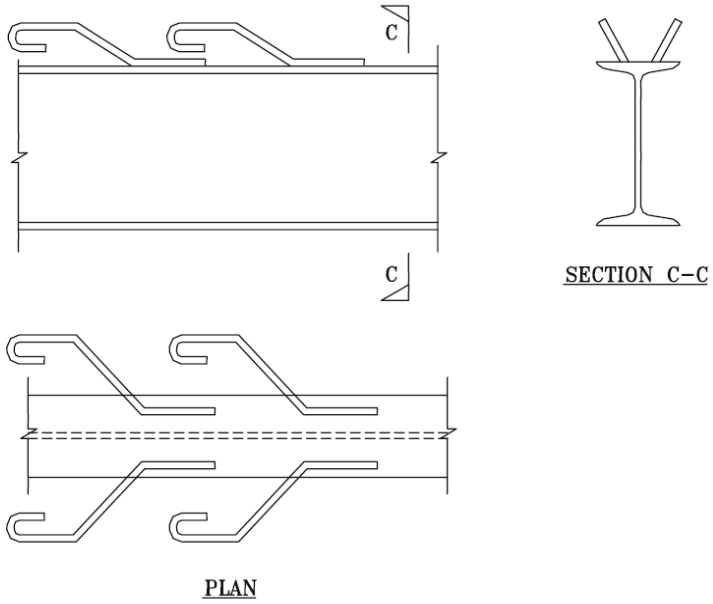

(i). Inclined mild steel bars welded to the top flange of steel unit [7].

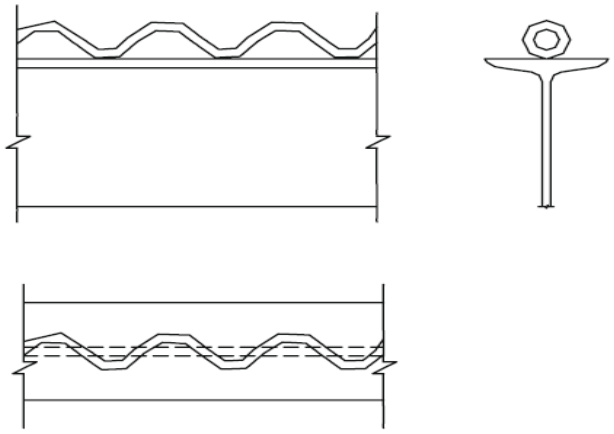

(ii). Helical connector

Figure 1.10: Typical bond or anchorage connectors [7].

1.6 Plate girder

Plate girders are built-up flexural members used to resist high bending moments and shear forces over long spans where the standard rolled or compound beams cannot satisfy the design requirements. Plate girders consist of two flange plates welded to web plate to form an I-section as seen in Figure (1.11). The major function of the flange plates is to resist axial compressive and tensile force caused by the applied bending moments. The primary aim of the web plate is to resist the applied shear forces [7].

Advantages use of plate girder:

- To reduce self-weight, the web thickness must be reduced to a minimum.
- Longitudinal and transvers stiffeners could be used to avoid web buckling.
- The designer has various choices to form plate girder and many designs, satisfy the design requirements, may be formed, but these designs may not be economical.
- The design of plate girder that satisfies the design requirements and minimizes its cost or weight is called optimum design.

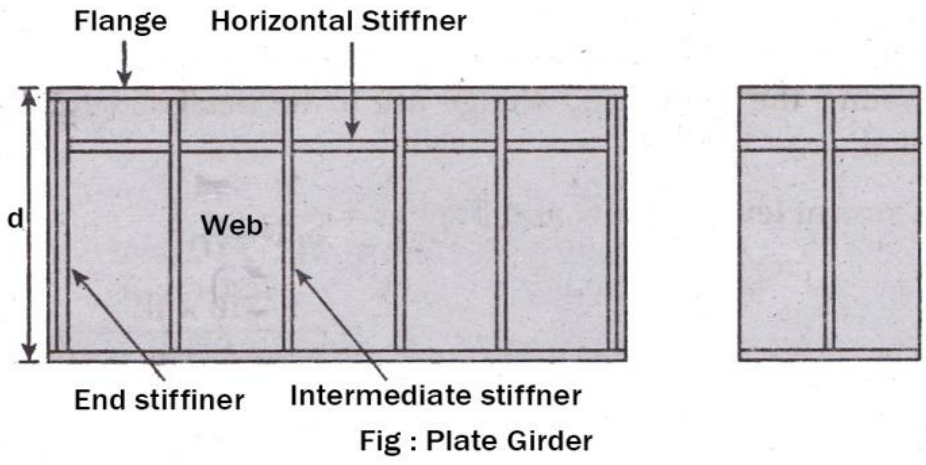

Figure 1.11 Plate girder section

1.7 Aim of the study:

The aim of this study is to find the values of the geometric dimensions of a plate girder and concrete deck which satisfy design requirements according to the provisions of the American Standard (ACI for concrete and AISC for steel) by using composite action and built-up section concept to introduce beam with high structural efficiency. Also, this study include; analysis the same suggested models by ANSYS to check the mode failures.

1.8 Scope of the Thesis

The present thesis consists of other five chapters. Chapter one deals with the general introduction when the chapter two reviews some previous work in optimum design and analysis of composite beam and Chapter three gives an introduction to the concepts of the design requirements of the composite beam used in this thesis. Chapter four explains in details the analysis of the suggested modes and the variation of its properties and capacity and also include analysis the same suggested models by ANSYS to check the mode failures. Finally, chapter five gives the conclusions drawn from this study and recommendations for future work.

CHAPTER TWO: LITERATURE REVIEW

2.1 General

Building with steel and composite elements experienced a renaissance during the 1980's, resulting in a profusion of new construction concepts and structural details.[1] In civil engineering applications, when a hot-rolled steel I-Beam section is insufficient to resist the bending moment or shear loading over a long span, a built-up plate girder is employed to satisfy the serviceability of a required section. This built-up plate girder is geometrically fabricated like those of steel I-Beam sections. The top and bottom flanges, which may have the same width and thickness or may vary in their widths and thickness, are welded to stiffened or unstiffened web panels. Moreover, those I-Beams and built-up plate girders are designed to resist the bending moment with their flanges, while, the shear stresses are carried by the web panel [2]. plate girders composed of angles connected to a web plate, with or without cover plates, were extensively used in United States on long spans in early railroad bridges during the period 1879-1900. Beginning with 1950s when welding became widely used, welded plate girders composed from three plates gradually replaced riveted girders [8]. Plate girders have advantages in the optimum use of material compared with rolled sections and the designer has greater freedom to vary the section to correspond with changes in the applied forces. Also, plate girders are easier to transport and erect than box girders and are aesthetically more pleasing than trusses. Thus plate girders are extensively used in civil engineering construction [2]. It is always required that designers use the well-known attributes of steel material to specify optimal engineering designs that would minimize the costs and satisfy the structural safety and design requirements [2]. The structural behavior of steel plate girders has been investigated by several researchers.

2.2 Concrete- Steel Composite Structures

In 2001, Adeli and Kim [10] developed a cost objective function which includes the costs of concrete, steel beams and shear studs using neural dynamics model programming for the composite truss and beams. A structural optimization method was applied to the analyzed models. The optimization was performed by the nonlinear programming approach (NLP). Their cost function included the costs of concrete, structural steel, reinforcement, shear studs, anti-corrosion paint, fire protection paint, sheet-steel cutting costs, welding costs, and the costs of the formworks. The conclusions were that composite trusses of spans exceeding 18 m are generally the most structural systems need to be optimized to get an optimized cost and weight.

In 2005, Kripka [11] presented a formulation procedure to minimize the volume of concrete in reinforced concrete building grillages. An association of the displacement method with optimization techniques implemented to obtain the optimized cross-sectional dimensions which lead to the smallest volume of concrete, attending to the ultimate loads (failure) and service loads (deflections). The constraints imposed in the formulation of the problem related to the limitation of the displacements include the effects of instantaneous and long-term deflections, considering an equivalent inertia with the contribution of concrete between cracking. The determination of the minimum height to each cross-section due to the flexural strength can be performed by fixing neutral axis position or by the maintenance of the section as under reinforced. Due to the relative complexity of the formulation as well as to the existence of local minima, even for a small number of variables, a stochastic method was chosen, being implemented the Simulated Annealing. In order to verify the efficiency of the proposed procedure, some of the analyzed

structures are presented, as well as the results obtained from the implementation of the proposed formulation.

In 2009, Degertekin and Hayalioglu [12] presented the optimum design of geometrically non-linear steel space frames using tabu search. The design algorithm obtains minimum weight frames by selecting suitable sections from a standard set of steel sections such as American Institute of Steel Construction (AISC) wide-flange (W)shapes. Strength constraints of American Institute of Steel Construction Load and Resistance Factor Design (AISC) specification, maximum drift (lateral displacement), interstorey drift and size constraints for columns were imposed on frames. The performance of the tabu search was compared with simulated annealing and genetic algorithms for two steel space frames taken from the literature. The comparisons showed that the tabu search algorithm resulted in lighter frames.

In 2010, Hasançebi and Doğan [13] applied a simulated annealing integrated solution algorithm to the optimum design of single-span steel truss bridges subjected to gravity loadings. In the optimum design process of a bridge the members are sized simultaneously as the coordinates of the upper chord nodes are determined such that the least design weight is attained for the structure. The design constraints and limitations are imposed in accordance with serviceability and strength provisions of ASD-AISC (Allowable Stress Design Code of American Institute of Steel Institution) specification. A numerical example is presented, where optimum designs produced according to nine alternative topological forms of single - span truss bridges are compared for a selected span length of 600 ft (182.88 m) to quantify the influence of choice of a topological form on the final design weight of the bridge.

In 2012, Axinte and Carmen [14] performed an optimization of the composite structures by the Neuro-linguistic programming (NLP) approach. The formulation included the cost steel beams and box girders. The use of the built-up section for the

plate girder made it more adaptable to optimization techniques and offers large savings in composite structures. The design, resistance and deflection inequality constraints for composite I welded beams were defined in accordance with the Eurocodes in order to satisfy the requirements of both the ultimate and the serviceability limit states. The optimization was performed for simply supported composite structures, for different combinations of spans and loads. The optimization also considered different economic conditions: different structural steel grades, four defined spans from 4 to 10 m, various uniformly distributed imposed loads from 5 kN/m (dead weight) to 10 kN/m taking into account the variation of the value of the imposed load. In this formulation, bearing stiffeners, welded connections and shear connectors are not taken into account. The concrete slab is tacking in account by the compressive strength (*fck*). A parametric study was conducted to compare the obtained optimal results. The task of the research was to define the spans and loads, at which each of the presented composite structures would show its advantages. The design variables consist of geometry dimensions, prestress tendon, shear and torsion reinforcement areas. Sensitivity analysis was performed for investigation of the effect of target reliability index level for ultimate and service limit states on the optimum solution. This studied evaluated the effect of target reliability index level for ultimate and service limit state on the optimal total cost of PC box girder bridges.

2.3 Plate Girders

In 1975, Johnson and May [15], presented an approximate method applicable only to simply supported beams with distributed load and uniformly spaced connectors. In this method, simple rules were derived for estimating the ultimate flexural strength and the deflections in service of composite beams with partial shear connection. The method was based on

the assumption that both the ultimate flexural strength and deflection could be equated by linear function to the degree of interaction.

In 1980, Hirst and Yeo [16] analyzed traditional shape of composite steel concrete beams to show how it is possible to modify the material properties of standard finite element to make them equivalent to a connecting system of composite construction. The analysis was applied in the elastic range and also to predict the load- deflection characteristics of a composite beam up to ultimate load. Two dimensional representations using eight-noded curved parabolic isoparametric element in plane stress were adapted. The stiffness of the connecting elements were determined on the assumption that they deformed essentially in shear and bending.

In 1981, Arizum and Hamada [17], presented a nonlinear finite element analysis of composite beams with elastic-plastic behavior of concrete, steel and shear connectors. A composite beam element with an assemblage of beam elements for the concrete slab and steel beam and a spring element for the shear connectors were used. The stress-strain curves of concrete and steel, and load-slip curve of shear connectors were presented by bilinear functions. The method can be applied to simply supported and continuous composite beams with both regularly and irregularly spaced shear connectors. The advantages of the method were the reduction of the degrees of freedom by fair amount comparing with the other finite element procedures and simpler manipulation for the analysis of material nonlinearity. The analysis showed that the bending stiffness of the partial composite beam was less than that of similar beams with continuously spaced connectors.

In 1999, Manfredi and Fabbrocino [18], studied the modeling of steel-concrete composite beams under negative bending. Negative bending moments acting in the support regions of continuous composite beams generate tensile stresses in the concrete slab and compressive stresses in the lower steel profile. As a result, the

mechanical behavior of these beams is strongly nonlinear even for low stress levels, due not only to the slip at the beam slab interface, but also to cracking in the slab. Therefore, an adequate theoretical modeling should take account of the interactions between the structural steel and the concrete slab by shear connectors and also between steel rebars and concrete in tension by bond phenomenon. Model of steel and concrete composite beams subjected to negative bending is presented. It accounts for the slip occurring at both the beam-slab interface and the steel reinforcement-concrete interface. Some numerical results, obtained using a suitable numerical procedure, are discussed to show the capacity of the model.

In 2001, Maiorana et al. [19] developed linear buckling analysis of plates with longitudinal stiffeners having various shapes and positions and subjected to axial force, in-plane bending and shear. The aim of the study was to give some new practical insights about the shape and optimum position of longitudinal stiffener in webs when axial force, bending moment and shear act. In this work the problem of elastic stability of square and rectangular stiffened panels subjected to axial compression and bending moment or shear was studied by means of the Finite Element Code Strand7. Plate elements with four nodes and six degrees of freedom for each node were used in this study. The following conclusions were drawn from the study: For panels subjected to axial force and in-plane bending moment; the optimum position of the longitudinal stiffener along the height of a web panel depends on the load condition. In particular, regarding the case of pure bending, the optimum position corresponds to one fifth of the height starting from the compressed edge. Increasing the compressive component with respect to the flexural one, the optimum position of the stiffener moves down until the central position for uniform compression. A stiffener with a closed-section (rectangular, triangular, and trapezoidal) has a better performance than a stiffener with an open section having

the same area of the cross-section. For panels subjected to shear, the optimum location of the longitudinal stiffener corresponds to the half of the height of the panel. A stiffener with a closed-section (rectangular, triangular, and trapezoidal) has a better performance than a stiffener with an open section having the same area of the cross-section. The elastic critical load increases when the aspect ratio of the panel (vertical stiffeners spacing-to-web depth) decreases. For both panels exposed to axial force and in-plane bending moment and shear, stiffeners with small flexural rigidity are not able to allow the entire plate to behave as two separate subpanels in relation to local buckling.

In 2004**,** Nie and Xiao [20], studied Static loading tests were conducted on 16 steel–concrete composite beams and two steel beams to investigate shear resisting mechanisms and the strength of composite beams. The main experimental parameters were the shear span aspect ratio of the simply supported beams, and the width and thickness of the concrete flanges. Based on strain measurements, stress in the steel beam was analyzed using theories of elasticity and plasticity, and the vertical shear that the steel beam resisted was calculated. The shear resistance of the concrete flange was then obtained by subtracting the steel shear contribution from the total load applied. It was found that the concrete flange could sustain 33–56% of the total ultimate shear applied to the composite beam specimens, contrary to the typical assumption of neglecting the concrete shear contribution in most design codes and specifications. A shear strength equation that considers the shear contributions of both the steel beam and the concrete flange is proposed.

In 2005, Liang and Ronagh [21], used the finite element method to investigate the flexural and shear strengths of simply supported composite beams under combined bending and shear. A three-dimensional finite element model has been developed to account for geometric and material nonlinear behavior of composite

beams, and verified by experimental results. The verified finite element model is then employed to quantify the contributions of the concrete slab and composite action to the moment and shear capacities of composite beams. The effect of the degree of shear connection on the vertical shear strength of deep composite beams loaded in shear is studied. Design models for vertical shear strength including contributions from the concrete slab and composite action and for the ultimate moment–shear interaction is proposed for the design of simply supported composite beams in combined bending and shear. The proposed design models provide a consistent and economical design procedure for simply supported composite beams.

In 2007, Korkess and Yousifany [22], studied the behavior of structural continuous composite steel-concrete beams, which are widely used in building and bridge constructions. Therefore, the structural behavior of composite beams under negative moment is a significant subject. However experimental tests in this field are very rarely and information about the efficiency of shear connection when the slab is under tension are really few. In this research, available experimental tests on composite steel-concrete beams under negative bending are theoretically analyzed using the finite element software ANSYS. ANSYS computer program is a large-scale multipurpose finite element program which may be used for solving several cases of engineering analyses. The proposed three-dimensional model is able to simulate the overall flexural behavior of composite beams. These covers; load-deflection behavior, longitudinal slip at the steel-concrete interface, and distribution of shear studs. The reliability of the model is demonstrated by comparison with available experiment and alternative numerical analysis which showed 9-10% difference.

In 2008, Mohammed [23], tested ten composite beams, designed to fail in bending. Varied degrees of shear connection are used. Regions of positive (sagging)

bending moment and negative (hogging) bending moment are taken into account. Two types of loading, central point load and two-point loads are considered. The behavior of beams under loading was observed. Ultimate loads, concrete and steel strains, deflections, and end slip, were recorded. The reduction of the degrees of shear connection from 100 % to 33.3 % causes increasing strains, mid span deflection, and end slip. The values of recorded items for the case of sagging bending beams were lower than those recorded for the hogging bending beams. The tested composite beams were analyzed using nonlinear one dimensional and three-dimensional finite element models. An ANSYS 5.4 program code was used to analyze the three-dimensional model. The adopted finite element models were found to predict the deflections, strains, and end slip distribution, in a reasonable agreement with the test results.

In 2008, Neto et al. [24] investigated the sensitivity analysis and optimal design by use of generalized Timoshenko modelling of composite beam structures. This research described a new approach to design the cross-section layer orientations of composite laminated beam structures. The beams are modelled with realistic cross-sectional geometry and material properties instead of a simplified model. The variational asymptotic beam section analysis (VABS) methodology was used to compute the cross-sectional model for a generalized Timoshenko model, which was embedded in the finite element solver FEAP. Optimal design was performed with respect to the layers' orientation. The design sensitivity analysis was analytically formulated and implemented. The direct differentiation method is used to evaluate the response sensitivities with respect to the design variables. Thus, the design sensitivities of the Timoshenko stiffness computed by VABS methodology are imbedded into the modified VABS program and linked to the beam finite element solver. The laminate ply orientations were considered as design variables and the

direct differentiation method was used to derive the response sensitivities with respect to the design variables. Using two different approaches, it was possible to verify that the optimization strategy that employs maximum displacement as a performance criterion does not ensure critical load improvement of the optimum designs. The modified method of feasible directions and sequential quadratic programming algorithms were used to seek the optimal continuous solution of a set of numerical examples. The results showed that using two simple composite beams with different cross-sectional geometries, optimal design improved the twist–bending buckling critical load. However, using the torsion and bending components of the generalized Timoshenko stiffness matrix as the goal function of the optimization procedure, several optimum designs obtained led to improvements in the critical bending buckling load. Moreover, the optimum designs of the cantilever beam with a composite box cross-section led to mirror antisymmetric box beams and stretch bending coupling, since the mirror symmetry is required for twist–bending coupling. Therefore, the results demonstrate that the methodology presented may be used to obtain feasible designs that support twist–bending buckling load improvement.

In 2008, Optimum design of steel reinforced concrete (SRC) composite beams were investigated by Zheng et al. [2]. An optimal design scheme of single objective and discrete variables is proposed to design SRC frame beams. In the optimum scheme, the design variables included the layout dimensions of SRC frame structure, structural member sections, strength of concrete and steel, and dimensions of steel shapes. The objective function is cost of the entire materials applied to construct SRC frame structure. This paper used a discrete variable mixing penalty function optimization algorithm to design SRC frame beams, which is one of mathematical programming methods. The method has extremely strict logic and is suitable for the

SRC frame design. As some of the parameters impact the convergence process in optimum scheme, for different initial condition the convergence process varies obviously, and sometimes the process will be longtime. To improve versatility and stability of the method, it is needed to do more systematic analysis research on the entire optimum process and its parameters. The constraint conditions were the main requirements stated in Chinese code for design of SRC structures, basic design rules, reasonable calculating theories and indispensable constructions, as well as some mature and consistent conclusions confirmed by experimental studies on calculating methods of SRC structures based on the bond-slip theory between steel shape and concrete.

In 2009, Alinia et al. [25] designed and analyzed a number of full-scale plate girders to determine their shear failure mechanism characteristics. Nonlinear large deflection finite element analyses were performed. The four-noded- reduced integrated element of the ABAQUS software was selected. Several transversely stiffened plate girders having identical depth and panel width of 1 m in spans of 2, 4 and 6 m were considered. Parametric studies regarding web thickness, flange dimensions and end-posts were carried out. The following results were found from their analyses: Shear-induced plastic hinges occur only in the flanges of end panels after formation a partial-inclined yield zones in webs. The formation of plastic hinges is due to the shear deformation of girders, directly pertained the stiffness of end-posts and flange dimensions. the location of plastic hinges is not directly related to the stresses imposed by the inclined tension fields. When the flange thickness is more than three times the web thickness, failure mode is always in shear and if this ratio is less than two, flexure failure mode governs. In the intermediate ranges, the failure mode depends on the web slenderness ratio. Compact webs collapse in flexural mode, while slender webs fail in shear. The addition of end-posts provides

more fixity to flange plates and increases the ultimate resistance of plate girders. Eurocode 3 the most conservative ultimate capacity for plate girders gives The AISC results for medium to stocky flanges produce closest results to the FEM. The AASHTO results always overestimate the capacity.

Cho and Shin (2011) [26] investigated the elastic web bend-buckling behavior of I-section girders with a longitudinal stiffener. A three-dimensional finite element analysis was used to obtain the bend-buckling caused by moment The effect of the non-symmetry of the cross section, the location of the longitudinal stiffener, the boundary conditions along the transverse and longitudinal stiffeners, the spacing of the transverse web stiffeners, the flexural rigidity of the longitudinal stiffener and the slenderness of the web were studied. It was found that the optimum location of the longitudinal stiffener is at (0.425 D) from the inner surface of the compression flange, where D. is the depth of the web in compression in elastic range. The subpanel between the compression flange and the longitudinal stiffener buckles when the distance between the compression flange and the longitudinal stiffeners is more than (0.425 D). Also, it was found that the AASHTO LRFD, and Eurocode-3 equations give a conservative value for bend-buckling compared with the finite element analysis The transverse and longitudinal stiffeners that satisfy the AASHTO LRFD requirements were shown to have sufficient rigidity to restrain the web from lateral buckling.

In 2012, Faluyi and Arum [27] utilized the Constrained Artificial Bee Colony (CABC) algorithm and the Generalized Reduced Gradient (GRG) algorithm to optimize the design of plate girder for minimum weight with fixed values for the span and steel yield strength of the girder. They considered a simply supported plate girder having a uniform cross section, homogenous material, and without longitudinal stiffeners. The cross-sectional areas of the girder and stiffeners were

minimized subject to the provisions of the Code of Practice BS 5950-1: 2000 and guides in Steel Designers' Manual (2003). The results obtained using the GRG and the CABC algorithms were very close and demonstrated a significant reduction in weight of the beam.

In 2012**,** Khalaf [28], studied a composite beam is an accumulation of different materials so as to forming a single unit to exploit the prominent quality of these materials according to their position within the cross-section of the composite beam. The present study investigates the structural behavior of six simply supported composite beams, in which a reinforced concrete T-beam is connected together with a steel channel located at the bottom of a T-beam by means of headed stud shear connectors. The used degrees of shear connection are (100%, 75%, 50%, and 38%) of full connection. The study also examined six reinforced concrete T-beams without steel channel. Three-dimensional nonlinear finite element analysis has been used to conduct the numerical investigation for the general behavior of the beams which are subjected to central point load. ANSYS 12.1 program code was used to estimate the ultimate loads, deflections, stresses, strains, end slip and curvatures. Perfect bond between the reinforcing bars and the concrete was assumed. The load on beams was applied monotonically in increments up to failure. Ultimate loads, deflections, stresses, strains, end slip and curvatures were noticed. The reduction of the degree of shear connection from 100% to 38% causes increasing strain, mid span deflection and end slip with an average of 3.95%, 13%, and 111% respectively, and decrease in ultimate load with an average of 7.3%. The composite beam (concrete T-steel channel) increased the strength as compared with the ordinary reinforced concrete T-beam, the increase in ultimate load ranging from 35% to 52% with an average of 44%. In order to observe the efficiency of the finite element model a comparison

between the numerical results with available experimental work was made. The maximum difference in ultimate load is less than 5.3%.

In 2014, Lee et al. [29] investigated the moments of inertia of the transverse stiffeners required to prevent both elastic buckling and post-buckling so as to allow a plate girder web panel to develop its potential shear strength. This study first investigated the moments of inertia of transverse stiffeners required to maintain straight web for elastic buckling through linear buckling finite element analysis, and new design equations were developed. Then, nonlinear finite element analyses were carried out in order to determine the moments of inertia the transverse stiffeners required to maintain straight web during post- of buckling. From the nonlinear FEA results, a new design equation is formulated post-buckling based on the design equations developed for elastic buckling. It was found that the design equation for elastic buckling in AISC and AASHTO LRFD specifications is too conservative especially when the aspect ratio is greater than 1.0. Also, the design equation for post-buckling in AISC and AASHTO specifications resulted in designs that are too conservative due to oversimplification.

In 2015, Optimal design of frequency dependent of composite steel concrete beams for low mass and high damping was presented by Hamdaoui et al. [30]. An optimal design approach for choosing the most suitable material for high damping and low mass for a sandwich beam is investigated. Two frequency dependent visco-elastic materials (PVB and 3M ISD112) were considered. The damping characteristics (eigenfrequencies and damping ratios) of the sandwich beam are determined by solving a non-linear eigenvalue problem. A multi-objective optimization approach based on evolutionary algorithms is used to find the Pareto surface theory that minimizes the mass and maximizes the damping. The optimization variables are the thicknesses of the visco-elastic and elastic layers. The

total beam thickness is kept constant and its maximal deflection under its own weight is limited to its thickness. It is found that the Pareto front for ISD112 material reduces to one point while for the PVB it is composed of several points. It is shown that choosing the most appropriate material for high damping and low weight depends on the importance of each criterion.

In 2017, Erdal Et al. [31] Optimum design of composite corrugated web beams using hunting search algorithm. Optimum design of corrugated composite beams is presented in term of application of a hunting search algorithm to demonstrate the robustness of the proposed algorithm. A recent stochastic optimization algorithm coded that is based on hunting search is used for obtaining the solution of the design problem. In the optimization process, besides the thickness of concrete slab and studs, web height and thickness, distance between the peaks of the two curves, the width and thickness of flange are considered as design variables. The design constraints are respectively implemented from BS EN1993-1:2005 (Annex-D, Eurocode 3) BS-8110 and DIN 18-800 Teil-1. Furthermore, these selections are also carried out such that the design limitations are satisfied and the weight of the composite corrugated web beam is the minimum.

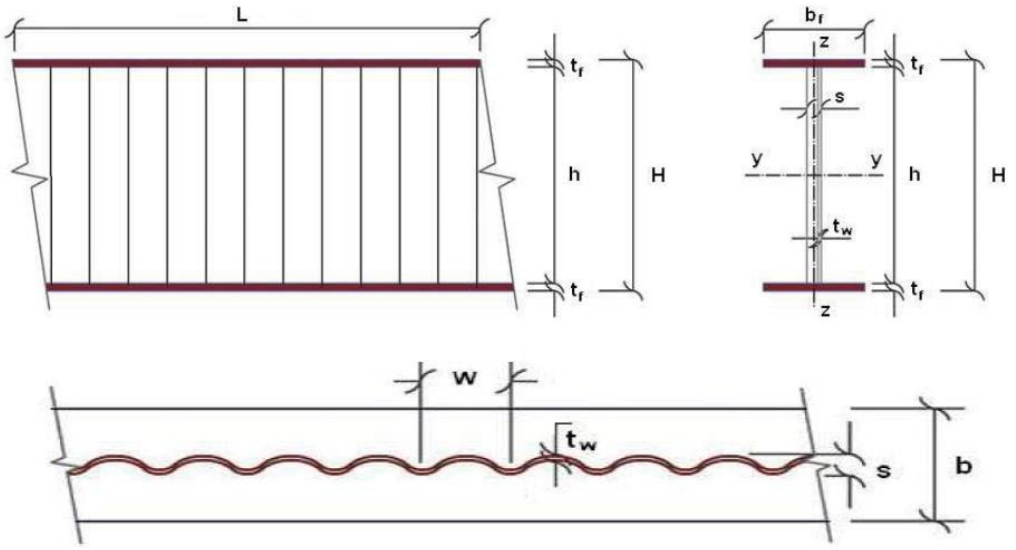

Figure 2- 1 The demonstration of Composite Corrugated Web Beam [31].

In 2019, Yossef et al. [32] investigated the cost optimization of composite floor systems with castellated steel beams. The cost optimization of the internal composite floor bays with castellated steel beams was studied using a genetic algorithm. A computed flowchart, input variables, constraints, and output variables are presented. The cost optimal function was defined using a price list of the different floor components. The accuracy of the model was validated by comparison with two literature examples. Comparative simulations were conducted to explore the effect of various influential parameters in optimal design, and the number of floor divisions, dimensions of hexagonal openings, and number of web openings were considered. The results showed that the optimization of 32 composite castellated bays, with different numbers of floor divisions, did not show any significant difference in the total cost, whereas, the maximum standard deviation was 4.8% of the mean value for the bay cost. Therefore, only a practical value of the spacing between beams (B) is recommended. For edge girders the degree of shear connection (h = 0.4) would provide competitive design for composite castellated girders. To minimize the cut length, the limit of hexagonal web dimension was introduced. The

web opening dimension ratio (e/tw) can vary from 35 to 55, the ratio of (2dh/e) must be less than 1.455, and a is nearly 30°. To reduce web post buckling, the web opening dimension ratio (e/tw) can vary from 19 to 34, the ratio of the opening height to width (2dh/e) must be less than 2.28, and a is between 54.8 and 76.5°, with a mean value 62.12°. Increasing the end distance is not recommended for optimization because it does not affect the material cost. Finally, the partially fixed connections with a restraint factor R = 0.75 for the main girder end could save about 10% of the composite bay cost compared with the simple end connection.

In 2022, El-Aghoury et al. [33] investigated the optimum design of fully composite, unstiffened, built-up, hybrid steel girder using nonlinear programming (NLP), artificial neural network (ANN), genetic algorithm (GA), ant colony (AC), and harmony search (HS) techniques. The aim of this research is to develop simple and practical equations to determine the optimum cross section dimensions for both shored and unshored, simply supported, hybrid and nonhybrid, composite steel beam under static loads. To achieve that goal, a research program of two phases was carried out. The first phase was generating a database of 504 composite beams with different steel grades for flanges and webs, subjected to different values of bending moment. The cross section of each beam in the database was optimized using GRG technique to minimize the cost considering the unit price of each steel grade. In the second phase, the generated database was divided into training and validation subsets and used to develop two predictive models using Nonlinear Regression (NLR) technique and Artificial Neural Network (ANN) technique to predict the optimum cross section dimensions and hence the optimum weight and cost. The accuracies of the developed models were measured in terms of average error percent. NLR and ANN models showed average error percent of 16% and 11%, respectively.

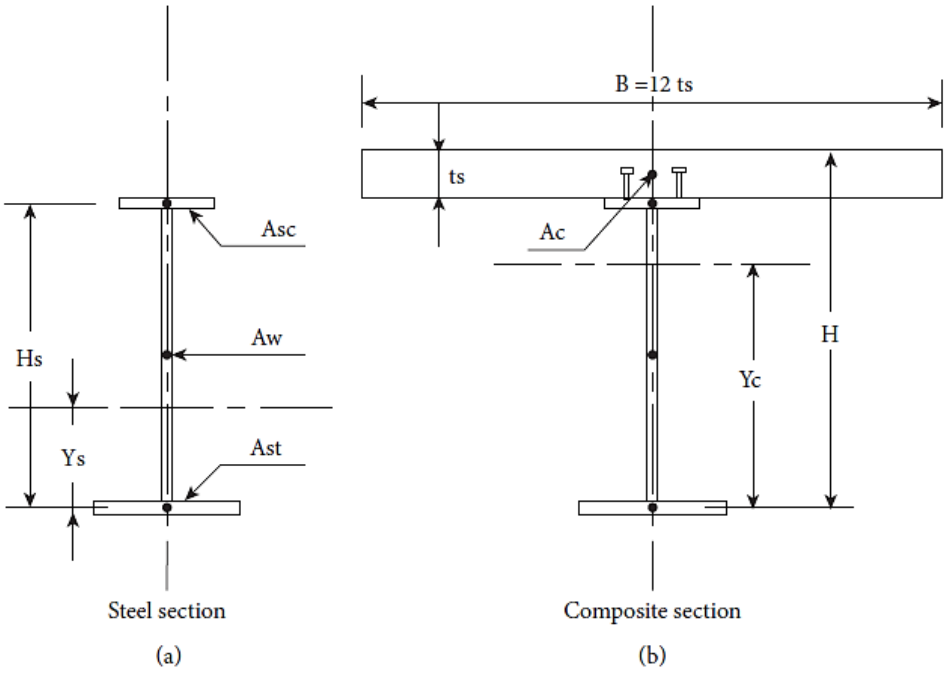

Figure 2.2 The considered built-up composite beam section. (a) Steel section. (b) Composite section [33].

CHAPTER THREE: DESIGN REQUIREMENT AND ANALYSIS BY FINITE ELEMENT

3.1 General

This chapter addresses the design and analysis of composite members composed built-up structural steel and concrete shapes structural concrete by equations and finite element analysis. In structural analysis, most problems are complex and accurate solutions are obtained for their governing equations only and for limited types of structures of load characteristics and simple engineering. Thus, numerical procedures such as FEM are used to obtain approximate solutions for realistic types of problems. FEM is an important technique provided solutions to a varied problem in all engineering fields. This work applies a nonlinear FEA for RCHBs exposed to static load to study the behavior of these beams.

3.2 Specification for concrete built up composite beam

3.2.1 General provision

In determining load effects in members and connections of a structure that includes composite members, consideration shall be given to the effective sections at the time each increment of load is applied.

3.2.2 Concrete and steel reinforcement

The design, detailing and material properties related to the concrete and reinforcing steel portions of composite construction shall comply with the reinforced concrete and reinforcing bar design specifications stipulated by the applicable building code, additionally the provisions in the Building Code Requirements for Structural Concrete and Commentary (ACI-318) and the Metric Building Code Requirements for Structural Concrete and Commentary (ACI 318M), [34]

subsequently referred to in Chapter I collectively as ACI 318, shall apply with the following exceptions and limitations: (a) ACI 318 provisions specifically intended for composite columns shall be excluded in their entirety. (b) Concrete and steel reinforcement material limitations shall be as specified in Section I1.3. (c) Transverse reinforcement limitations shall be as specified in Section I2.1a(b) and I2.2a(c), in addition to those specified in ACI 318. Minimum longitudinal reinforcement limitations shall be as specified in Sections I2.1a(c) and I2.2a(c). Concrete and steel reinforcement components designed in accordance with ACI 318 shall be based on a level of loading corresponding to LRFD load combinations. [35].

3.3 AISC Requirements for Built Up Steel Section

Web Proportions

Whether a girder web is noncompact or slender depends on h/t_w , the width-to-thickness ratio of the web, where h is the depth of the web from inside face of bottom flange to inside face of flange and t_w is the web thickness [35].

For noncompact web, the requirements for the double and single symmetric I-shaped sections are

$$3.67\sqrt{\frac{E}{F_y}} < \frac{h}{t_w} \leq 5.7\sqrt{\frac{E}{F_y}} \qquad \text{…..(3.1)}$$

$$\frac{\frac{h_c}{h_P}\sqrt{\frac{E}{F_y}}}{\left(0.54\frac{M_p}{M_y}-0.09\right)}\frac{h_c}{t_w} \leq 5.7\sqrt{\frac{E}{F_y}} \qquad \text{…..(3.2)}$$

For slender web, the requirements for the double and single symmetric I-shaped sections are

$$\frac{h}{t_w} \leq 5.7\sqrt{\frac{E}{F_y}} \quad \text{.....(3.3)}$$

$$\frac{h_c}{t_w} > 5.7\sqrt{\frac{E}{F_y}} \quad \text{.....(3.4)}$$

To prevent web buckling (to prevent vertical buckling of the compression flange into the web, web stiffeners can be added for stability. AISC F13.2 imposes an upper limit on the web slenderness. The limiting value of h/tw is a function of the aspect ratio, a/h, of the girder panels, which is the ratio of intermediate stiffener spacing to web depth.

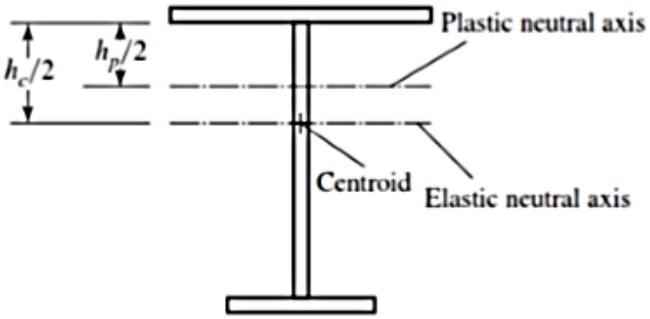

(a) I shape plate girder

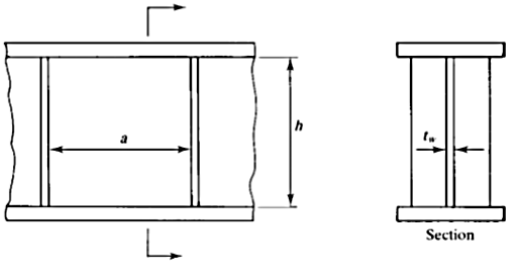

(b) Section of plate girder

Figure 3.1 Section of plate girder

Thus I-shaped members must also satisfy the following limits, where a is the clear distance between transverse stiffeners, and h is the height of the web between flanges

I-shaped members with slender webs shall also satisfy the following limits:

(a) When $\frac{a}{h} \leq 1.5$

$$\left(\frac{h}{t_w}\right)_{max} = 12.0\sqrt{\frac{E}{F_y}} \quad \ldots\ldots\ldots\ldots \quad (3.5)$$

(b)When $\frac{a}{h} > 1.5$

$$\left(\frac{h}{t_w}\right)_{max} = \frac{0.40E}{F_y} \quad \ldots\ldots\ldots\ldots \quad (3.6)$$

where

a =clear distance between transverse stiffeners, in. (mm)

In unstiffened girders, h/t_w shall not exceed 260. The ratio of the web area to the compression flange area shall not exceed 10.

Regarding the comparison between the stiffness and unstiffened web, the requirements for the unstiffened girder are

$$\frac{h}{t_w} \leq 260 \; and \; \frac{A_w}{A_{fc}} \leq 10$$

While for stiffened web, the requirements are:

$$\frac{a}{h} \leq 1.5 \quad \ldots\ldots\ldots\ldots \quad (3.7)$$

$$\frac{a}{h} > 1.5 \quad \ldots\ldots\ldots\ldots \quad (3.8)$$

$$\left(\frac{h}{t_w}\right)_{max} = 12\sqrt{\frac{E}{F_y}} \quad \ldots\ldots\ldots\ldots \quad (3.9)$$

$$(\frac{h}{t_w})_{max} = \frac{0.42\ E}{F_y} \quad \text{..... (3.10)}$$

Where;

A_w = Area of the web = $h*t_w$

A_{fc} = Area of the compression flange = $b_{fc} * t_{fc}$

$0.1 <= I_{yc}/I_y <= 0.9$ (AISC Equation F13-2)

I_y = is the moment of inertia about the y-axis, and I

I_{yc} = is the moment of inertia about the y-axis referred to the compression flange.

3.4 Composite Section Capacity

The nominal strength of composite sections shall be determined in accordance with either the plastic stress distribution method, the strain compatibility method, the elastic stress distribution method, or the effective stress-strain method, as defined in this section. The tensile strength of the concrete shall be neglected in the determination of the nominal strength of composite members.

3.4.1 Plastic Stress Distribution Method

For the plastic stress distribution method, the nominal strength shall be computed assuming that steel components have reached a stress of (Fy) in either tension or compression, and concrete components in compression due to axial force and/or flexure have reached a stress of (0.85*f'c*), where (*f'c*) is the specified compressive strength of concrete, ksi (MPa).

3.4.2 Strain Compatibility Method

For the strain compatibility method, a linear distribution of strains across the section shall be assumed, with the maximum concrete compressive strain equal to

0.003 in./in. (mm/mm). The stress-strain relationships for concrete shall be obtained from tests or from ACI- Code equations [34].

3.4.3 Elastic Stress Distribution Method

For the elastic stress distribution method, the nominal strength shall be determined from the superposition of elastic stresses for the limit state of yielding or concrete crushing.

3.4.4 Effective Stress-Strain Method

For the effective stress-strain method, the nominal strength shall be computed assuming strain compatibility, and effective stress-strain relationships for steel and concrete components accounting for the effects of local buckling, yielding, interaction and concrete confinement.

3.5 Design approach:

3.5.1 Plastic stress distribution

A. Flexural Strength

The nominal flexural strength *Mn* of a plate girder is based on one of the limit states of tension flange yielding, compression flange yielding or local buckling (FLB), or lateral-torsional buckling (LTB).

B. Tension Flange Yielding

From Chapter 5, the maximum bending stress in a flexural member bent about its strong axis is

$F_b = M/S_x$ ……. (3.11)

where Six is the elastic section modulus about the strong axis.

Expressing the bending moment as a function of the section modulus and stress gives

$M = F_b * S_x$ ……. (3.12)

AISC F5 gives the nominal flexural strength based on tension flange yielding as

$M_n = F_y S_{xt}$ ……. (3.13)

where S_{xt} = elastic section modulus referred to the tension side.

C. Compression Flange Strength

The compression flange nominal strength is given by

$M_n = R_{bg} F_{cr} S_{xc}$ ……. (3.14)

Where;

R_{bg} = bending strength reduction factor

F_{cr} = critical compressive flange stress, based on either yielding or local buckling

S_{xc} = elastic section modulus referred to the compression side

The bending strength reduction factor is given by

$$\text{Rpg} = 1 - \frac{a_w}{1200+300a}\left(\frac{h_c}{t_w} - 5.7\sqrt{\frac{E}{F_y}}\right) \leq 1.0\ldots \quad \ldots\ldots\ldots \quad (3.15)$$

(AISC Equation F5-6) …….

Where

$$a_w = \frac{h_c\, t_{w1}}{b_{fc} t_{fc}} \leq 10 \qquad \text{AISC Equation F4} - 12) \quad \ldots\ldots\ldots \quad (3.16)$$

b_{fc} = width of the compression flange

t_{fc} = thickness of the compression flange

The critical compression flange stress F_{cr} depends on whether the flange is compact, noncompact, or slender. The AISC Specification uses the generic notation l, l_p, and l_r to define the flange width-to-thickness ratio and its limits.

From AISC Table B4.1b.

D. Lateral-Torsional Buckling

The nominal lateral-torsional bucking strength is given by the bending strength reduction factor is given by

$$R_{pg} = 1 - \frac{a}{1200+300a_w}\left(\frac{h}{t_w} - 5.7\sqrt{\frac{E}{F_y}}\right) \leq 1.0 \quad \text{..... (3.17)}$$

Where:

$$a_w = \frac{h_c t_w}{b_{fc} t_{fc}} \leq 10 \quad \text{..... (3.18)}$$

b_{fc} =width of the compression flange

fc =thickness of the compression flange

(The upper limit of 10 in Equation F4-12 is not actually part of the AISC Equation, but AISC F5.2 stipulates that limit). The critical compression flange stress Fcr depends on whether the flange is compact, noncompact, or slender. The AISC Specification uses the generic notation λ, λ_p,and $\lambda_r$to define the flange width-to-thickness ratio and its limits. From AISC Table B4.1b,

$$\lambda = \frac{2\, b_f}{t_f} \quad \text{..... (3.19)}$$

$$\lambda p = 0.38\sqrt{\frac{E}{F_y}} \quad \text{..... (3.20)}$$

$$\lambda r = 0.95\sqrt{\frac{k_c E}{F_L}} \quad \text{..... (3.21)}$$

$$k_c = \frac{4}{\sqrt{\frac{h}{t_w}}} \quad \text{..... (3.22)}$$

F_L=0.7 f_y for girders with slender webs.

If $\lambda \leq \lambda_p$ the flange is compact. The limit state of yielding will control, and $F_{cr}=F_y$ resulting in

$$k_c = R_{pg} F_y S_{xc} \quad \text{..... (3.23)}$$

If $\lambda_p < \lambda \leq \lambda_r$, the flange is noncompact. Inelastic FLB will control, and

$$F_{cr} = F_y - 0.3F_y\left(\frac{\lambda-\lambda p}{\lambda r-\lambda p}\right) \quad \text{..... (3.24)}$$

If $\lambda > \lambda_r$, the flange is slender, elastic FLB will control, and

$$F_{cr} = \frac{0.9EK_c}{\left(\frac{b_f}{2t_f}\right)} \quad \text{..... (3.25)}$$

Lateral-Torsional Buckling

The nominal lateral-torsional bucking strength is given by

$$M_n = R_{pg} F_{cr} S_{xc} \quad \text{..... (3.26)}$$

Whether lateral-torsional buckling will occur depends on the amount of lateral support—that is, the unbraced length Lb. If the unbraced length is small enough, yielding or flange local buckling will occur before lateral-torsional buckling. The length parameters are Lp and Lr, where;

$$L_p = 1.1\, r_1\sqrt{\frac{E}{F_y}} \quad \ldots\ldots\ldots\ldots \quad (3.27)$$

$$L_r = r_1\sqrt{\frac{E}{0.7F_y}} \quad \ldots\ldots\ldots\ldots \quad (3.28)$$

r_t =radius of gyration about the weak axis for a portion of the cross section consisting of the compression flange and one-third of the compressed part of the web. For a doubly symmetric girder, this dimension will be one-sixth of the web depth. (See Figure 10.7.) This definition is a conservative approximation of rt (see the user note in AISC F4.2). The exact definition is given by AISC Equation F4-11.

If $L_b \leq L_p$, there is no lateral torsional buckling.

If $L_p < L_b \leq L_r$, Failure will be by inelastic LTB, and

$$F_{cr} = c_b F_y - 0.3F_y\left(\frac{L - Lp}{Lr - Lp}\right) \leq F_y \quad \ldots\ldots\ldots\ldots \quad (3.29)$$

If $L_b > L_r$, failure will be by elastic LTB, and

$$F_{cr} = \frac{{C_b}^2 E}{\left[\frac{L_b}{r_1}\right]^2} \leq Fy \quad \ldots\ldots\ldots\ldots \quad (3.30)$$

C_b is defined by AISC Equation F1-1 and is covered in Chapter 5 of this book

3.6 Composite Section Description

3.6.1 Mode 1

Traditional concrete steel composite section with minimum reinforcement for shrinkage. The mode 1 adopted to be reference.

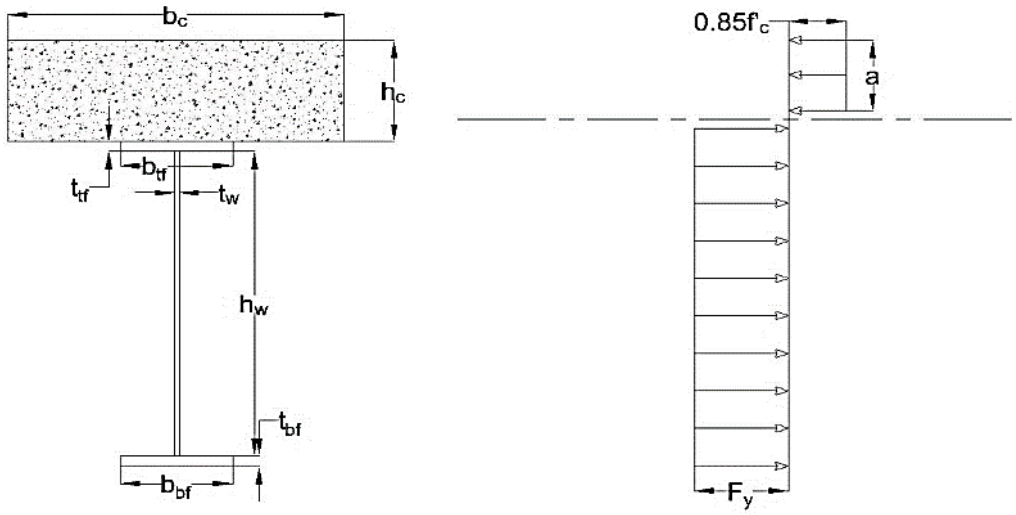

Figure 3.2 composite beam concrete and steel built up I section

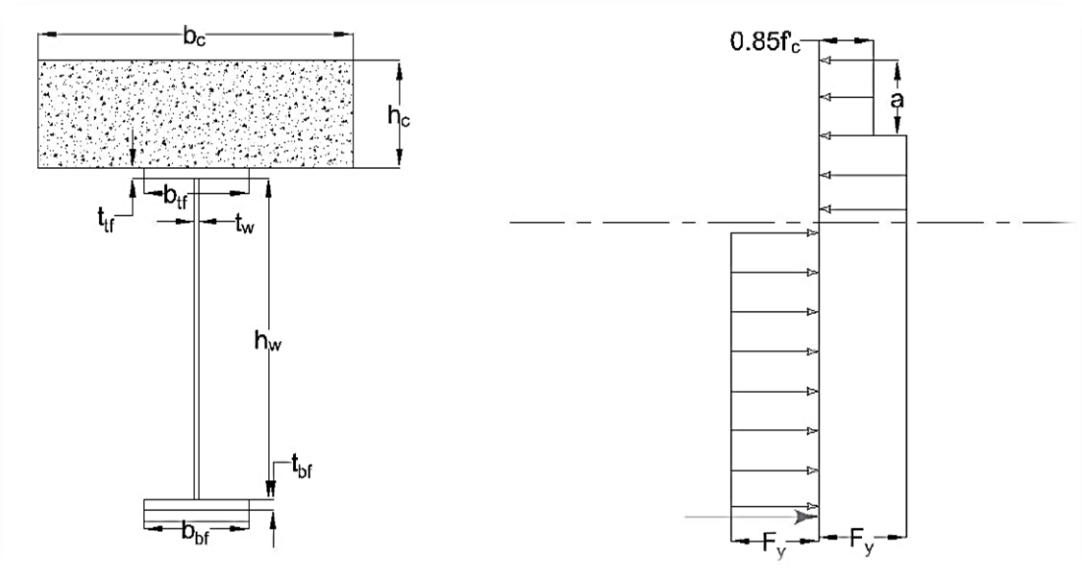

Figure 3- 3 composite beam concrete and steel built up I section with cover plate at bottom flange

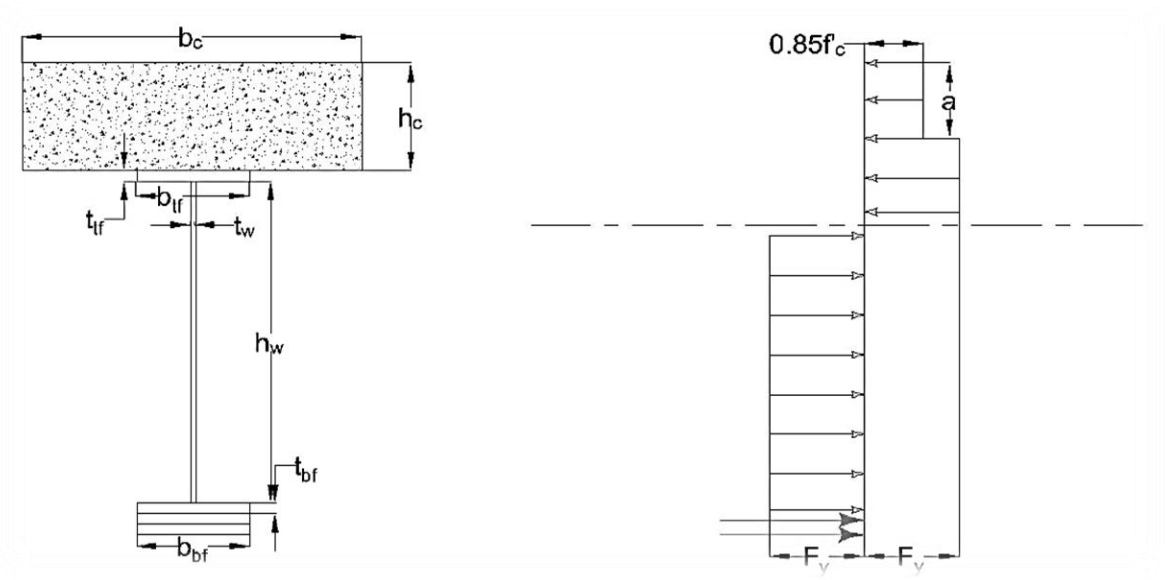

Figure 3- 4 composite beam concrete and steel built up I section with double cover plate at bottom flange

Table 3.1 Specimens Matrix-Traditional Composite mode details

No.	Gr.	Var.	Code	Fc'	fy_f	fy_w	t_{tf}	t_{bf}	t_w	b_c	h_c	b_{tf}	b_{bf}	h_w
1	1	fc'	C-Is-1	35	420	345	20	20	8	600	200	200	200	600
2			C-Is-2	45	420	345	20	20	8	600	200	200	200	600
3			C-Is-3	55	420	345	20	20	8	600	200	200	200	600
4	2	fy_f	C-Is-4	35	275	345	20	20	8	600	200	200	200	600
5			C-Is-5	35	420	345	20	20	8	600	200	200	200	600
6			C-Is-6	35	575	345	20	20	8	600	200	200	200	600
7	3	fy_w	C-Is-7	35	420	275	20	20	8	600	200	200	200	600
8			C-Is-8	35	420	345	20	20	8	600	200	200	200	600
9			C-Is-9	35	420	420	20	20	8	600	200	200	200	600
10	4	t_{bf}	C-Is-10	35	420	345	20	20	8	600	200	200	200	600
11			C-Is-11	35	420	345	20	30	8	600	200	200	200	600
12			C-Is-12	35	420	345	20	40	8	600	200	200	200	600
13	5	t_w	C-Is-13	35	420	345	20	20	6	600	200	200	200	600

14			C-Is-14	35	420	345	20	20	8	600	200	200	200	600
15			C-Is-15	35	420	345	20	20	10	600	200	200	200	600
16	6	b_c	C-Is-16	35	420	345	20	20	8	200	200	200	200	600
17			C-Is-17	35	420	345	20	20	8	400	200	200	200	600
18			C-Is-18	35	420	345	20	20	8	600	200	200	200	600
19	7	b_{bf}	C-Is-19	35	420	345	20	20	8	600	200	200	200	600
20			C-Is-20	35	420	345	20	20	8	600	200	200	300	600
21			C-Is-21	35	420	345	20	20	8	600	200	200	400	600
22	8	h_w	C-Is-22	35	420	345	20	20	8	600	200	200	200	600
23			C-Is-23	35	420	345	20	20	8	600	200	200	200	700
24			C-Is-24	35	420	345	20	20	8	600	200	200	200	800

3.6.2 Mode 2

Description: steel built up section with web opening located in the steel web to make full connection with concrete deck reinforced with minimum reinforcement for shrinkage

Aim: upgrading section capacity for dominated depth

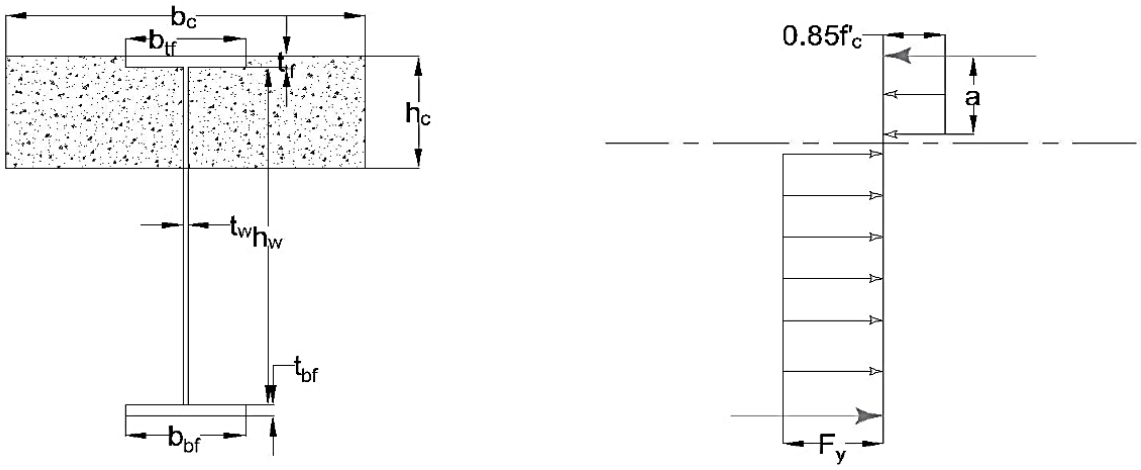

Figure 3. 5 Composite section of merged concrete-steel compressive region

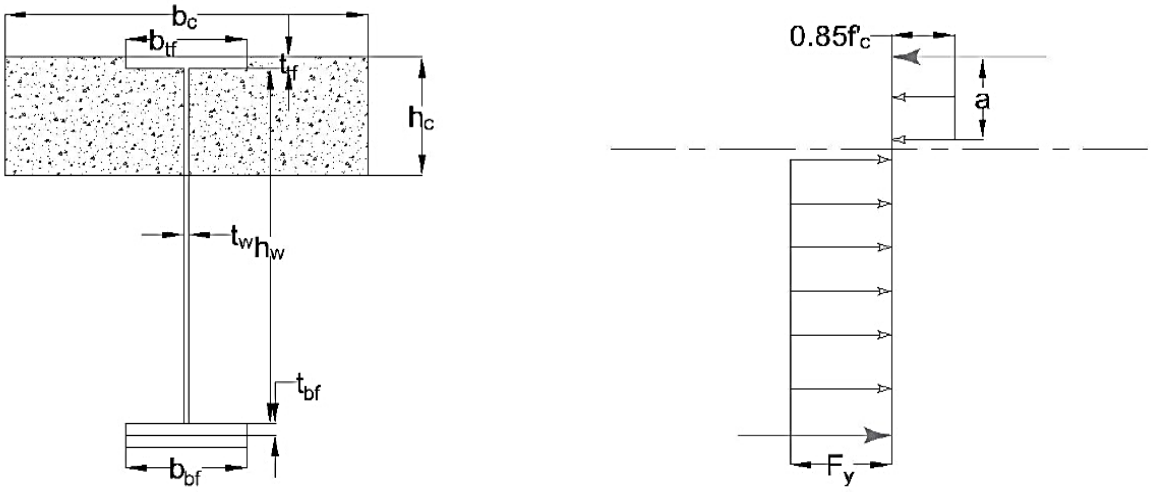

Figure 3. 6 Composite section of merged concrete-steel compressive region with cover plate at bottom flange

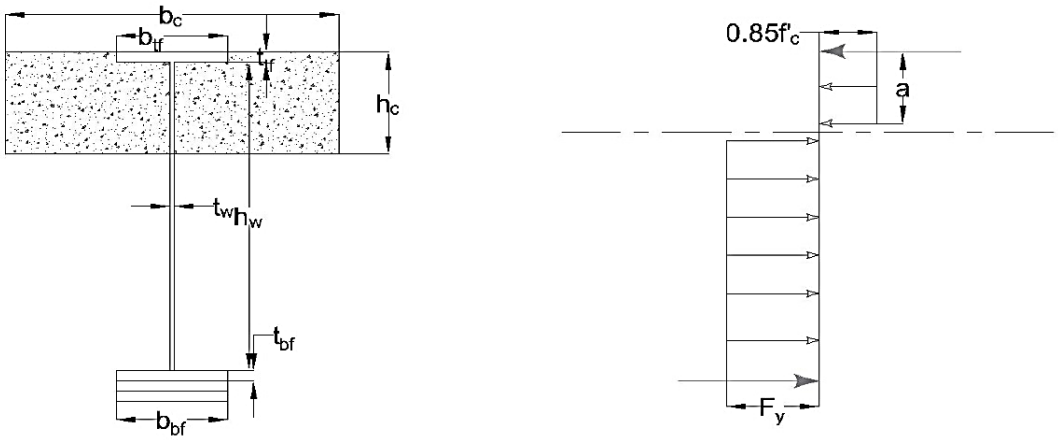

Figure 3. 7 Composite section of merged concrete-steel compressive region with double cover plate at bottom flange

Table 3.2 specimen's matrix details of composite section- Mode II

No.	Var.	Code	fc'	fy_f	fy_w	t_{tf}	t_{bf}	t_w	b_c	h_c	b_{tf}	b_{bf}	h_w	A_{sf}	A_{sw}
1	Bottom flange thickness	C-Is#-1	35	420	345	10	8	8	600	200	200	200	600	1600	4800
2		C-Is#-2	35	420	345	10	10	8	600	200	200	200	600	2000	4800
3		C-Is#-3	35	420	345	10	12	8	600	200	200	200	600	2400	4800
4		C-Is#-4	35	420	345	10	14	8	600	200	200	200	600	2800	4800
5		C-Is#-5	35	420	345	10	16	8	600	200	200	200	600	3200	4800
6		C-Is#-6	35	420	345	10	18	8	600	200	200	200	600	3600	4800
7		C-Is#-7	35	420	345	10	20	8	600	200	200	200	600	4000	4800
8		C-Is#-8	35	420	345	10	22	8	600	200	200	200	600	4400	4800
9		C-Is#-9	35	420	345	10	24	8	600	200	200	200	600	4800	4800
10		C-Is#-10	35	420	345	10	26	8	600	200	200	200	600	5200	4800
11		C-Is#-11	35	420	345	10	28	8	600	200	200	200	600	5600	4800
12		C-Is#-12	35	420	345	10	30	8	600	200	200	200	600	6000	4800

3.6.3 Mode 3

Description: concrete built up U shape section of intermated proposed flanged plates with minimum reinforcement for shrinkage

Aim: to turn the web compactness from slender to compact so as to utilizing the section to resist compression force for high depth section

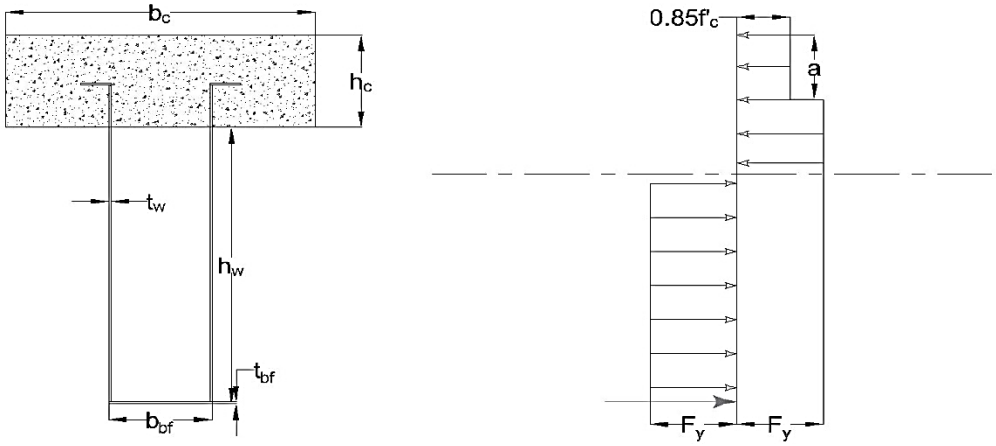

Figure 3- 8 Composite section of multi flanged U steel section

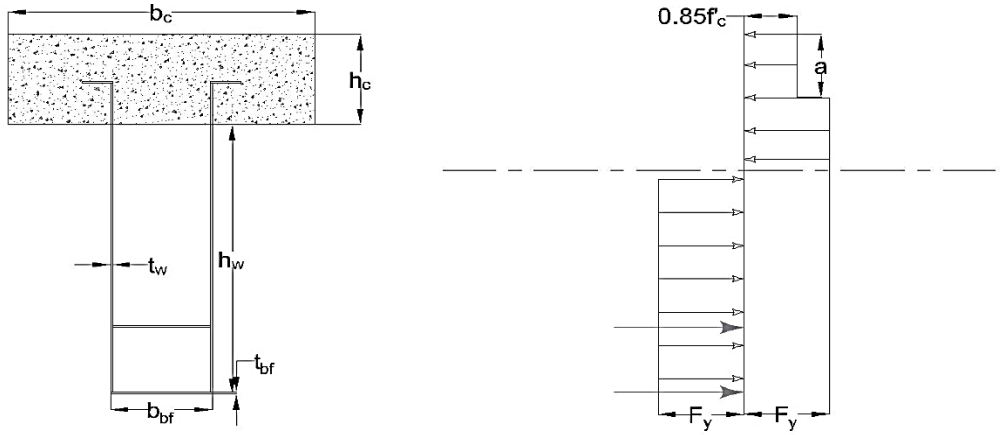

Figure 3- 9 Composite section of multi flanged U steel section with one intermediate flange

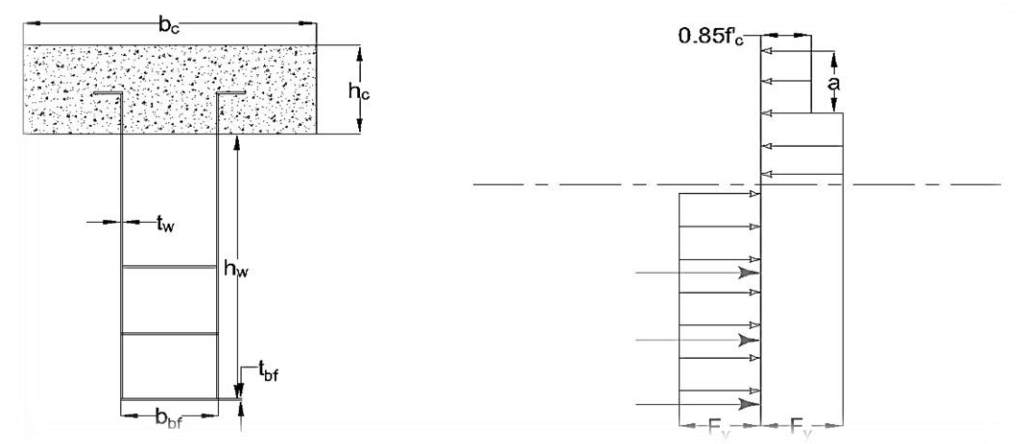

Figure 3- 10 Composite section of multi flanged U steel section with Two intermediate flange

Table 3.3 Specimens Details - ModeIII

No.	Var.	Designation	N_f	Fc'	f_{yf}	f_{yw}	t_{tf}	t_{bf}	t_w	b_c	h_c	b_{tf}	b_{bf}	h_w	A_{sf}	A_{sw}
1	Intermediate flanges numbers, Nf	C-Us-1	1	35	420	345	10	10	4	600	200	200	200	600	2000	4800
2		C-Us-2	1	35	420	345	10	20	4	600	200	200	200	600	4000	4800
3		C-Us-3	1	35	420	345	10	30	4	600	200	200	200	600	6000	4800
4		C-Us-4	2	35	420	345	10	10	4	600	200	200	200	600	2000	4800
5		C-Us-5	2	35	420	345	10	20	4	600	200	200	200	600	4000	4800
6		C-Us-6	2	35	420	345	10	30	4	600	200	200	200	600	6000	4800
7		C-Us-7	3	35	420	345	10	10	4	600	200	200	200	600	2000	4800
8		C-Us-8	3	35	420	345	10	20	4	600	200	200	200	600	4000	4800
9		C-Us-9	3	35	420	345	10	30	4	600	200	200	200	600	6000	4800

3.7 Nonlinear Finite Element Analysis of Structures

A lot of phenomenal problems in solid mechanics are nonlinear. However, in several applications, using linear formulation will be proper and practical solution to obtain an engineering solution. Otherwise, other problems may require analysis with nonlinear property if obtained realistic results such as high deflection and post-

yielding, in addition the analysis of nonlinear behavior of steel structures is required to understand the behavior of such structures [35]. Depending on nonlinear sources, the nonlinear problems involve three types [36], these types are:

a- Problems including material nonlinearity.
b- Problems including geometric nonlinearity.
c- Problems including both materials and geometric nonlinearity.

In finite element method, the complex structure is first divided (discretized) into a limited number of individual non-overlapping components known as 'elements' over which the variables are interpolated. These elements are connected together in number of discrete points along their periphery known as 'nodal points' or 'nodes' as revealed in Figure (3-10) [36].

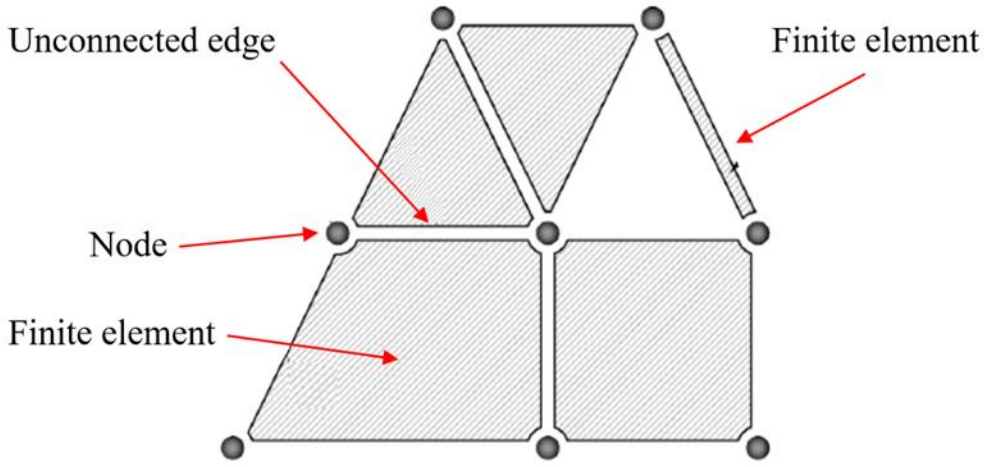

Figure 3- 11 Finite element discretization [36].

For all elements, stiffness matrix and applied load vector are calculated and then assembled to give respectively, a global stiffness matrix with global load vector for the complete structure. The resulting rhymester of simultaneous equations is solved for unknown nodal variables which for structural problems are the displacement components [36].

3.7.1 Basic Steps in Finite Element Method

Saeed Moaveni in 1999 [37], introduced basic steps for any problem used finite element analysis to provide a solution as shown below:

a) Pre-processing Phase:

1) Create and discretize the solution domain into finite elements; making the problem division into elements and node.
2) Assuming shape function to define the physical behavior of an element; that is, to provide the element solution, the approximate continuous function is supposed.
3) Develop matrices for each different element.
4) Assemble stiffness matrices of the current elements to present the whole problem and build a general stiffness matrix.
5) implement boundary conditions, initial conditions, and loading.
6) A group of linear or nonlinear algebraic equations are solved at the same time to get nodal outcomes, like displacement values or shear force, moments, or other significant outcome such as stresses and strains that can be evaluated for the nodes or the elements.

b) Solution Phase:

The resulting series algebraic equations is solved to obtain nodal results, such as displacement at different nodes.

c) Post Processing Phase:

Obtain additional important information, like the values of principal stresses, moment, shear force, etc.

3.8 Finite Element Formulation

3.8.1 Basic Finite Element Relationships

The derivation of stiffness matrix for selected element is the basic stage in any FEA, which relates $\{a\}$ the nodal displacement vector to$\{f\}$ the nodal force vector. Three conditions should be satisfied to derive this relation:

1) Compatibility of strains and displacements (kinematic condition).
2) Equations of equilibrium (equilibrium condition).
3) Stress-strain relations (constitutive relations).

By using the principle of virtual displacement, stiffness matrix of element can be determined, which states that, if the work done by the external forces on a structural system is equal to the increase in strain energy of the system for any set of tolerable virtual displacements, then the system is in equilibrium [38].

When a body is exposed to a series of exterior forces, the displacement vector at any point within the element, $\{U\}_e$, is given by,

$$\{U\}_e = [N].\{a\}_e \quad \ldots\ldots (3.31)$$

Where, [N] is a matrix for shape functions, and $\{a\}_e$ is the nodal displacements column vector. At any point the strain calculated by differentiating Eq. (3.32),

$$\{\varepsilon\}_e = [L].\{U\}_e \quad \ldots\ldots (3.32)$$

Where, $[L]$ is the differential operator matrix. In extended form, the strain vector can be termed as,

$$\{\varepsilon\}_e = \begin{Bmatrix} \varepsilon_x \\ \varepsilon_y \\ \varepsilon_z \\ \gamma_{xy} \\ \gamma_{yz} \\ \gamma_{xz} \end{Bmatrix} = \begin{Bmatrix} \frac{\partial u}{\partial x} \\ \frac{\partial v}{\partial y} \\ \frac{\partial w}{\partial z} \\ \frac{\partial u}{\partial y} + \frac{\partial v}{\partial x} \\ \frac{\partial v}{\partial z} + \frac{\partial w}{\partial y} \\ \frac{\partial w}{\partial x} + \frac{\partial u}{\partial z} \end{Bmatrix} \quad \ldots\ldots (3.33)$$

Substitution of Eq. (3.32) into Eq. (3.32) gives,

$$\{\varepsilon\}_e = [B].\{a\}_e \quad \ldots\ldots (3.34)$$

where [*B*] is matrix of strain-nodal displacement, which is given by,

$$[B] = [L].[N] \quad \ldots\ldots (3.35)$$

With the strains within the element are known, the stress vector can be illustrated by using the stress-strain relationship as:

$$\{\sigma\}_e = [D].\{\varepsilon\}_e \quad \ldots\ldots (3.36)$$

where [*D*] is the constitutive matrix and $\{\sigma\}_e$ is:

$$\{\sigma\}_e = [\sigma_x\ \sigma_y\ \sigma_z\ \tau_{xy}\ \tau_{yz}\ \tau_{xz}]^T \quad \ldots\ldots (3.37)$$

From Eq. (3.34) and (3.36), the stress-nodal displacement relationship can be displayed as,

$$\{\sigma\}_e = [D].[B].\{a\}_e \quad \ldots\ldots (3.38)$$

To depict the force-displacement relationship, a principle of virtual displacement is utilized. If a random virtual nodal displacement, $\{a^*\}_e$, is executed, the external work, W_{ext}, will be the same to the internal work, W_{int} ,

$$W_{ext} = W_{int} \quad \ldots\ldots (3.39)$$

in which

$$W_{ext} = \{a^*\}_e^T . \{f\}_e \quad \ldots\ldots (3.40)$$

and

$$W_{int} = \int_e \{\varepsilon^*\}_e^T . \{\sigma\}_e . dv \quad \ldots\ldots (3.41)$$

where $\{f\}_e$ is the vector of nodal force. Substitution of Eq. (3.34) into Eq. (3.41), yields,

$$W_{int} = \{a^*\}_e^T . \int_v [B]^T . \{\sigma\}_e . dv \quad \ldots\ldots (3\text{-}42)$$

From Eq. (3.37) and (3.42),

$$W_{int} = \{a^*\}_e^T . \int_v [B]^T . [D] . [B] . dv . \{a\}_e \quad \ldots\ldots (3.43)$$

Then Eq. (3.39) can be written as,

$$\{a^*\}_e^T . \{f\}_e = \{a^*\}_e^T . \int_v [B]^T . [D] . [B] . dv . \{a\}_e \quad \ldots\ldots (3.44)$$

or,

$$\{f\}_e = \int_v [B]^T . [D] . [B] . dv . \{a\}_e \quad \ldots\ldots (3.45)$$

letting:

$$[K]_e = \int_v [B]^T . [D] . [B] . dv . \quad \ldots\ldots (3.46)$$

then

$$\{f\}_e = [K]_e.\{a\}_e \qquad \ldots\ldots (3.47)$$

where, $[K]_e$ is stiffness matrix for an element.

The comprehensive stiffness matrix, $[K]$, can be achieved by direct addition of the elements stiffness matrices after transforming from the local to the global coordinates, therefore,

$$[K] = \sum_n \int_v [B]^T.[D].[B].dv \qquad \ldots\ldots (3.48)$$

$\{f\}$, the vector of total external force is then,

$$\{f\} = [K].\{a\} \qquad \ldots\ldots (3.49)$$

where, $\{a\}$ is the vector of unknown nodal point displacement.

3.8.2 Strain-Displacement Matrix

At any point in the brick element (8 nodes) the strain vector is relating to the nodal displacements vector by Eq. (3.33), which may be written in this form as:

$$\begin{Bmatrix} \varepsilon_x \\ \varepsilon_y \\ \varepsilon_z \\ \gamma_{xy} \\ \gamma_{yz} \\ \gamma_{zx} \end{Bmatrix} = \sum_{i=1}^{8} \begin{bmatrix} \frac{\partial N_i}{\partial x} & 0 & 0 \\ 0 & \frac{\partial N_i}{\partial y} & 0 \\ 0 & 0 & \frac{\partial N_i}{\partial z} \\ \frac{\partial N_i}{\partial y} & \frac{\partial N_i}{\partial x} & 0 \\ 0 & \frac{\partial N_i}{\partial z} & \frac{\partial N_i}{\partial y} \\ \frac{\partial N_i}{\partial z} & 0 & \frac{\partial N_i}{\partial x} \end{bmatrix} \begin{Bmatrix} u_i \\ v_i \\ w_i \end{Bmatrix} \qquad \ldots\ldots (3.45)$$

where, the 6x3 matrix is the strain-displacement matrix$[B]$, which includes the global shape functions derivatives, N_i.

Since the shape function are explained in term of local coordinate, then a rapport between the shape functions derivatives in the two coordinate systems must be defined. This relationship can be existing by using the chain rule as follows:

$$\begin{aligned}\frac{\partial N_i}{\partial s} &= \frac{\partial N_i}{\partial x}\cdot\frac{\partial x}{\partial s}+\frac{\partial N_i}{\partial y}\cdot\frac{\partial y}{\partial s}+\frac{\partial N_i}{\partial z}\cdot\frac{\partial z}{\partial s}\\ \frac{\partial N_i}{\partial t} &= \frac{\partial N_i}{\partial x}\cdot\frac{\partial x}{\partial t}+\frac{\partial N_i}{\partial y}\cdot\frac{\partial y}{\partial t}+\frac{\partial N_i}{\partial z}\cdot\frac{\partial z}{\partial t}\\ \frac{\partial N_i}{\partial r} &= \frac{\partial N_i}{\partial x}\cdot\frac{\partial x}{\partial r}+\frac{\partial N_i}{\partial y}\cdot\frac{\partial y}{\partial r}+\frac{\partial N_i}{\partial z}\cdot\frac{\partial z}{\partial r}\end{aligned} \quad \ldots\ldots (3.51)$$

In matrix form, Eq. (3.51) can be expressed as,

$$\begin{Bmatrix}\frac{\partial N_i}{\partial s}\\ \frac{\partial N_i}{\partial t}\\ \frac{\partial N_i}{\partial r}\end{Bmatrix}=\begin{bmatrix}\frac{\partial x}{\partial s} & \frac{\partial y}{\partial s} & \frac{\partial z}{\partial s}\\ \frac{\partial x}{\partial t} & \frac{\partial y}{\partial t} & \frac{\partial z}{\partial t}\\ \frac{\partial x}{\partial r} & \frac{\partial y}{\partial r} & \frac{\partial z}{\partial r}\end{bmatrix}\begin{Bmatrix}\frac{\partial N_i}{\partial x}\\ \frac{\partial N_i}{\partial y}\\ \frac{\partial N_i}{\partial z}\end{Bmatrix} \quad \ldots\ldots (3.52)$$

The Jacobian matrix [*J*] is the 3x3 matrix, therefore,

$$\begin{Bmatrix}\frac{\partial N_i}{\partial s}\\ \frac{\partial N_i}{\partial t}\\ \frac{\partial N_i}{\partial r}\end{Bmatrix}=[J]\begin{Bmatrix}\frac{\partial N_i}{\partial x}\\ \frac{\partial N_i}{\partial y}\\ \frac{\partial N_i}{\partial z}\end{Bmatrix} \quad \ldots\ldots (3.53)$$

The shape functions are utilized to define the element geometry for the iso-parametric element. Therefore, the Cartesian coordinates of any point within the element are given by,

$$x(s,t,r) = \sum_{i=1}^{8} N_i(s,t,r) \cdot x_i$$
$$y(s,t,r) = \sum_{i=1}^{8} N_i(s,t,r) \cdot y_i \quad \ldots\ldots (3.54)$$
$$z(s,t,r) = \sum_{i=1}^{8} N_i(s,t,r) \cdot z_i$$

where, x_i, y_i and z_i are the global coordinates of node i.

Making use of Eq. (3.45), the Jacobian matrix can be written as,

$$[J]=\begin{bmatrix} \sum_{i=1}^{8} \frac{\partial N_i}{\partial s} \partial x_i & \sum_{i=1}^{8} \frac{\partial N_i}{\partial s} \partial y_i & \sum_{i=1}^{8} \frac{\partial N_i}{\partial s} \partial z_i \\ \sum_{i=1}^{8} \frac{\partial N_i}{\partial t} \partial x_i & \sum_{i=1}^{8} \frac{\partial N_i}{\partial t} \partial y_i & \sum_{i=1}^{8} \frac{\partial N_i}{\partial t} \partial z_i \\ \sum_{i=1}^{8} \frac{\partial N_i}{\partial r} \partial x_i & \sum_{i=1}^{8} \frac{\partial N_i}{\partial r} \partial y_i & \sum_{i=1}^{8} \frac{\partial N_i}{\partial r} \partial z_i \end{bmatrix} \quad \ldots\ldots (3.55)$$

By inverting the Jacobian matrix, the global derivatives of the shape functions can be attained;

$$\begin{Bmatrix} \frac{\partial N_i}{\partial x} \\ \frac{\partial N_i}{\partial y} \\ \frac{\partial N_i}{\partial z} \end{Bmatrix} = [J]^{-1} \begin{Bmatrix} \frac{\partial N_i}{\partial s} \\ \frac{\partial N_i}{\partial t} \\ \frac{\partial N_i}{\partial r} \end{Bmatrix} \quad \ldots\ldots (3.56)$$

3.8.3 Element Stiffness Matrix

The stiffness matrix for an element as given in Eq. (3.46) can be written as [38]:

$$[K]_e = \iiint_v [B]^T.[D].[B].dv \quad \ldots\ldots (3.57)$$

in which dv represents the volume of the element in the global coordinates and can be expressed as:

$$dv = dx.dy.dz \quad \ldots\ldots (3.58)$$

In local coordinates it can be written as:

$$dv = |J|.ds.dt.dr \quad \ldots\ldots (3.59)$$

where, $|J|$ is the determinate of the Jacobian matrix.

Substituting Eq. (3.37) into Eq. (3.38), the element stiffness matrix is then given by,

$$[K]_e = \int_{-1}^{+1}\int_{-1}^{+1}\int_{-1}^{+1}[B]^T.[D].[B].|J|.ds.dt.dr \quad \ldots\ldots (3.60)$$

3.9 Material Modeling

3.9.1 Concrete Modeling

A. Plasticity Approach

There are many constituent models which have been established to evaluate the concrete response under different stress states. Some of the main constitutive models are the elasticity-based models and the plasticity-based model. The plasticity-based model is relying in this work, which provides a mathematical relationship that describes the elasto-plastic response of materials. ANSYS provides several options to characterize different kinds of material behavior, such as bilinear isotropic (with work hardening) and multi-linear isotropic hardening. For concrete, the concrete crushing in compression algorithm is similar to a plasticity law [39]. This algorithm is similar to a multilinear work hardening uniaxial stress-strain relationship based on rate independent Von-Mises yielding criterion. Rate independent plasticity constitutes an irreversible straining that occurs in a material once the yield surface is reached. The yield term which means that value of stress that causing yield to the material, while, the rule of flow after the yield point determines the plastic straining

direction. The hardening rule defines the changes in yield surface with gradually changing in yield. Even though this approach represents the behavior in the strain hardening region, the softening in the curve can't be defined adequately by the hardening plasticity theory after the point of peak stress [40].

B. Material Nonlinearity

This nonlinearity arise due to time independent behavior, like plasticity, and behavior of time dependent behavior like creep and viscoelastic / viscoplastic behavior. Stress-strain relationship is the prime feature that explains the material behavior. A nonlinear structural behavior is caused by the nonlinearity of the stress-strain curve of the material. Varied factors can affect the material's stress-strain properties, such as load history, environmental circumstances, and the needed time to apply loads. A variation in nonlinear material behavior models are offered in ANSYS program, including plasticity, creep, nonlinear elastic, viscoelasticity, and hyper elasticity [39]. Figure (3-11) shows a typical non-linearity of concrete stress-strain curve.

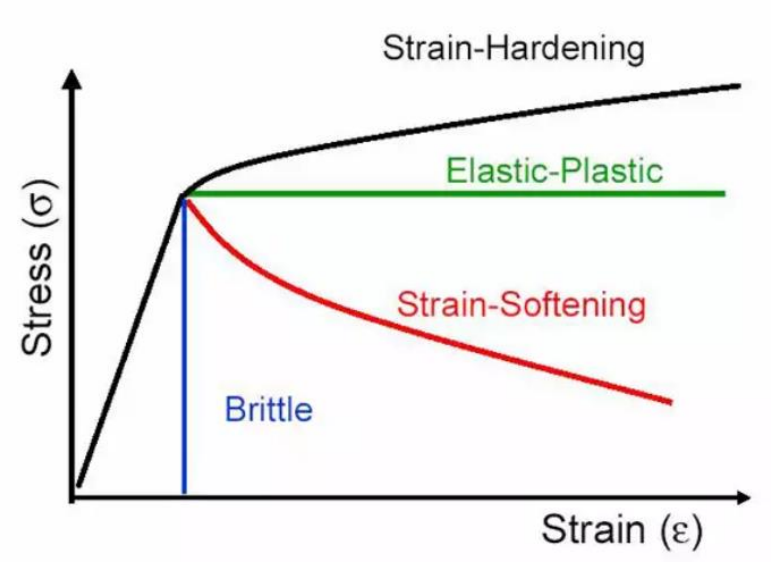

Figure 3- 12 Non-Linear Material Response [39].

C. Multilinear Stress-Strain Relationship

A typical stress-strain behavior for concrete exposed to uniaxial compression is illustrated in Figure (3-12). It is approximately linear up to about (0.3-0.5) times the ultimate strength of concrete $\left(f_c^{'}\right)$ [41]. stress-strain curve explains a progressive increase in bend that occurs up to level of stress of $\left(0.75\ f_c^{'}\right) to \left(0.9\ f_c^{'}\right)$, after which the stress-strain curve bends pointedly and oncoming to the summit point at $\left(f_c^{'}\right)$. Then, the stress-strain curve descends until failure occurs because of the concrete crushing. High strength concrete (HSC) behaver is linear with higher stress than the normal strength concrete (NSC). The strain at the maximum stress is approximately (0.003) (although high strength concretes have somewhat a little higher strain at peak stresses). On the descending portion of the stress-strain curve, higher strength concrete tends to behave in more brittle manner, with the fast stress dropping more than NSC as exhibited in Figure (3-12) [41].

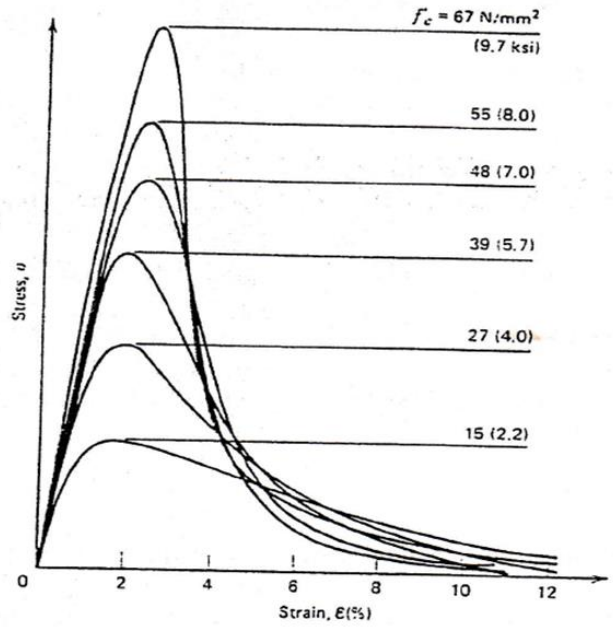

Figure 3- 13 Uniaxial compressive strain curve for concrete with different strength [41].

Young modulus for concrete (E_c) is a function in term of compressive strength ($f_c^{'}$). For normal strength concrete, the empirical equation found in the ACI 318M-11 [34] is used ,

$$E_c = 4700\sqrt{f_c'}\ , \qquad (MPa) \qquad \ldots\ldots (3.61)$$

For high strength concrete, Hsu and Hsu [42] reported values for the modulus of elasticity,

$$E_c = 124.31 f_c' + 22653\ , \qquad (MPa) \qquad \ldots\ldots\ (3.62)$$

Where, (E_c) is the slope of stress-strain curve of concrete in (MPa), which equal to dividing the stress over strain.

The Poisson's ratio for concrete subjected to uniaxial compression ranges between (0.15 to 0.22). In current investigation a value of (0.2) is selected for analyzing RC beams [43-45].

In ANSYS, the concrete behavior for uniaxial compression is defined by a piece-wise linear stress-strain curve, starting from the origin, and increases with positive values for stresses and strains. The slope of the first segment of the curve corresponds to the elastic modulus of the material and other segments have slopes less than first segment slope.

The idealized uniaxial stress-strain sketch for concrete specimen can be get by using the following equations for numeration the multilinear isotropic stress-strain values for the concrete as shown in Figure (3-13) [46] as follows:

$$f_c = \varepsilon\ E_c \qquad for \qquad 0 \le \varepsilon \le \varepsilon_1 \qquad \ldots\ldots (3.63)$$

$$f_c = \frac{\varepsilon E_c}{1+\left(\frac{\varepsilon}{\varepsilon_\circ}\right)^2} \qquad for \qquad \varepsilon_1 \le \varepsilon \le \varepsilon_\circ \qquad \text{. . . . . (3.64)}$$

$$f_c = f_c^{'} \qquad for \qquad \varepsilon_\circ \le \varepsilon \le \varepsilon_{cu} \qquad \text{……(3.65)}$$

$$\varepsilon_1 = \frac{0.3 f_c^{'}}{E_c} \text{ (Hooke's law)} \qquad \text{……(3.66)}$$

$$\varepsilon_\circ = \frac{2 f_c^{'}}{E_c} \qquad \text{……(3.67)}$$

Where;

$f'c$ = stress at any strain ε, MPa

ε = strain at stress f

ε_o =strain at ultimate compressive stress $f'c$ and,

E_c = concrete elastic modulus, MPa.

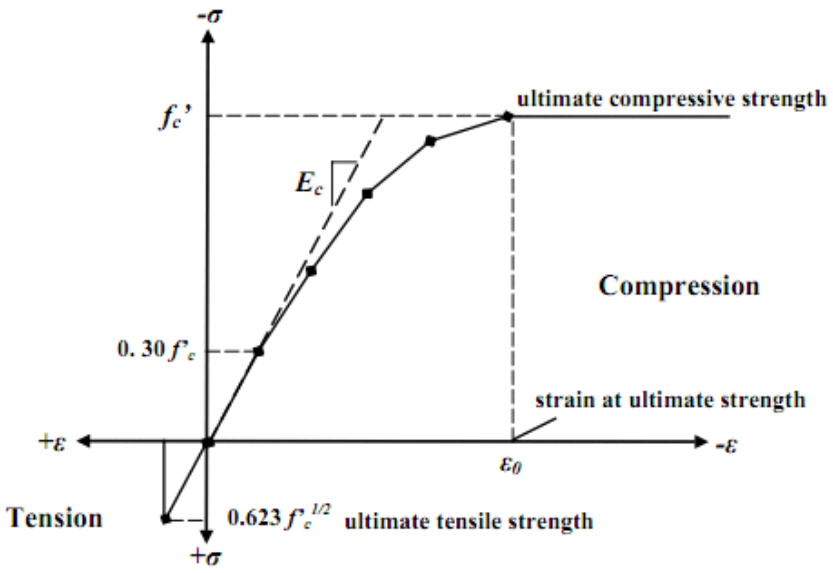

Figure 3- 14 Simplified stress strain for NSC. [34]

For HSC, stress-strain equation is used

$$f_c = f_c' \frac{n\,\beta\,(\varepsilon/\varepsilon_o)}{n\,\beta - 1 + (\varepsilon/\varepsilon_o)^{n\,\beta}} \quad \ldots\ldots (3.68)$$

$$\beta = \left(\frac{f_c'}{65.23}\right)^3 + 2.59 \quad \ldots\ldots (3.69)$$

$$\varepsilon_o = 1.29 \times 10^{-5} f_c' + 2.114 \times 10^{-3} \quad \ldots\ldots (3.70)$$

Where, f_c is the stress at any strain ε in (MPa).

f_c' is the ultimate compressive strength at strain ε_o in (MPa).

n is a parameter that depends on material strength , n=1 for $0 < \varepsilon < \varepsilon_o$.

β is a parameter that depends on the shape of the stress-strain curve.

The ascending branch of stress-strain curve for HSC is more linear and steeper and the strain at maximum strength is greater. This is because HSC is more homogenous than NSC and has less internal micro cracking for the same axial strain imposed, that becomes active only at a high load. After the maximum strength is reached, the descending branch of the curve gets steeper and drops suddenly for HSC due to the brittle failure of HSC, this behavior results because the broken surface initiates through the aggregate particles because of the greater matrix strength and this leads to form a much smoother cracked surface, thus sudden failure happens [46] as shown below.

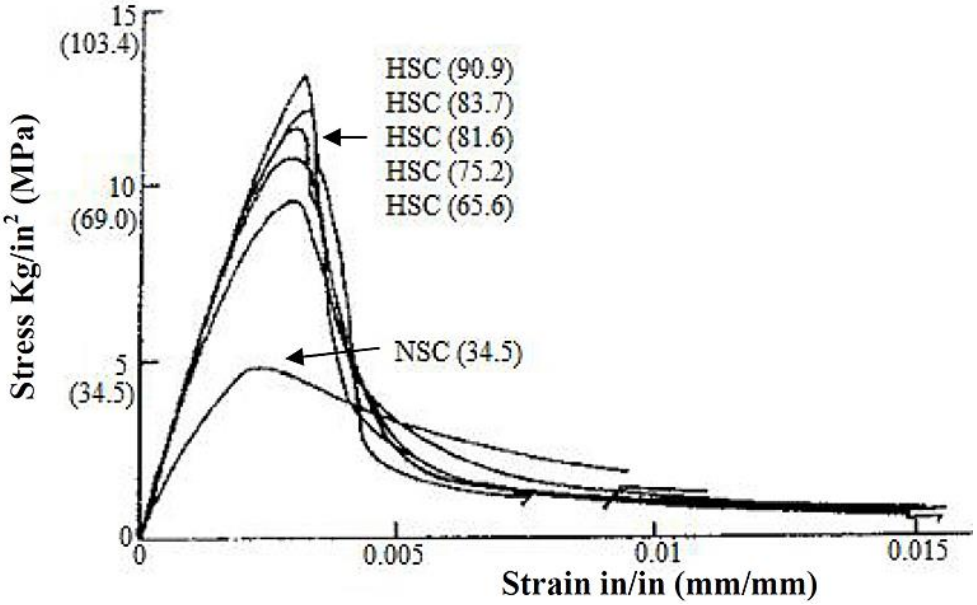

Figure 3.15 Stress-Strain Curve of HSC in Compression [46].

As revealed in Figure (3-15) When the volumetric strain ($\varepsilon_v = \varepsilon_1 + \varepsilon_2 + \varepsilon_3$) is found initially to be almost linear up to about to (here1, 2, 3 are subscripts representing direction of principal stresses and strains). At this point, the direction (or sign) of the volumetric strain is reversed, resulting in a volumetric expansion near or at ($f'c$). The stress corresponding to the minimal value of volumetric strain beyond which no further reduction in volume occur is termed critical stress [47].

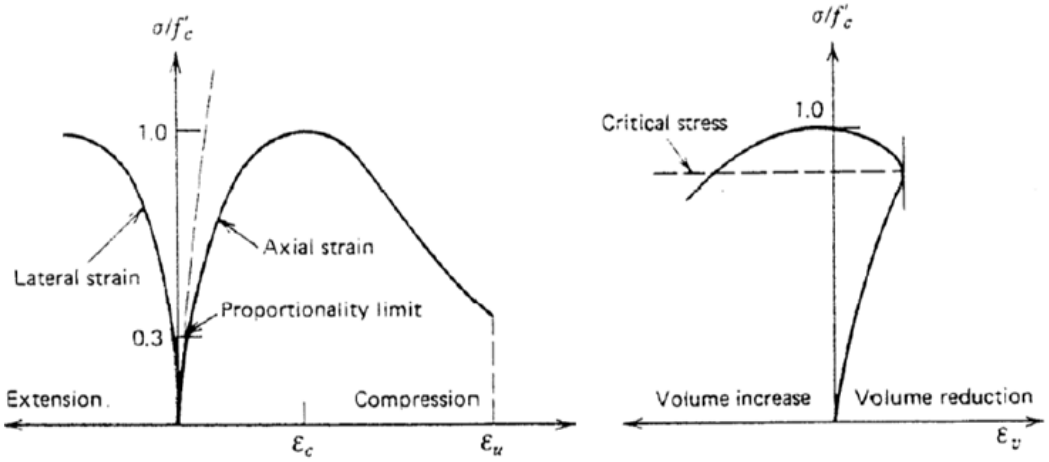

Figure 3.16 Typical stress-strain curves for concrete in uniaxial compression test (a)Axial and lateral strains. (b) Volumetric strain (εv= ε1+ ε2+ ε3) [47].

In the nearness of maximum stresses concrete subjecting to compression reveals inelastic volume increase. This phenomenon, termed as volume dilatancy, is usually attributed to the gradual micro cracking in concrete during loading, as explained in Figure (3-16) [47].

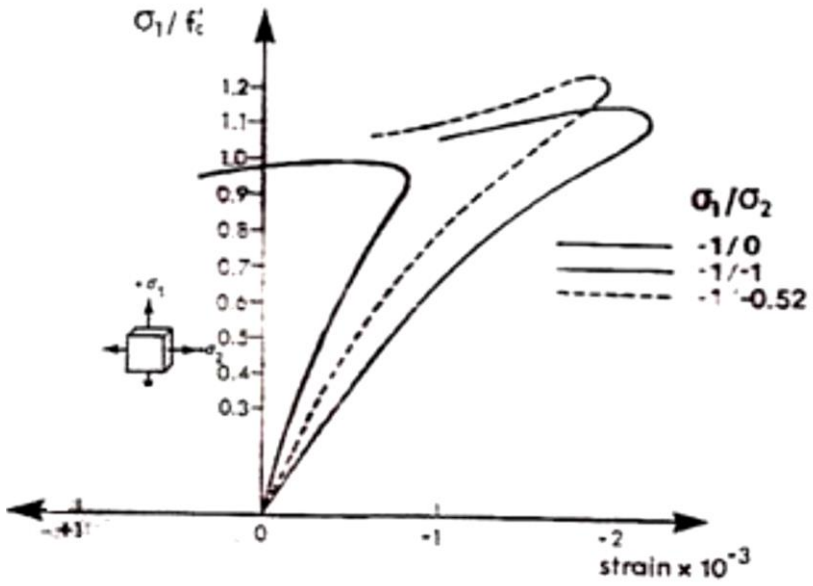

Figure 3.17 Stress-volumetric strain curves [47].

C.1 Tensile Behavior of Concrete

The general concrete behavior under uniaxial tensile loading is similar to an extent the behavior observed in uniaxial compression. The crack propagation direction for uniaxial tension is normal to the stress direction. A decrement in the available load-stress capacity due to growth of every new crack and this reduction will be the reason of an increasing in the stresses at critical crack tips. The failing in tension occurs because a few connected cracks instead of numerous cracks, as it is for compressive states of stress. The ratio between uniaxial tensile strength (f_t) and compressive strength (f_c') may vary significantly but regularly ranges from (8-12)%. The modulus of elasticity under uniaxial tension is fairly higher and Poisson's ratio

somewhat lower than in uniaxial compression [47]. The direct tensile strength of concrete is problematic to measure and is normally taken as $\left[(0.3)\,to\left(0.4\sqrt{f_c'}\right)\right]$. Usually, either the modulus of rupture (f_r) or the split cylinder strength (f_t) is utilized to estimate the tensile strength of concrete. The value of the modulus of rupture of concrete differs quite extensively but is normally taken as $\left(0.62\sqrt{f_c'}\right)$. The split cylinder tensile strength is usually somewhat lower, at approximately $\left[(0.45)\,to\left(0.55\sqrt{f_c'}\right)\right]$ in (MPa) [47]. The behavior of HSC exposed to uniaxial tension was studied by Li and Ansari (2000) [48] which was an experimental investigation consisted of testing (NSC) with *f'c* values ranged from (41 to 103) MPa. Typical stress-deformation responses of the NSC and HSC in tension are explained in Figure (3-17).

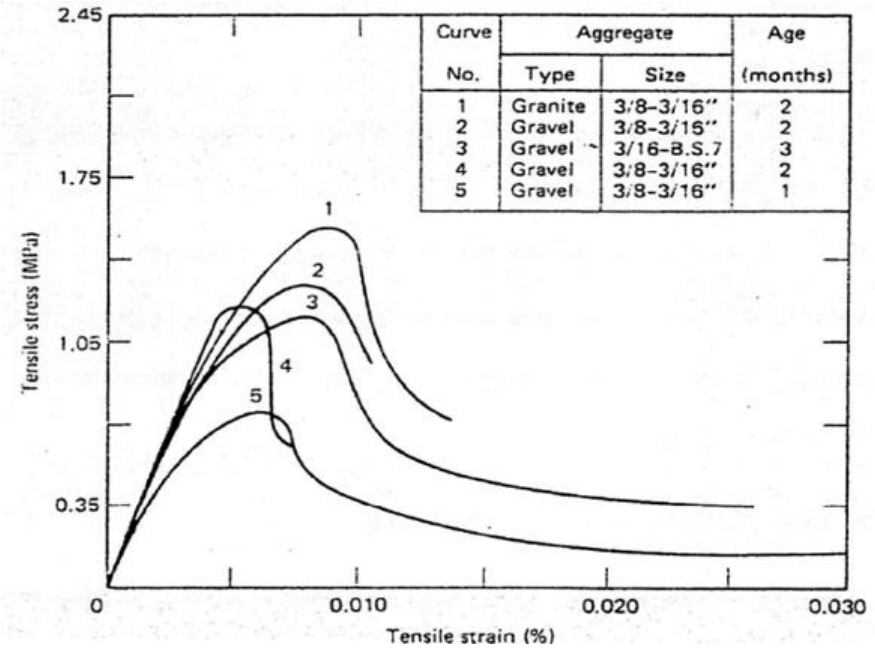

(a) Stress-strain relationship for NSC.

Figure 3- 18 Typical tensile stress-strain curve for concrete [47].

D. Post - Cracking Model (Tension Stiffening Model)

Upon cracking, the stresses normal to cracked plane are released as the cracks propagate. To simulate this behavior in connection with the FE designing of RC beams, a tension stiffening concept is usually used [48]. This concept is based on fact that some of the tensile stresses can be carried by the concrete among the cracks because of bond action between the steel bars and the surrounding concrete. This capability is gradually weakened because of the emergence of new cracks. Additionally, to expand the numerical stability of the solution, the influence of tension stiffening was presented in several models. In the current work, the tension stiffening of RC after cracking was characterized by providing a linearly descending branch as revealed in Figure (3-18). This model is given by:

(a) For $\varepsilon_{cr} \le \varepsilon_n \le \alpha_1 \varepsilon_{cr}$

$$f_n = \left(\frac{\alpha_2 \ f_{cr}}{\alpha_1 - 1} \right) \left(\alpha_1 - \frac{\varepsilon}{\varepsilon_{cr}} \right) \qquad \ldots\ldots (3.71)$$

(b) For $\varepsilon_n \ge \alpha_1 \varepsilon_{cr}$

$$f_n = 0 \qquad \ldots\ldots (3.72)$$

where, (f_n, ε_n) is the stress and strain normal to the crack plane,

$(f_{cr}, \varepsilon_{cr})$ is the cracking stress and strain,

(α_1) is the rate of stress released as the crack widens

(α_2) is the sudden loss of stress at the instant of cracking

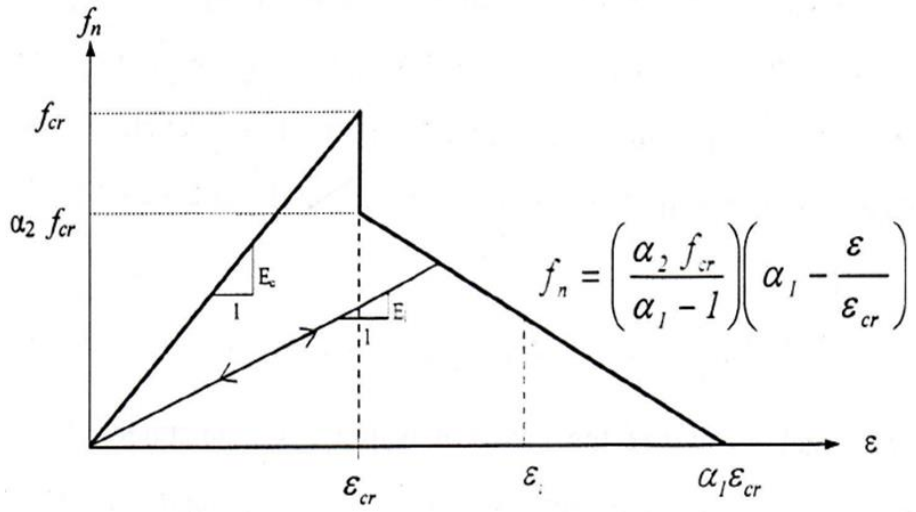

Figure (3-18): Pre and post-cracking behavior of normal strength concrete [48].

E. Failure criteria for concrete

The actual behavior and strength of concrete materials are very complex because they depend on many factors like the mechanical and physical properties of the aggregate, cement paste and loading nature. No single mathematical model can describe the strength of real concrete materials completely under all conditions, so, simple models or criteria are utilized to represent the properties that are essential to the problem being considered [45].

Willam and Warnke, [49] developed a mathematical model able to inspect failure for concrete materials under multiaxial stress state.

Both cracking mode and crushing failure are accounted for. This model is modelled by usage of these equations:

$$\frac{F}{f_c'} - S \geq 0 \qquad \ldots\ldots (3.73)$$

where, (F) is the function of principal state $(\sigma_{xp}, \sigma_{yp}, \sigma_{zp})$, (S) is the failure surface defined in term of principal stresses with five input parameters

$(f_c', f_t, f_{cb}, f_1 \text{ and } f_2)$, (f_c') is the peak uniaxial compressive strength, (f_t) is the peak uniaxial tensile strength, (f_{cb}) is the crucial biaxial compressive strength, (f_1) is the peak compressive strength for a case of biaxial compression superimposed on hydrostatic stress state (σ_h^a), (f_2) is the crucial compressive strength for a state of uniaxial compression superimposed on hydrostatic stress state (σ_h^a), and (σ_h^a) is the ambient hydrostatic stress state [45].

Failure surface is discrete into hydrostatic (volume changing) and deviatoric (shape changing) sections as shown in Figure (3-10). The hydrostatic section forms a meridional plane which contains the equisectrix $(\sigma_1 = \sigma_2 = \sigma_3)$ as an axis of revolution. The deviatoric section located in normal plane to the equisectrix (intermittent line). Defining the deviatoric trace is done by polar coordinate (r, θ) where (r) is the position vector locating the failure surface with angle (θ). The failure surface is defined as:

$$f(\sigma_m, \tau_m, \theta) = \frac{1}{2}\frac{\sigma_m}{f_c'} + \frac{1}{r(\theta)}\frac{\tau_m}{f_c'} - 1 = 0 \qquad \ldots\ldots (3.74)$$

where, $(\sigma_m \text{ and } \tau_m)$ is the average stress components defined as:

$$\sigma_m = \frac{1}{3}(\sigma_1 + \sigma_2 + \sigma_3) = \frac{1}{3} I_1 \qquad \ldots\ldots (3.75)$$

$$\tau_m^2 = \frac{2}{5} J_2 \qquad \ldots\ldots (3.76)$$

where, (I_1) is the first stress invariant, (J_2) is the second deviatoric stress invariant and (ρ) is the apex of the surface.

The free parameters of failure surface (ρ) and (r) are identified from the uniaxial compressive strength(f_c'), biaxial compressive strength (f_{cb}) and uniaxial tensile strength(f_t). If Eq. (3.44) is not satisfied, there is no attendant cracking or crushing. in another way, cracks will develop in material if any principal stress is tensile, while crushing will happen if all main stresses are compressive.

Willam and Warnke [49] succeeded in finding an expression for a failure cross section, since it can meet not only the conditions of symmetry, smoothness and convexity, but also it degenerates to circle if $(r_1 = r_2)$. This means that the cylindrical Von Mises model and the conical Drucker-Prager model are all special cases of Wiliam and Warnke failure formulation [50].

The failure surface can be indicated with a total of five strength parameters $(f_c', f_t, f_{cb}, f_1 \text{ and } f_2)$ in addition to an ambient hydrostatic stress state(σ_h^a), as exhibited in Figure (3-10). (f_c') and (f_t) can be specified from two simple tests, and the other constants can be determined from Willam and Warnke [49]:

$$f_{cb} = 1.2\, f_c' \quad \ldots\ldots (3.77)$$

$$f_1 = 1.45\, f_c' \quad \ldots\ldots (3.78)$$

$$f_2 = 1.725\, f_c' \quad \ldots\ldots (3.79)$$

However, these values are valid only for stress states where the condition stated below is satisfied:

$$|\sigma_h| \le \sqrt{3}\, f_c' \quad \ldots\ldots (3.80)$$

where

(σ_h) is the hydrostatic stress state = $\frac{1}{3}(\sigma_{xp} + \sigma_{yp} + \sigma_{zp})$ …… (3.81)

The condition of Eq. (3.41) applies to stress situations with a low hydrostatic stress component.

Figure (3-19), the lower curve represents all stress states in which $(\theta = 0^\circ)$, while the upper curve represents stress states for $(\theta = 60^\circ)$. The axis (ξ) represents hydrostatic length.

The concrete failure is categorized into four domains, each domain consisted of three principal stresses as follows:

1st domain: $(0 \geq \sigma_1 \geq \sigma_2 \geq \sigma_3)$ (compression – compression – compression).

2nd domain: $(\sigma_1 \geq 0 \geq \sigma_2 \geq \sigma_3)$ (tension – compression – compression).

3rd domain: $(\sigma_1 \geq \sigma_2 \geq 0 \geq \sigma_3)$ (tension – tension – compression).

4th domain: $(\sigma_1 \geq \sigma_2 \geq \sigma_3 \geq 0)$ (tension – tension – tension).

The concrete will crack if any principal stress is a tensile stress, while crushing will occur if all principal stresses are compressive.

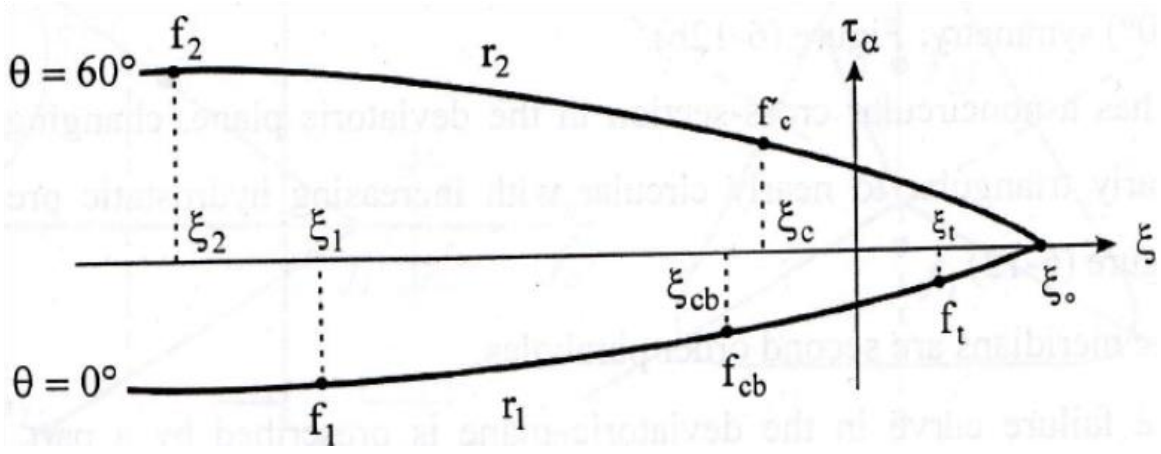

Figure 3- 19 Profile of the failure surface as function of five parameters [49] .

F. Cracking modeling

The internal stresses and deflections of RC structures are affected by cracking. This phenomenon can be modeled in FE schemes either as discrete cracking approach, or as smeared cracking approach.

In the discrete cracking approach, the disconnecting or separating of the concrete element nodes through which the cracking is passing, requires additional nodes to occupying the same location, and connected by linkage elements. This physically appealing representation has computational difficulties in that it requires node renumbering after the emergence of the cracks and there is restriction on the crack propagation direction count on mesh layout [50].

The smeared crack paradigm was presented by Rashid [51]. He represents cracks as a change in the material property of the element over which the cracks are supposed to be smeared and offers cracks generation without the redefinition of the finite element topology. In this study, smeared crack model was used.

It is supposed that concrete turn into orthotropic after cracking with zero young modulus in normal direction to the crack. Both methods are exhibited in Fig (3-20).

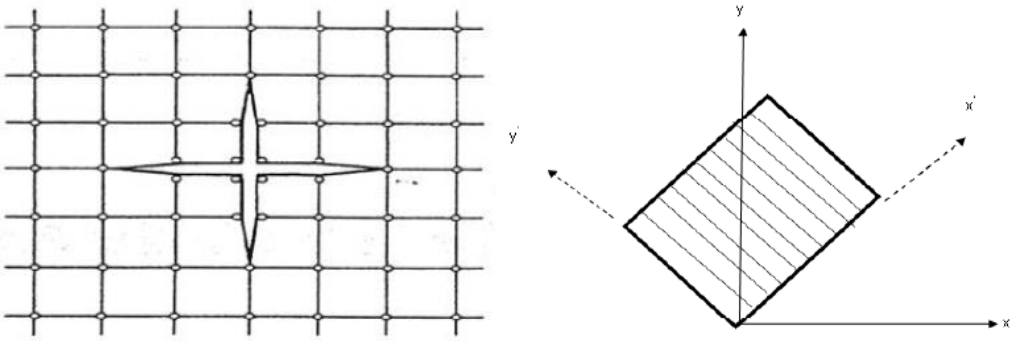

(a) 2D Discrete Crack Model. (b)Smeared Crack Model.

Figure 3- 20 Cracking Modeling [50].

G. Shear Transfer and Tensile Crack Coefficient

Concrete is supposed to behave linearly in tension up to the beginning of cracking. When concrete started to cracking, shear stiffness will reduce. However, cracked concrete can transmit shear forces partially because of aggregate interlock and property of dowel action existed in steel reinforcement. The shear transmission mechanism affected by several factors: the reinforcement ratio, bar size, bar arrangement, concrete cover depth, the concrete type and aggregate size. The coefficient of shear transfer (β) represents the circumstances of the face of the crack. βc and βt refer to the coefficients of closed and open cracks.

The value of β ranges from 0.0 to 1.0, with 0.0 representing a smooth crack (whole shear loss) and 1.0 referring to rough crack (no shear loss). There are a number of investigations for modeling RC structures with using varied values of these coefficient. From these studies, βt frequently ranges from 0.05 to 0.65, and βc varies from 0.25 to 1. Using these coefficients below 0.2 will cause a problem in convergence. a number of preliminary analyses were carried out to assess the influence of βt and βc on the model behavior [52]. In this study, βt ranged between (0.25-0.4) and βc ranged between (0.3-0.9) for different specimens.

Reduction stiffness factor for cracked tensile condition for all beams equal to 0.9 was used to define this factor. There are many research studies that used for RC structures a tensile stiffness multiplier of 0.6 to simulate an abrupt dropping in tensile stress to 60% of the rupture stress; followed by a linearly descending curve to zero stress, many researchers used values ranged among 0.45 and 0.95 for PSC beams in FE for flexural test. Depending on these studies, and taking into account the good results obtained in the numerical studies by using ANSYS considering this factor equal to 0.9 [53 & 54].

H. Crushing Modeling

If the material fails in uniaxial, biaxial, and triaxial compression at integration point, this material is supposed to crush at that point. Under this condition, material strength is supposed to have degraded to an extent such that the stiffness contribution of an element at this integration point [50].

3.9.2 Reinforcement Behavior

Since the reinforcing bars are typically long and comparatively slender, they can commonly be supposed to be capable of transmitting axial forces only. For the FE models, the uniaxial stress - strain relation for steel was idealized as a bilinear curve, representing elastic- perfect plastic behavior, Figure (3-21) explained this representation. This relation is supposed to be identical in tension and in compression. In present work, the (E_T), strain hardening modulus is presumed to be the same value of yield stress approximately for the longitudinal bar and stirrups. This value was neatly chosen to obtain convergence [55]. Poisson's ratio μ = 0.3 was utilized for the steel reinforcement.

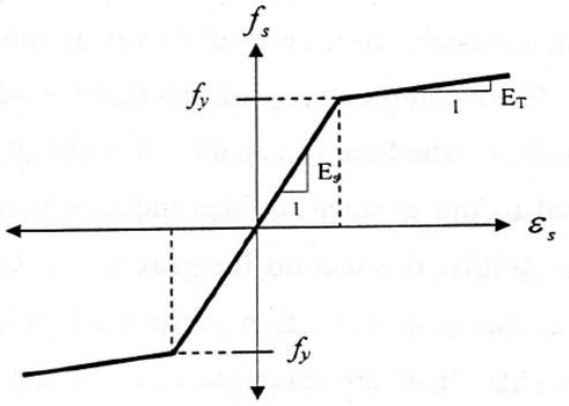

Figure 3- 21 Modeling of reinforcing bars [55].

3.10 ANSYS Computer Program

The computer program ANSYS is a sturdy and interesting engineering finite element package that may be utilized to solve a lot of problems. FEM has become a most commonly method used to study the stress, deformation, and other engineering parameters. FEM uses complicated mathematical equations to accurately approximate how the complex structure reacts to a certain load or condition. FE bundles like ANSYS solve thousands or millions of these equations to find a solution for a model. Handling all these equations as a whole be difficult and mostly impossible to solve manually. ANSYS is an inclusive general-purpose FE computer program that contains different elements implemented in the program. ANSYS has the capacity of solving linear and nonlinear problems including the influence of cracking, crushing, yielding of reinforcement, creep… etc. To use ANSYS or any another FEA software Smartly, it should that one first fully understands the underlying basic concepts and limitation of the FEM. In this work, the material parameters that must taking into consideration to investigate the RCHBs behavior that are young modulus (E_c), compressive strength $f'c$, and the tensile strength (f_t). Also, young modulus (E_s) and the yielding strength (f_y) of steel are considered. Furthermore, the geometry factors considered are the beam width, effective depth, longitudinal reinforcement area and shear reinforcement area [50].

3.11 Nonlinear Solution Techniques

The FE derivation process returns a set of simultaneous equations:

$$[K]\{U\}=\{F^a\} \quad \ldots\ldots (3.82)$$

where, $[K]$ is the stiffness matrix, $\{U\}$ is the nodal displacements vector and $\{F^a\}$ is the applied loads vector. For linear elastic problems Eq. (3.52) is untied to

calculate the solution of the unknown displacement $\{U\}$. In the case of nonlinear system, the $[K]$ stiffness matrix is a function of the unknown displacement (or their derivatives). Then the Eq. (3.51) cannot be exactly computed before determining of the unknown displacement $\{U\}$. There are three techniques for solving the nonlinear Eq. (3.52); the basic technique can be categorized into [56]:

1) An Incremental or stepwise procedure, Figure (3-22 a).
2) An iterative or Newton procedure, Figure (3-22 b).
3) An Incremental- Iterative procedure, Figure (3-22 c).

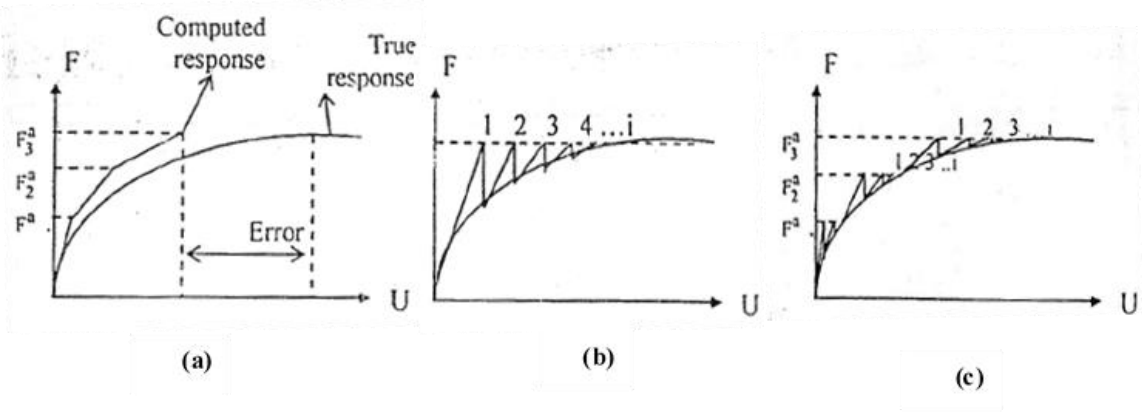

Figure 3- 22 Basic technique for solving the nonlinear equation (a) Incremental. (b) Iterative. (c) Incremental-Iterative [56].

In the incremental proceedings, the application load is changed in many small increments, and the structure is expected to react linearly during each increment with its stiffness recalculation based on geometry of the structural member and member end actions at the finish of the previous load increment. This is a simple procedure that does not require any iteration, except errors are probable to compile after many increments unless so fine increments are used, Figure (3-22a).

In the iterative procedure, all applied load is in one increment at the first iteration, the out of balance forces are then computed and used in next iteration until

the last converged solution will be in equilibrium, such that the internal load vector would equal the applied load vector or within some tolerance. This process can be written as:

$$\left[K_i^T\right]\{\Delta U_i\} = \{F^a\} - \{F^{nr}\} \quad \ldots\ldots (3.83)$$

$$\{U_{i+1}\} = \{U_i\} + \{\Delta U_i\} \quad \ldots\ldots (3.84)$$

where, $\left[K_i^T\right]$ is the stiffness matrix, (i) is the subscript representing the current equilibrium iteration and $\{F^{nr}\}$ is the internal load vector.

This procedure fails to produce information regarding the intermediate stage of loading. For structural analysis including path-dependent nonlinearities increments are in equilibrium to correctly follow the path of the applied load. This can be achieved by using the combined incremental-iterative method. In the combined-iterative procedure, a combination of an incremental and iterative scheme is utilized. The load is stratified incrementally, and iterations are performed to obtain converged solution corresponding to the stage of loading under consideration, as exhibited in Figure (3-22c).

The incremental-iterative solution procedures have been utilized in this study. Full Newton-Raphson procedure is applied. The stiffness matrix is formed at every iteration. The benefits of this procedure may give more accurate result and used to avoid the convergence problem. The procedure disadvantage is that require large effort to form and resolve the stiffness matrix [56].

3.12 Analysis Termination Criteria

In the physical examination under load control, structure collapse takes place when no further loading can be continued. This is typically indicated in the numerical

tests by successively increasing iterative displacements and a continuous growth in the dissipated energy. Hence, the iterative process convergence cannot be accomplished. A maximum number of iterations for each increment are definite to stop the nonlinear solution if the convergence limit could not achieve for this study. It has been detected that the default number about (250) of iterations is generally sufficient to predict the solution divergence and failure. number of iterations Mainly depends on the type of problem and the nature of the input, range of nonlinearities, and tolerance value. In the present work a maximum range number equal (200) is adopted for load control problems.

3.13 Convergence Criteria

The iteration is accompanying for every incremental load until convergence is attained.

The convergence criterion for any nonlinear analysis in structural problems can be categorized into [57]:

1) Force criterion.
2) Displacement criterion.
3) Stress criterion.

The displacement criterion utilized in this study. In displacement criterion, the incremental displacements at iteration (i) and the total displacements are determined. The solution is considered to be in convergence when the criteria of an incremental displacements is within a given tolerance for norm of the total displacements; infinite norm is used and takes the form:

$$\left\|\{\Delta U_i\}\right\| = \left(\max\left|\Delta U_i\right|\right) \le T_n \left(\max\left|\Delta U_i\right|\right) \quad \ldots\ldots (3.85)$$

where, U may equal u, v, w or θ_z.

For force criteria the norm of the residual forces at end of each iteration are tested versus the current applied forces norm as:

$$\|\{R\}\| = \left(\sum R_i^2\right)^{0.5} \leq T_n \left(\sum F_i^2\right)^{0.5} \quad \ldots\ldots (3.86)$$

where, $\{R\}$ is a residual vector:

$$\{R\} = \{F^a\} - \{F^{nr}\} \quad \ldots\ldots (3.87)$$

To control the convergence through an analysis of model in this work, for this process as follows:

1) Using the full new Raphson.
2) Using shear transmission coefficient βt and βc more than 0.2 .
3) Tangent modulus for steel reinforcement equal approximately to the yield stress (f_y) and input data of CFRP sheet.
4) The tolerance (T_n) is taken equal to (0.05) near the ultimate load.
5) Increasing the iteration number to 200.

3.14 ANSYS Finite Element Model

3.14.1 SOLID65 Element Description

SOLID 65 is utilized for the modeling of solid material with and without rebar (reinforcing bars). For example, this ability of solid is utilized to simulate the concrete material with its condition and properties. There is a need to define the failure surface and this is done by using the maximum compressive and tensile strength. Concrete element started to crack when the principal tensile stress is located in any direction outside the surface of the failure. After that, Young modulus will suffer dropping in its value reaching to zero in parallel direction to the principal tensile stress. Crushing begins to happen when the principal stresses are compressive

and located outside the failure surface. Subsequently, Young modulus is reached to zero, and the element efficiency vanishes [58].

The most significant feature of SOLID65 is that it can represent the non-linearity of the material used. SOLID65 has an ability to cracks, crushes, plastic deformation, and creep. The element is defined by isotropic material properties. The geometry, node position, and coordinate system for SOLID65 are exhibited in Figure (3-23) [58].

3.14.1.1 Shape Functions of SOLID65 Element

To model concrete, three-dimensional brick elements are utilized. To express the displacements at any point within the element in terms of nodal displacement, shape functions for SOLID65 are utilized, which are interpolation functions.

Using the shape functions, the displacement components (u, v, w) at a specific point can be found as follows [56],

$$u = \frac{1}{8}\,[u_I(1-s)(1-t)(1-r) + u_J(1+s)(1-t)(1-r) + u_K(1+s)(1+t)(1-r) + u_L(1-s)(1+t)(1-r) + u_M(1-s)(1-t)(1+r) + u_N(1+s)(1-t)(1+r) + u_O(1+s)(1+t)(1+r) + u_P(1-s)(1+t)(1+r)] \quad \ldots\ldots (3.88)$$

$$v = \frac{1}{8}\,[v_I(1-s)] \ldots \text{(analogous to u)} \quad \ldots\ldots (3.89)$$

$$w = \frac{1}{8}\,[w_I(1-s)] \ldots \text{(analogous to u)} \quad \ldots\ldots (3.90)$$

where, (s, t, and r) are the local coordinates and they are normalized, ranging from -1 to +1, and are not necessarily orthogonal to one another [56].

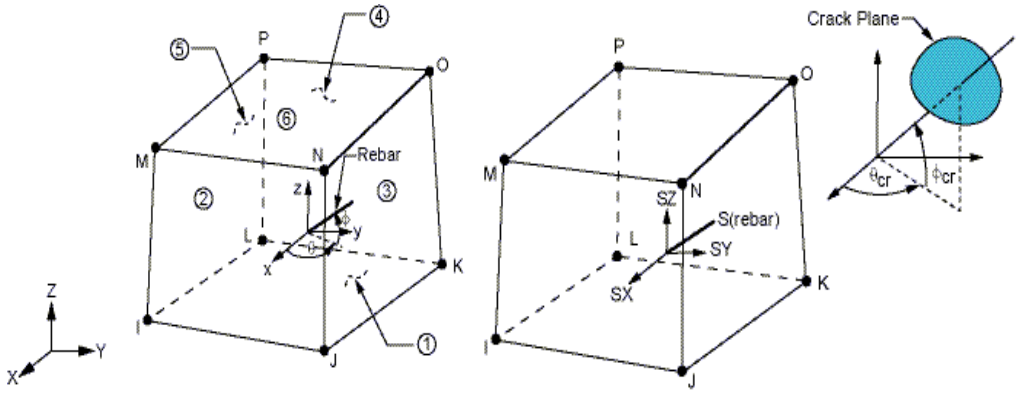

a) SOLID65 geometry b) SOLID65 stress output

Figure 3- 23 SOLID65 element for representing the concrete [56].

3.14.1.2 Input Data for SOLID65

Input data for SOLID65 element has one solid material and up to three rebar material in different direction. This element can contain another material through the volume of SOILID65 which defined as the rebar volume divided by the total element volume is equal to zero. Additional concrete material data such as the shear transfer coefficient, tensile strength, and compressive strength are described in Table (3.6).

Table 3.4 SOLID65 input data [56].

Constant	Meaning
1	Shear transfer coefficient for open cracks
2	Shear transfer coefficient for closed cracks
3	Uniaxial tensile cracking stress
4	Uniaxial crushing stress
5	Biaxial crushing stress
6	Ambient hydrostatic stress state
7	Biaxial crushing stress under the ambient hydrostatic stress
8	Uniaxial crushing stress under the ambient hydrostatic stress.
9	Stiffness multiplier for cracked tensile condition

3.14.2 LINK180 Element Description

It is a truss (or spar) element which may be utilized in many of engineering problems. LINK180 is utilized to modeling trusses, springs, links, sagging cables etc. This spar element is a uniaxial tension-compression element. As in a pin-jointed structure, no consideration of bending in this element. Plasticity and stress stiffening are contained within. The element is chosen, in this research, to modelling steel reinforcement which workings as main steel reinforcement and stirrups.

By using shape functions of the LINK180 element, the displacement components (*u*,*v*, and *w*) at a particular point can be found as follows [51]:

$$u = 1/2\left[u_I(1-s) + u_J(1+s)\right] \quad \ldots\ldots (3.91)$$

$$v = 1/2\left[v_I(1-s) + v_J(1+s)\right] \quad \ldots\ldots (3.92)$$

$$w = 1/2\left[w_I(1-s) + w_J(1+s)\right] \quad \ldots\ldots (3.93)$$

A geometry, nodes positions, and coordinate system for LINK180 are presented in Figure (3-24) [56].

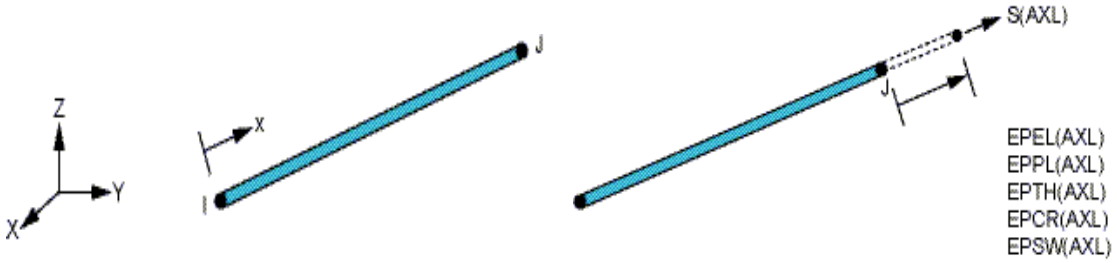

a) LINK 180 geometry b) LINK 180 stress output

Figure 3- 24 LINK180 for representing steel reinforcement [56].

Input data for LINK180 element are the cross sectional area for used bar, initial strain, and the material properties. In mounting a FE model, three alternative representations of reinforcement can commonly be utilized, these are [53]:

Discrete Representation

Discrete representation has commonly been utilized. The reinforcement in discrete modeling uses one dimensional bar that are linked to concrete mesh nodes as shown in Figure (3-24 a). Therefore, the concrete and steel reinforcement bar will construct at the same nodes and same occupied regions. Full displacement compatibility between SOLID65 for concrete and LINK180 for steel rebar is significant benefit of the discrete representation. The weaknesses in this method that the constraint of the mesh and increase in number of the constructed elements.

Embedded Representation

The embedded representation is often used with high order iso-parametric elements. The bar element is constructed in by keeping reinforcing steel displacements compatible with an adjacent concrete element as displayed in Figure (3-24b). When reinforcement is complex, this model is very useful. The reinforcement steel stiffness matrix is evaluated unconnectedly and added to that of the concrete to obtain the inclusive stiffness matrix. The disadvantage of this method is that there are extra degrees of freedom increase the computational and numerical treatment.

Smeared (Distributed) Representation

This method of modelling supposes that steel reinforcement is distributed uniformly through concrete elements in the defined region of the FE mesh as displayed in Figure (3.24 c). For example, this method is utilized for modelling wire mesh to simulate the occurred cracks, and for large structural members to decrease

number of used elements. Also, where the presence of reinforcement does not have significantly effect on the overall structural behavior.

In discrete model method, which is utilized in this work, reinforcement is constructed by LINK180 at shared node with SOLID65. As a result, there are ‘‘perfect bond” between the concrete core and steel rebar, as presented in Figure (3-24).

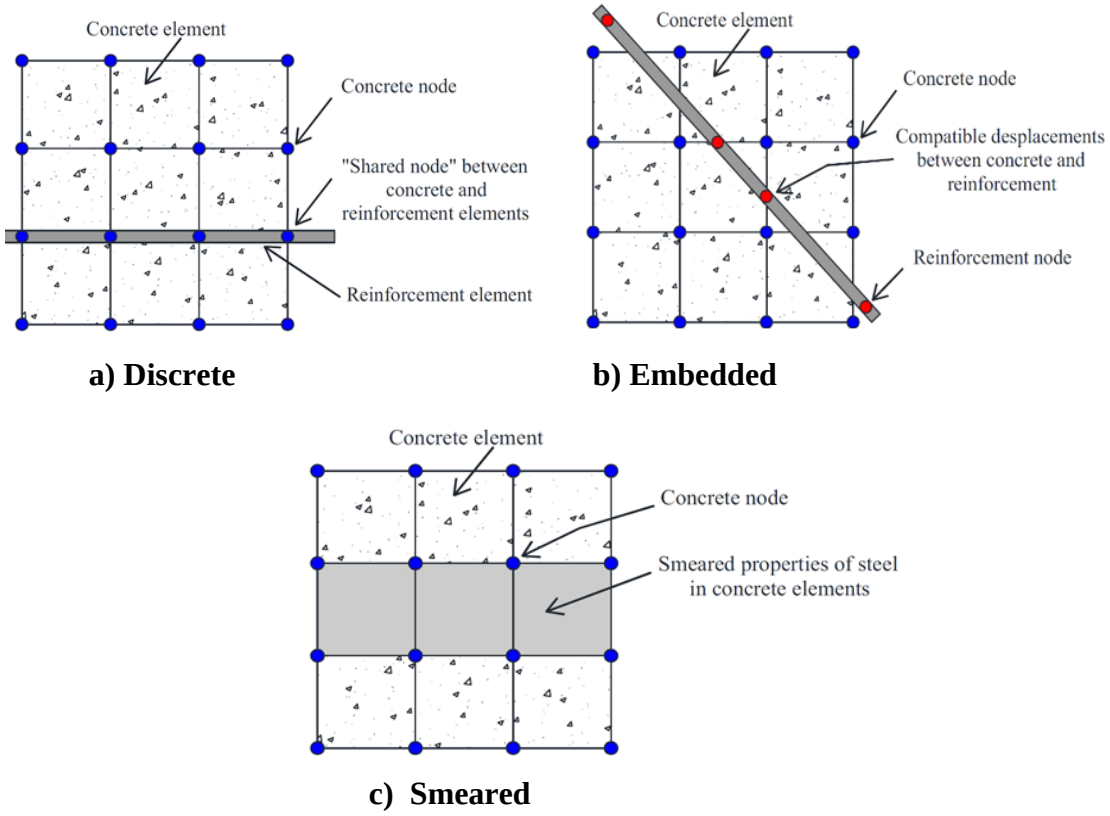

Figure 3.25 Models for reinforcement in reinforced concrete [53] .

The above is termed to limitation, because from the experimental testing, cracking, crushing, and loss of concrete cover because of bond-slip failures. The desired technique for the modeling of steel reinforcement is selected based on the problem nature [53].

3.14.3 SOLID185 Element Description

A SOLID185 element is utilized for steel sections and plates at the supports and loading zones for the beam. This element with eight nodes, each node has three degrees of freedom. SOLID185 with translation in x, y, and z directions. A geometry and nodes positions for this element are exhibited in Figure (3-25). SOLID185 description are took from ANSYS 15 element library [56].

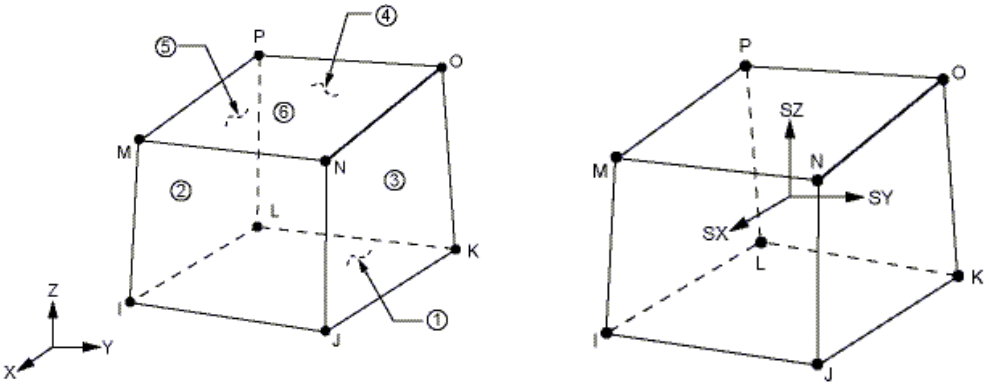

a) SOLID 185 homogeneous structural solid geometry

b) SOLID 185 homogeneous structural solid stress output

Figure 3. 26 SOLID 185 used to model steel plates and supports [56].

CHAPTER FOUR: RESULTS AND DISCUSSIONS

4.1. General

For long plate girder, the slab or deck effect in comparing with high section depth is relatively small and could be ignored in determining of section capacity and considering it as dead load. For small length, the composite section could be consisting of concrete and standard steel section and design traditionally. For intermediate length, where the compression force in deck could be contribute significantly in resistance forces, proper dimension selection and section configuration could be effect section moment capacity and the dominated failure mode.

4.2. The dominated Flexural limit states

Composite section is subjected to internal stress intensity which generates the tensile and compressive stress in the cross section. The compressive stress effects are of a significant buckling failure mode and could be considered as limit the strength of a beam section. The tensile stress intensity affected by the highly slenderness of steel element and so do not cause buckling failure modes, as strength dominated by steel yielding strength. The nominal flexural strength of section of relatively slender element is based on the different flexural limit states likewise:

1. Flanged local bulking (FLB)
2. Tension flange yielding (TFY)
3. compression flange yielding (CFY)
4. Lateral-torsional buckling (LTB)

In composite section, the top flange could be constrained and so, the flanged local bulking (FLB) omitted

4.3 Composite Section Configuration

Various materials can be arranged in an optimum configuration, with the target that the desirable characteristics of utilizing materials function in its perfect position. In Traditional composite section, concrete slabs rest over slandered or built-up steel beams with proper bonding. This study aimed to proposed and investigate two other configuration aspect of composite modes in addition to the traditional composite mode; generally, the introduced composite modes could be listed as the following:

1- Traditional composite mode
2- Composite section of merged concrete-steel compressive region
3- Composite section of multi flanged U steel section

The traditional composite section and the proposed sections are clearly illustrated in Figure 4.1

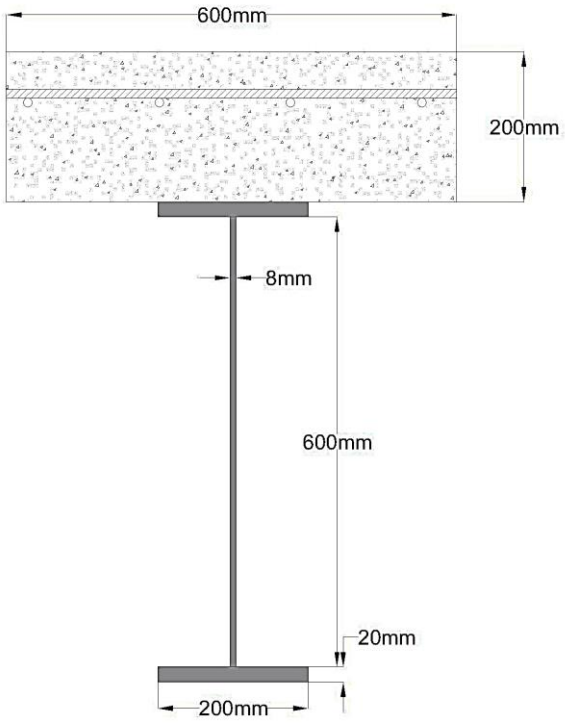

a. Traditional composite mode (Mode I)

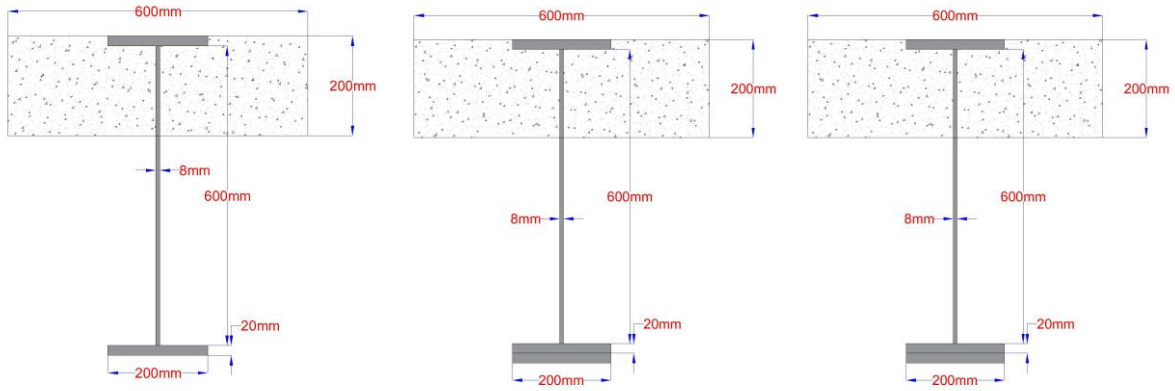

b. Composite section of merged concrete-steel compressive region (Mode II)

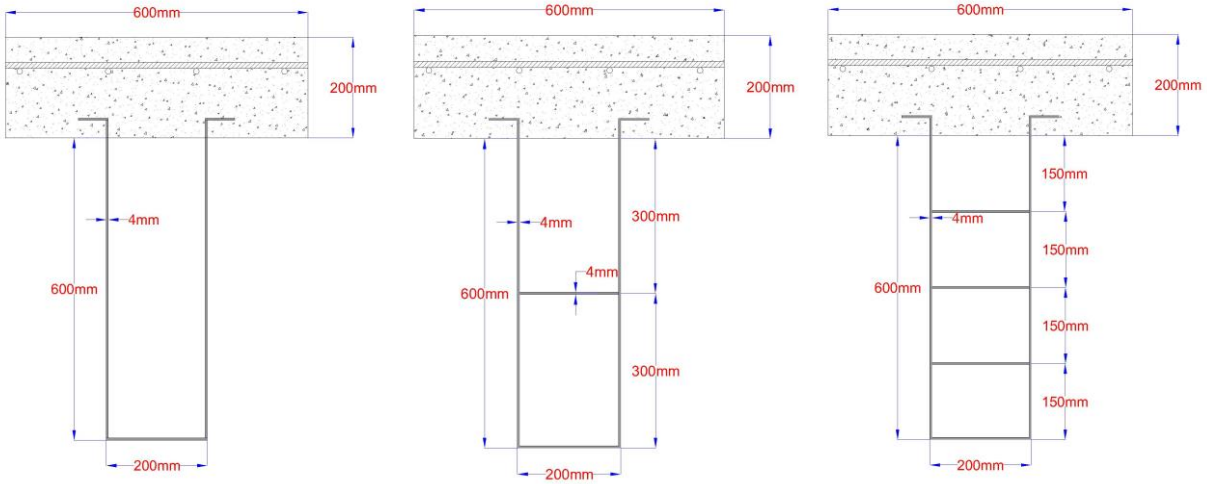

c. Composite section of multi flanged U steel section

Figure 4- 1 Concrete- built up steel section various composite modes

4.4. Traditional composite mode (Mode I)

Table 4. 1 exhibits the specimen's matrix details of the adopted traditional composite mode samples (Mode I). Eight groups are adopted and classified according to change a significant geometry characteristics or material properties of section consisting components (concrete deck and build up steel section)

Table 4- 1 Specimens Matrix-Traditional Composite mode details

No.	Gr.	Var.	Code	Fc'	fyf	fyw	ttf	tbf	tw	bc	hc	btf	bbf	hw
1	1	fc'	C-Is-1	35	420	345	20	20	8	600	200	200	200	600
2			C-Is-2	45	420	345	20	20	8	600	200	200	200	600
3			C-Is-3	55	420	345	20	20	8	600	200	200	200	600
4	2	fyf	C-Is-4	35	275	345	20	20	8	600	200	200	200	600
5			C-Is-5	35	420	345	20	20	8	600	200	200	200	600
6			C-Is-6	35	575	345	20	20	8	600	200	200	200	600
7	3	fyw	C-Is-7	35	420	275	20	20	8	600	200	200	200	600
8			C-Is-8	35	420	345	20	20	8	600	200	200	200	600
9			C-Is-9	35	420	420	20	20	8	600	200	200	200	600
10	4	tbf	C-Is-10	35	420	345	20	20	8	600	200	200	200	600
11			C-Is-11	35	420	345	20	30	8	600	200	200	200	600
12			C-Is-12	35	420	345	20	40	8	600	200	200	200	600
13	5	tw	C-Is-13	35	420	345	20	20	6	600	200	200	200	600
14			C-Is-14	35	420	345	20	20	8	600	200	200	200	600
15			C-Is-15	35	420	345	20	20	10	600	200	200	200	600
16	6	bc	C-Is-16	35	420	345	20	20	8	200	200	200	200	600
17			C-Is-17	35	420	345	20	20	8	400	200	200	200	600
18			C-Is-18	35	420	345	20	20	8	600	200	200	200	600
19	7	bbf	C-Is-19	35	420	345	20	20	8	600	200	200	200	600
20			C-Is-20	35	420	345	20	20	8	600	200	200	300	600
21			C-Is-21	35	420	345	20	20	8	600	200	200	400	600
22	8	hw	C-Is-22	35	420	345	20	20	8	600	200	200	200	600
23			C-Is-23	35	420	345	20	20	8	600	200	200	200	700
24			C-Is-24	35	420	345	20	20	8	600	200	200	200	800

4.4.1. Tension Flange Yielding (TFY)

Tension flange yielding limit state is occur in sections where the centroidal is not at mid-section and could be occur within built-up sections as the tension section capacity is less than the compression section capacity.

Table 4.2 lists the determined tension flange yielding moment capacity of the concrete- built up steel section composite beams. The variation of TFY moment capacities in term of concrete compressive strength, flange yield strength, web yield strength, bottom flange thickness, web thickness, concrete deck width, bottom flange width and steel girder full depth are exhibits in Figures (4.2 - 4.9) respectively. The variation of the adopted parameters affects the TFY moment capacities with various rates. The best improving associated with yield parameters that relate to bottom flange likewise strength, thickness and widths while the effect of concrete deck limited to effected width, besides; the webs' geometrical and material characteristics have slightly effect on the obtained TFY moment capacities. And always there are a certain limit of improving in scope of geometry and material adopted properties.

Table 4- 2 TFY Moment Capacity-Mode I

No.	Gr.	Var.	Code	T, N	C, N	a, mm	yf, mm	Yw, mm	M, kN.m	Relative rating
1	1	fc'	C-Is-1	3336000	3570000	94.12	572.94	272.94	1414.53	1.00
2			C-Is-2	3336000	4590000	73.20	583.40	283.40	1449.42	1.02
3			C-Is-3	3336000	5610000	59.89	590.05	290.05	1471.62	1.04
4	2	fyf	C-Is-4	2756000	3570000	61.62	589.19	289.19	1127.00	1.00
5			C-Is-5	3336000	3570000	94.12	572.94	272.94	1414.53	1.26
6			C-Is-6	3956000	3570000	128.85	555.57	255.57	1701.05	1.51
7	3	fyw	C-Is-7	3000000	3570000	94.12	572.94	272.94	1322.82	1.00
8			C-Is-8	3336000	3570000	94.12	572.94	272.94	1414.53	1.07
9			C-Is-9	3696000	3570000	94.12	572.94	272.94	1512.79	1.14
10	4	tbf	C-Is-10	3336000	3570000	94.12	572.94	272.94	1414.53	1.00
11			C-Is-11	4176000	3570000	141.18	549.41	249.41	1797.54	1.27
12			C-Is-12	5016000	3570000	188.24	525.88	225.88	2141.03	1.51
13	5	tw	C-Is-13	2922000	3570000	94.12	572.94	272.94	1301.53	1.00
14			C-Is-14	3336000	3570000	94.12	572.94	272.94	1414.53	1.09
15			C-Is-15	3750000	3570000	94.12	572.94	272.94	1527.53	1.17
16	6	bc	C-Is-16	3336000	1190000	282.35	478.82	178.82	1100.56	1.00
17			C-Is-17	3336000	2380000	141.18	549.41	249.41	1336.04	1.21
18			C-Is-18	3336000	3570000	94.12	572.94	272.94	1414.53	1.29
19	7	bbf	C-Is-19	3336000	3570000	94.12	572.94	272.94	1414.53	1.00
20			C-Is-20	4176000	3570000	141.18	549.41	249.41	1797.54	1.27
21			C-Is-21	5016000	3570000	188.24	525.88	225.88	2141.03	1.51
22	8	hw	C-Is-22	3336000	3570000	94.12	572.94	272.94	1414.53	1.00
23			C-Is-23	3612000	3570000	94.12	672.94	322.94	1754.46	1.24
24			C-Is-24	3888000	3570000	94.12	772.94	372.94	2122.00	1.50

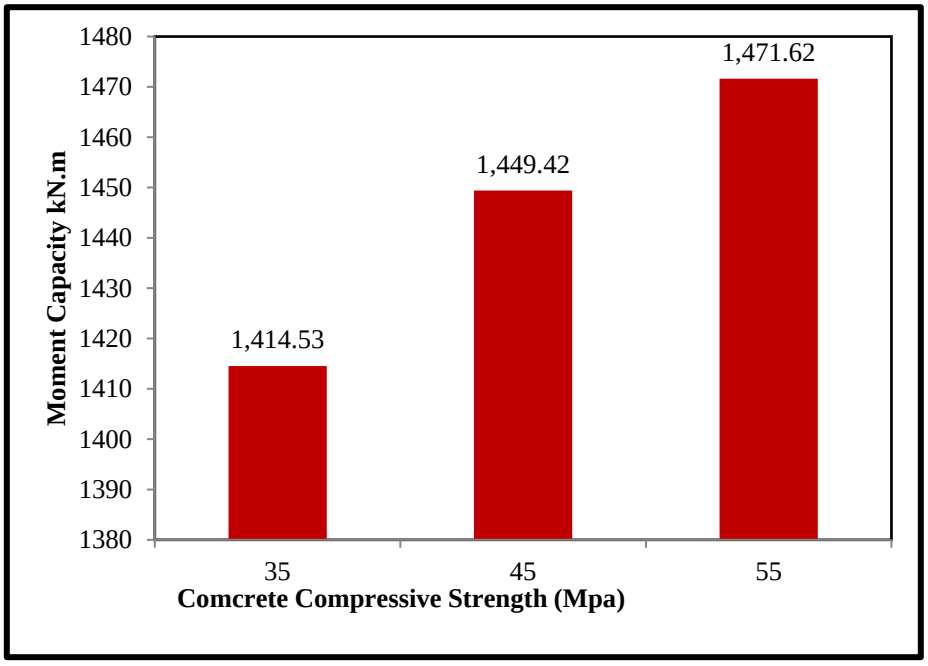

Figure 4- 2 Concrete compressive strength effects- Mode I

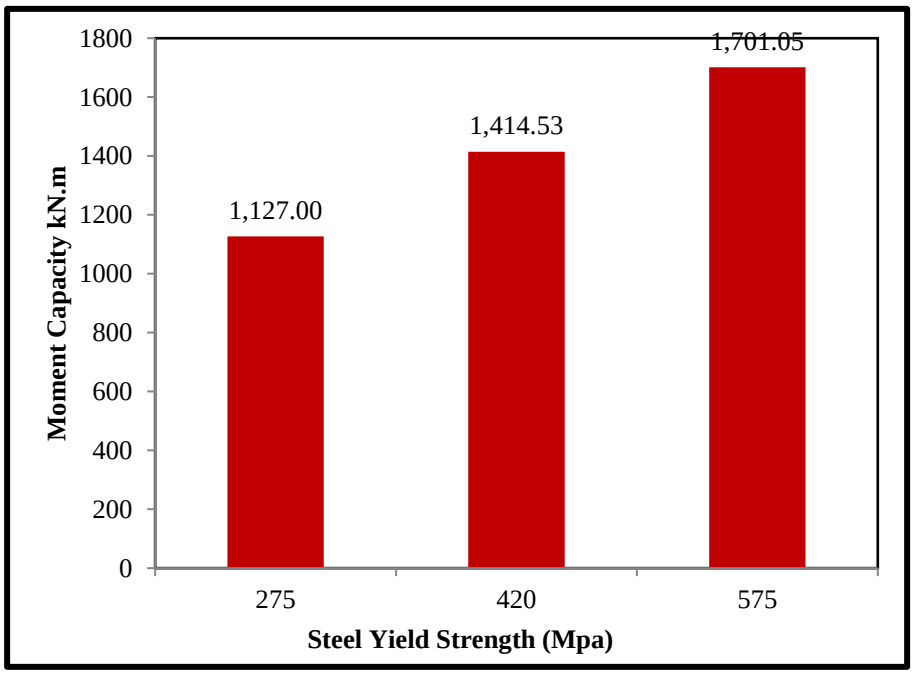

Figure 4- 3 Effect of flange steel yield strength on TFY moment capacity - Mode I

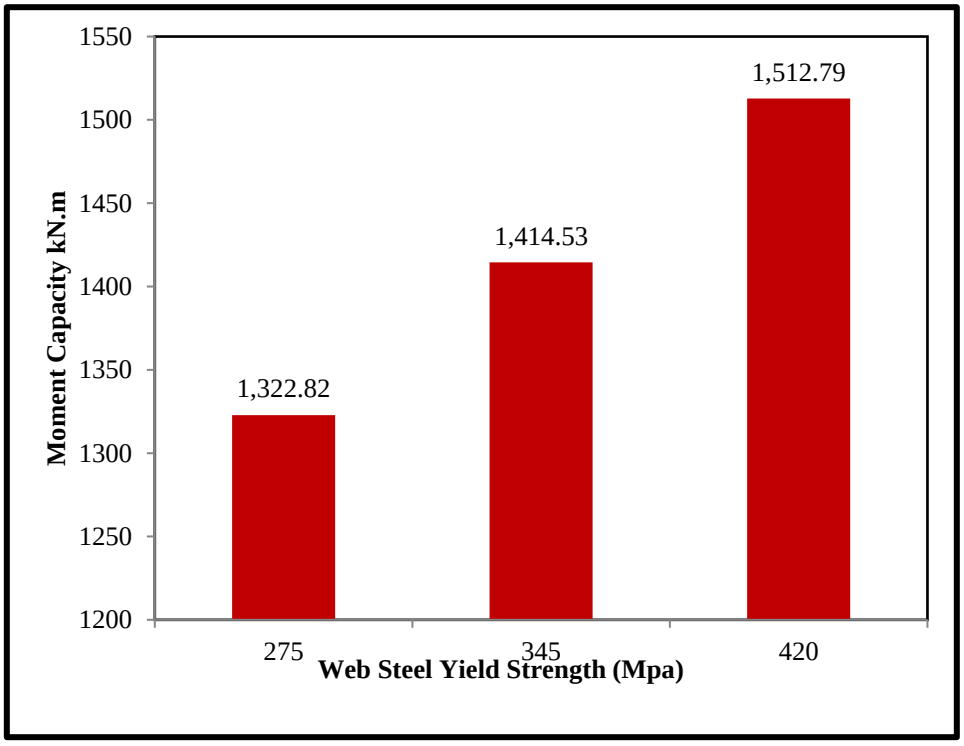

Figure 4- 4 Effect of web steel yield strength on TFY moment capacity - Mode I

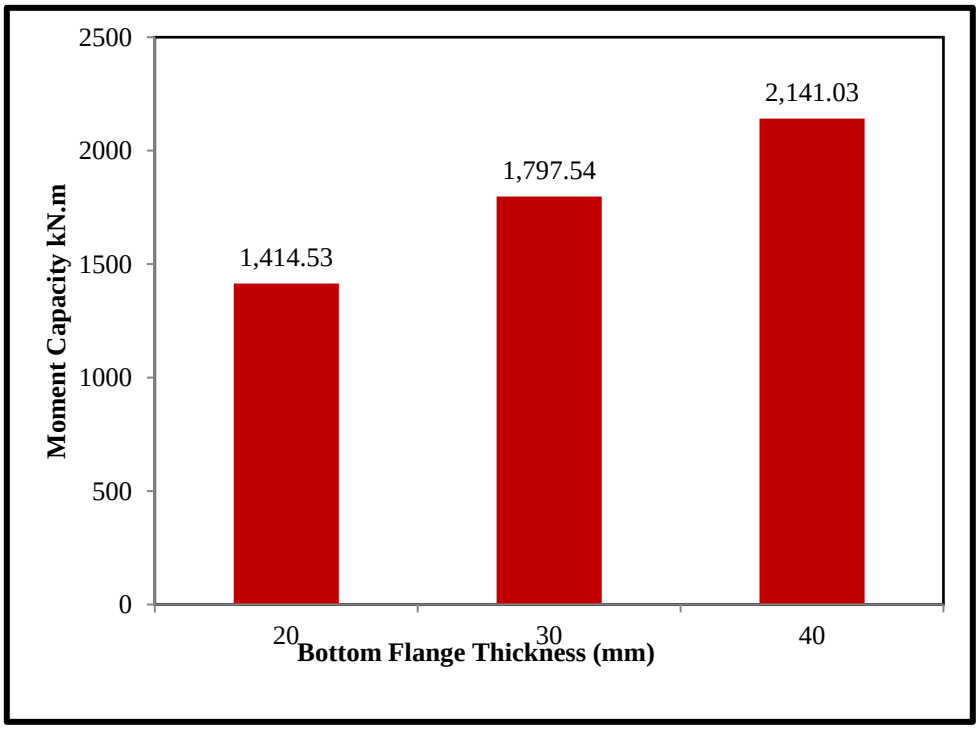

Figure 4- 5 Effect of bottom flange thickness on TFY moment capacity - Mode I

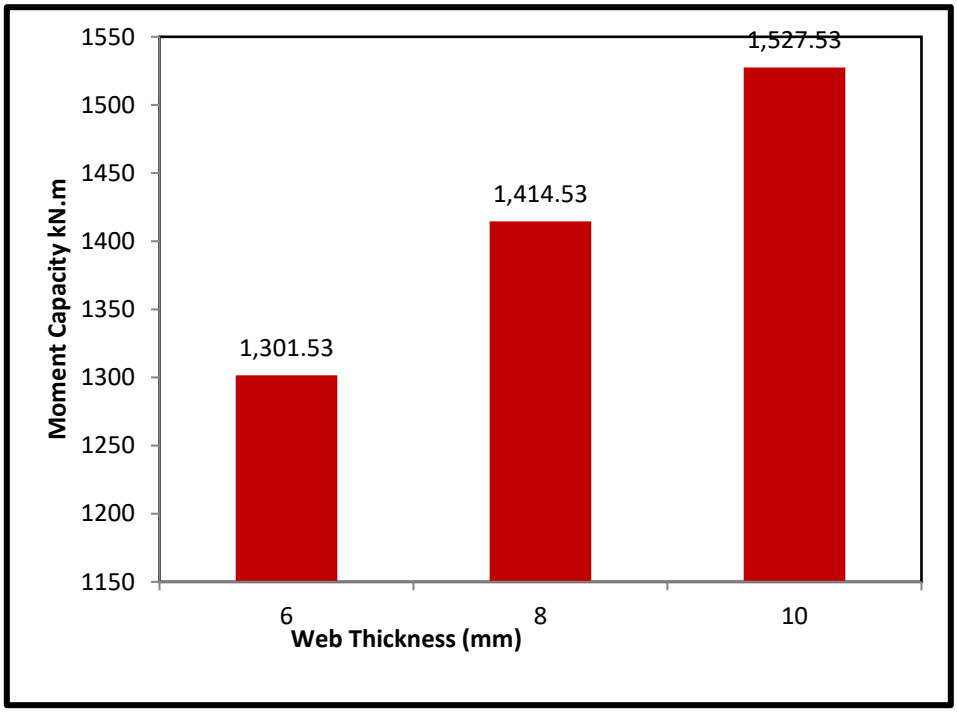

Figure 4- 6 Effect of bottom web thickness on TFY moment capacity- Mode I

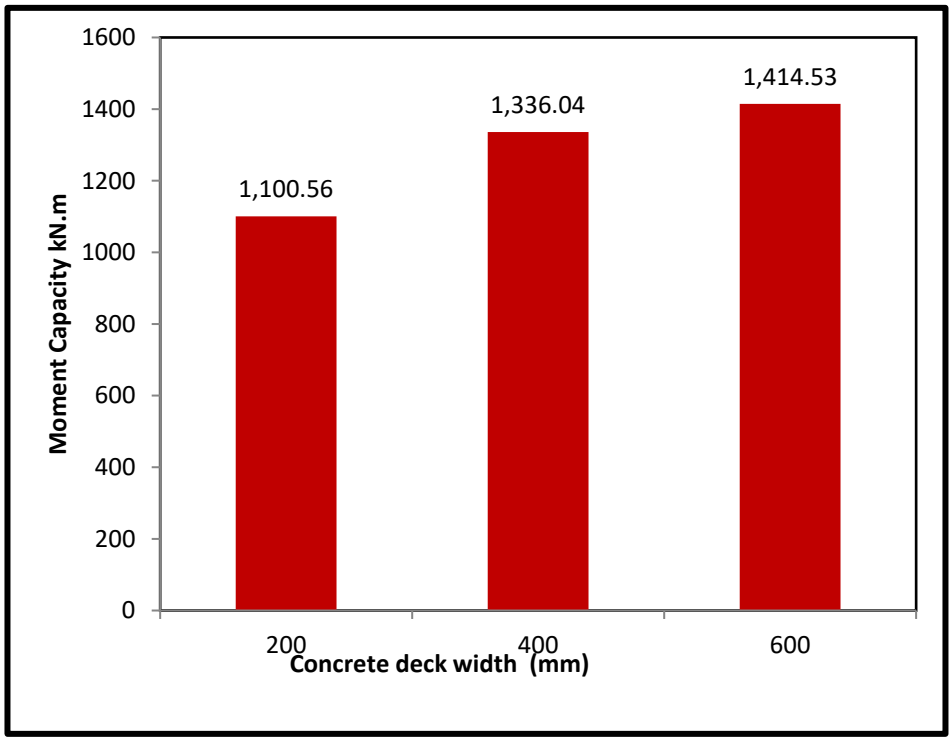

Figure 4- 7 Effect of bottom concrete deck width on TFY moment capacity- Mode I

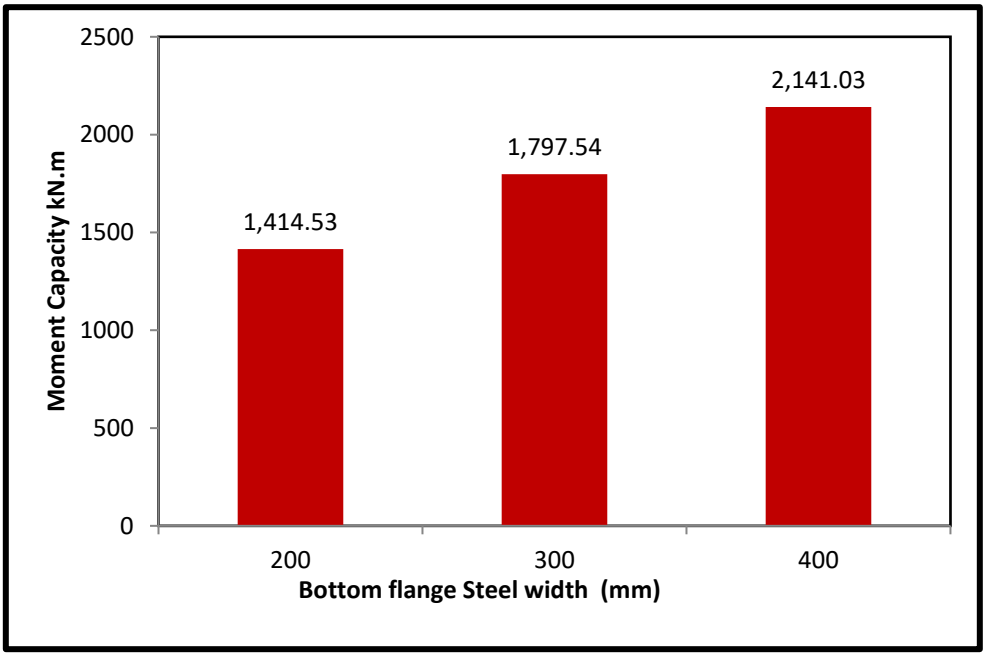

Figure 4- 8 Effect of bottom flange steel width on TFY moment capacity- Mode I

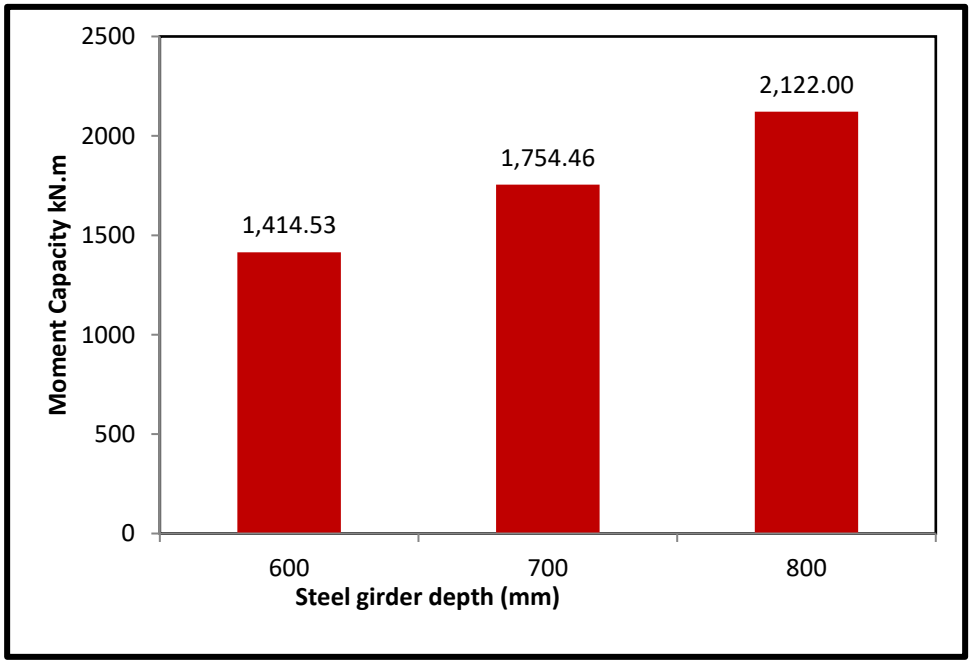

Figure 4- 9 Effect of steel girder depth on TFY moment capacity- Mode I

4.4.2. Compression Flange Yielding (CFY)

Compression flange yielding limit state occurs when a full yielding strength is attainted for compacted steel elements under the effect of compressive stress. The critical compression flange stress (Fcr) depends on the flange is compactness (compact, noncompact, or slender). The related Specification (AISC), uses the notation λ, λp, and λr to define the flange slenderness ratio (flange width-to-thickness ratio) and its limits. And due to the continuous constraining of top flange of steel section, the material will stresses to full strength of Fy.

Table 4.3 lists the determined compression flange yielding (CFY) moment capacities of the concrete- built up steel section composite beams. CFY moment capacities besides comparative analysis of TFY verse CFY moment capacities in term of concrete compressive strength, flange yield strength, web yield strength, bottom flange thickness, web thickness, concrete deck width, bottom flange width and steel girder full depth are exhibits in Figures (4.10 - 4.17) respectively.

Likewise, TFY, the variation of the adopted parameters affects the CFY moment capacities with various rates. The best improving associated with parameters that relate to bottom flange likewise strength, thickness and widths that effect the section strength to get 1.59 times of basic strength as these parameter changed with for a certain limits while the effect of concrete deck still slightly, and the full depth of built up steel section positively affects the strength. The comparative analysis between TFY and CFY shows that, the dominated failure mode is TFY where the rate of CFY moment capacities to TFY moment capacities more than 1 for all samples, the high rate is 1.36 and associated with concrete deck width, the highly rate diverging in comparing with those of other parameters, could be indicated that the deck width have the main effect that dominated other parameters in scope of target highly section moment capacity.

Table 4- 3 Moment Capacity (CFY)-Mode 1

No.	Gr.	Var.	Code	T, N	C, N	a, mm	yf	Yw	aw	Rpg	M, kN.m	Relative rating	MCFY/MTFY
1	1	fc'	C-Is-1	3336000	3570000	94.12	572.94	272.94	0.4	0.99	1500.76	1.00	1.06
2			C-Is-2	3336000	4590000	73.20	583.40	283.40	0.4	0.99	1501.12	1.00	1.04
3			C-Is-3	3336000	5610000	59.89	590.05	290.05	0.4	0.99	1501.35	1.00	1.02
4	2	fyf	C-Is-4	2756000	3570000	61.62	589.19	289.19	0.4	0.99	1159.59	1.00	1.03
5			C-Is-5	3336000	3570000	94.12	572.94	272.94	0.4	0.99	1500.76	1.29	1.06
6			C-Is-6	3956000	3570000	128.85	555.57	255.57	0.4	0.99	1844.62	1.59	1.08
7	3	fyw	C-Is-7	3000000	3570000	94.12	572.94	272.94	0.4	0.99	1391.62	1.00	1.05
8			C-Is-8	3336000	3570000	94.12	572.94	272.94	0.4	0.99	1500.76	1.08	1.06
9			C-Is-9	3696000	3570000	94.12	572.94	272.94	0.4	0.99	1617.68	1.16	1.07
10	4	tbf	C-Is-10	3336000	3570000	94.12	572.94	272.94	0.4	0.99	1500.76	1.00	1.06
11			C-Is-11	4176000	3570000	141.18	549.41	249.41	0.4	0.99	1961.46	1.31	1.09
12			C-Is-12	5016000	3570000	188.24	525.88	225.88	0.4	0.99	2382.62	1.59	1.11
13	5	tw	C-Is-13	2922000	3570000	94.12	572.94	272.94	0.3	0.99	1366.01	1.00	1.05
14			C-Is-14	3336000	3570000	94.12	572.94	272.94	0.4	0.99	1500.76	1.10	1.06
15			C-Is-15	3750000	3570000	94.12	572.94	272.94	0.5	0.99	1635.63	1.20	1.07
16	6	bc	C-Is-16	3336000	1190000	282.35	478.82	178.82	0.4	0.99	1497.53	1.00	1.36
17			C-Is-17	3336000	2380000	141.18	549.41	249.41	0.4	0.99	1499.95	1.00	1.12
18			C-Is-18	3336000	3570000	94.12	572.94	272.94	0.4	0.99	1500.76	1.00	1.06
19	7	bbf	C-Is-19	3336000	3570000	94.12	572.94	272.94	0.4	0.99	1500.76	1.00	1.06
20			C-Is-20	4176000	3570000	141.18	549.41	249.41	0.4	0.99	1961.46	1.31	1.09
21			C-Is-21	5016000	3570000	188.24	525.88	225.88	0.4	0.99	2382.62	1.59	1.11
22	8	hw	C-Is-22	3336000	3570000	94.12	572.94	272.94	0.4	0.99	1500.76	1.00	1.06
23			C-Is-23	3612000	3570000	94.12	672.94	322.94	0.4	0.99	1854.46	1.24	1.06
24			C-Is-24	3888000	3570000	94.12	772.94	372.94	0.4	0.99	2235.58	1.49	1.05

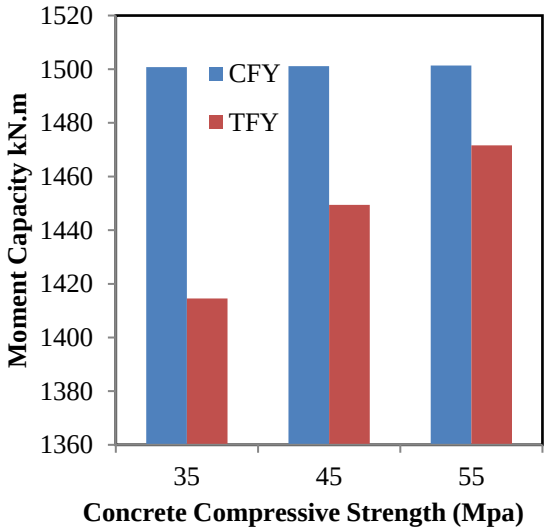

Figure 4- 10 Effect of concrete compressive Strength on moment capacity-TFY verse CFY

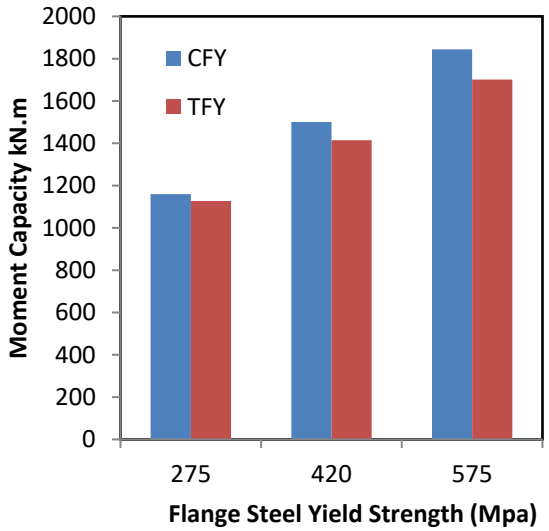

Figure 4- 11 Effect of flange steel yield strength on moment capacity- TFY verse CFY

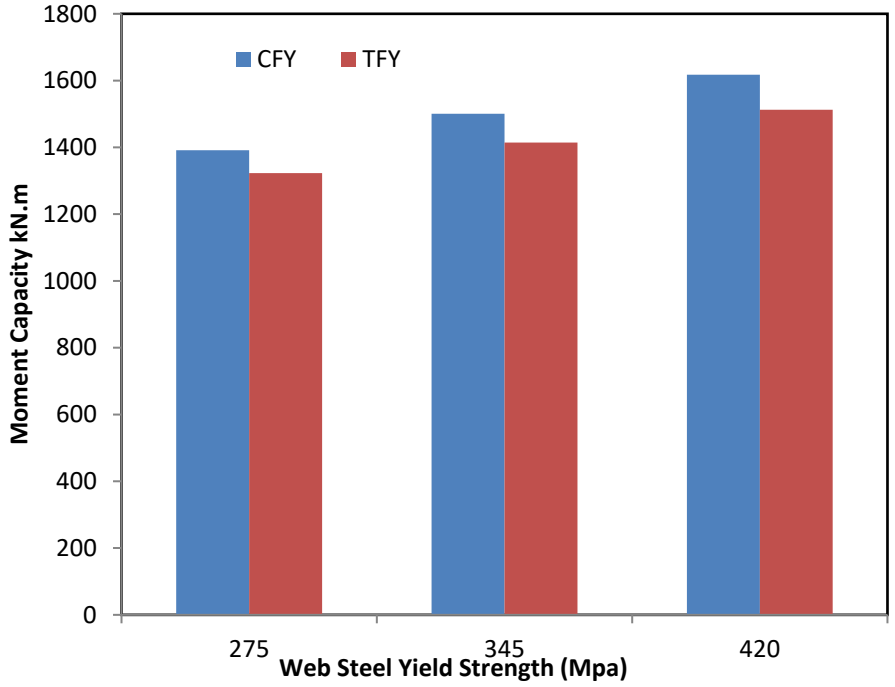

Figure 4- 12 Effect of web steel strength on moment capacity- TFY verse CFY

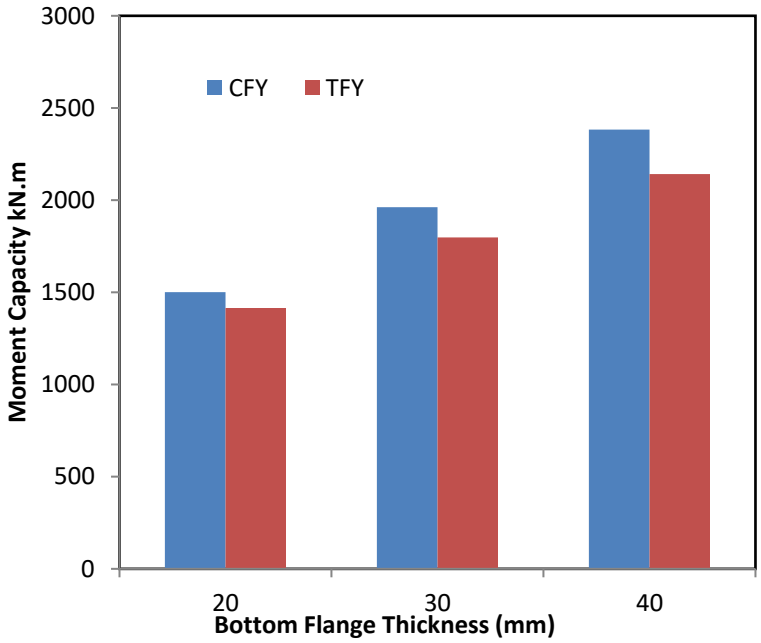

Figure 4- 13 Effect of bottom flange thickness on moment capacity- TFY verse CFY

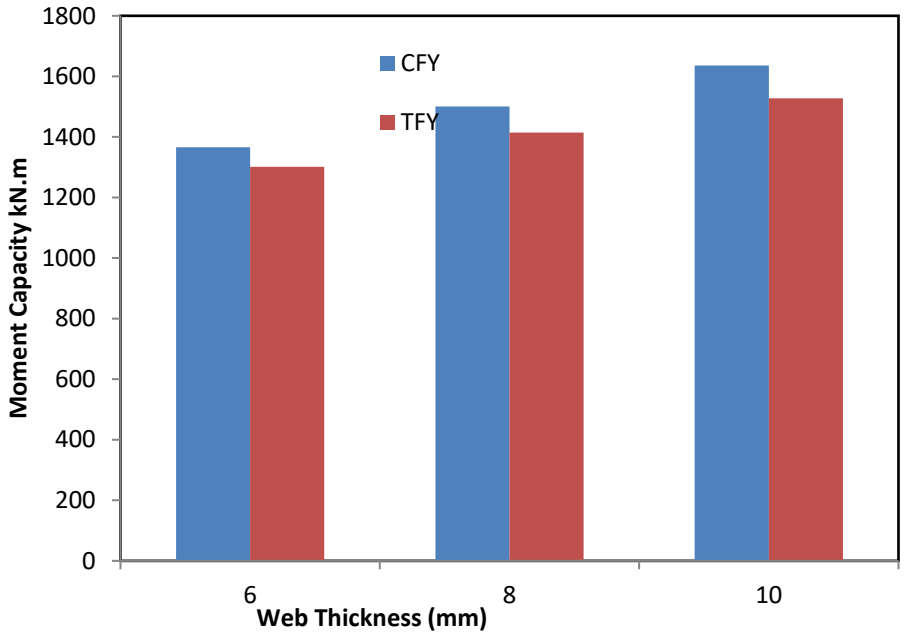

Figure 4- 14 Effect of web thickness on moment capacity- TFY verse CFY

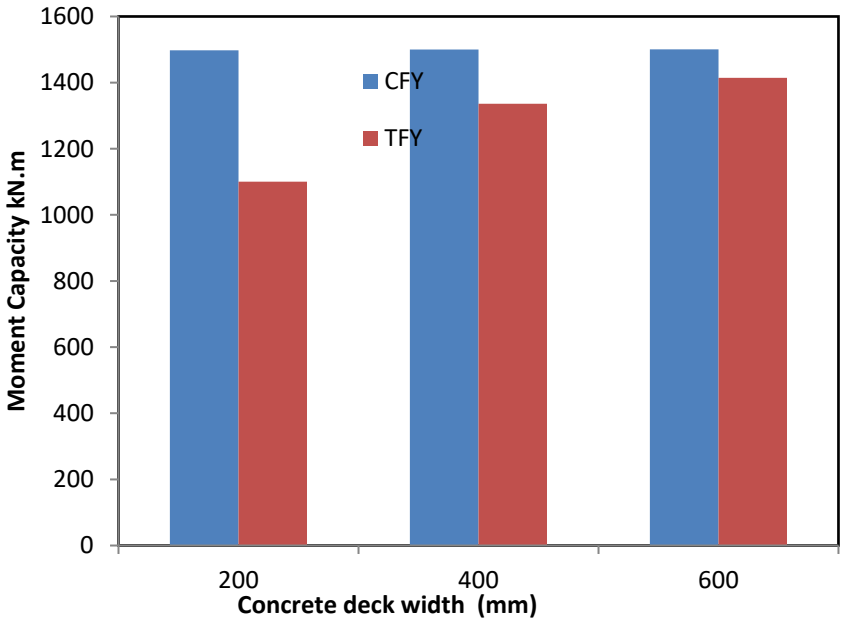

Figure 4- 15 Effect of concrete deck width on moment capacity- TFY verse CFY

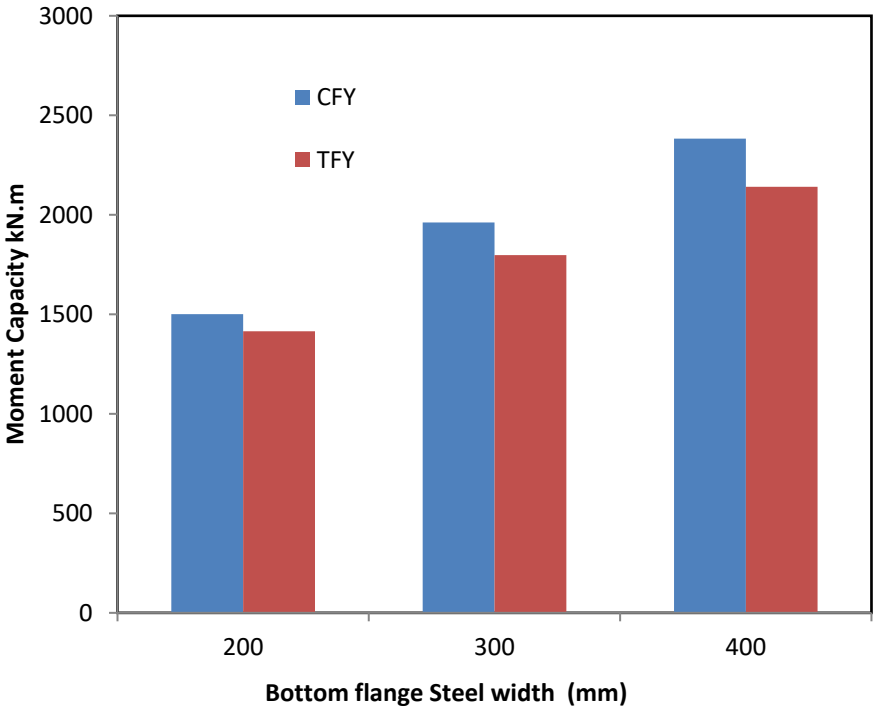

Figure 4- 16 Effect of bottom flange steel width on moment capacity- TFY verse CFY

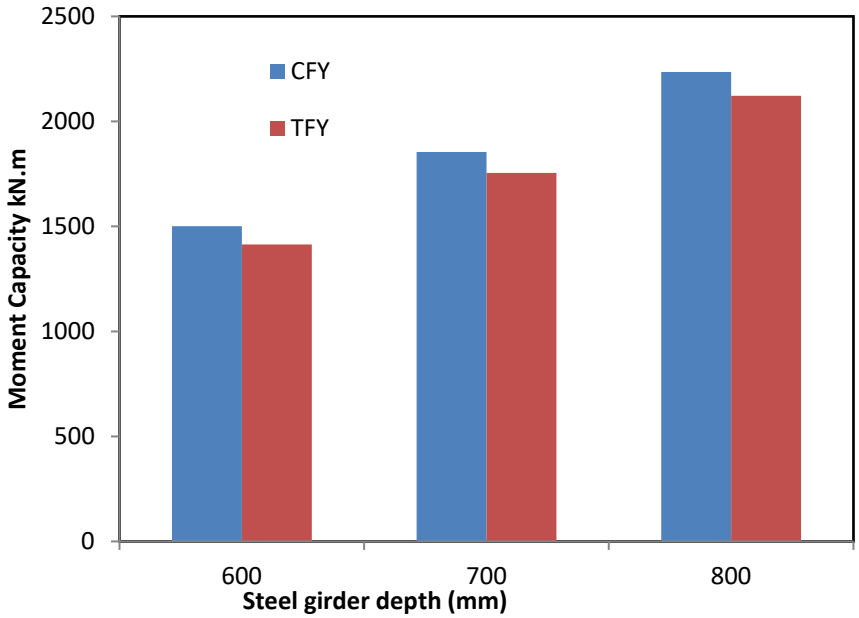

Figure 4- 17 Effect of steel girder depth on moment capacity- TFY verse CFY

4.4.3. Lateral-Torsional Buckling (LTB)

Lateral-Torsional Buckling limit state is overall lateral buckling of the compression flange of the section and occurs when a compression flange of beam lacks lateral support.

Whether lateral-torsional buckling will occur depends on the amount of lateral support—that is, the unbraced length Lb. If the unbraced length is small enough, yielding or flange local buckling will occur before lateral-torsional buckling. The length parameters are Lp and Lr. Table 4.4 lists the determined lateral-torsional buckling (LTB) moment capacity of the concrete- Built up steel section composite beams. The present constrain turned the assigned lateral-torsional buckling mode from elastic lateral-torsional buckling to plastic lateral – torsional buckling mode for a certain length domain, more than from (14 m to 20 m), the clearly strength different between two attainted modes are shown in Figure 4.18 which illustrates the effect of mid span constraining on LTB moment capacity in composite Mode I,

Table 4- 4 Unbraced length effect on LTB-Mode 1

No.	Var.	Code	r	Lr	LP	Lb	fcr	LTB-plastic	Lb	fcr	LTB-elastic
1	Unbraced length	C-Is-1	6.60	13.73	4.03	7	420.33	875.91	14	42.45	175.53
2			6.60	13.73	4.03	8	407.35	846.10	16	37.31	134.39
3			6.60	13.73	4.03	9	394.38	816.30	18	33.05	106.18
4			6.60	13.73	4.03	10	381.40	786.50	20	29.48	86.01

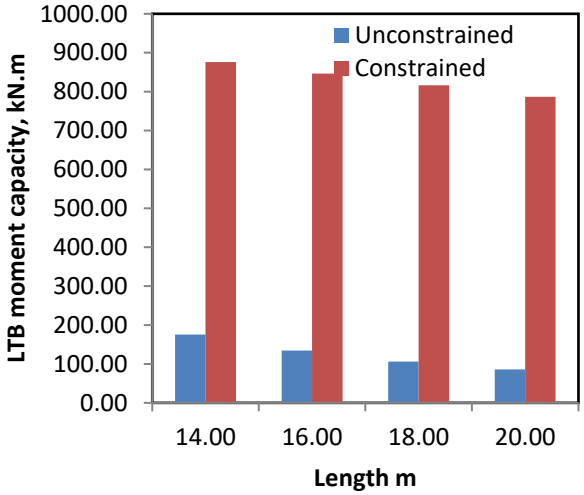

Figure 4- 18 Effect of mid span constraining on LTB moment capacity-Mode I

4.5. Composite section of merged concrete-steel compressive region: (Mode II)

Table 4.5 exhibits the specimen's matrix details of composite section Mode II, wide spectrum of sample are considered, the target variation is provided in the cover steel plate that provide in tension flange where the overall thickness of tension flange area varied from 8 mm to 30 mm.

Table 4- 5 specimen's matrix details of composite section- Mode II

No.	Var.	Code	fc'	fyf	fyw	ttf	tbf	tw	bc	hc	btf	bbf	hw	Asf	Asw
1	Bottom flange thickness	C-Is#-1	35	420	345	10	8	8	600	200	200	200	600	1600	4800
2		C-Is#-2	35	420	345	10	10	8	600	200	200	200	600	2000	4800
3		C-Is#-3	35	420	345	10	12	8	600	200	200	200	600	2400	4800
4		C-Is#-4	35	420	345	10	14	8	600	200	200	200	600	2800	4800
5		C-Is#-5	35	420	345	10	16	8	600	200	200	200	600	3200	4800
6		C-Is#-6	35	420	345	10	18	8	600	200	200	200	600	3600	4800
7		C-Is#-7	35	420	345	10	20	8	600	200	200	200	600	4000	4800
8		C-Is#-8	35	420	345	10	22	8	600	200	200	200	600	4400	4800
9		C-Is#-9	35	420	345	10	24	8	600	200	200	200	600	4800	4800
10		C-Is#-10	35	420	345	10	26	8	600	200	200	200	600	5200	4800
11		C-Is#-11	35	420	345	10	28	8	600	200	200	200	600	5600	4800
12		C-Is#-12	35	420	345	10	30	8	600	200	200	200	600	6000	4800

4.5.1. Tension Flange Yielding (TFY)

Table 4.6 lists the determined tension flange yielding (TFY) moment capacity of composite section of merged concrete-steel compressive region (Mode II). The results depict that, always there are an domain of cover plate thickness that compatible with main design criteria which maintain optimum section of compatible tension and compression force and do not affect the other modes to be attained, in current study the overall flange area steel thickness ranged between 8mm to 30 mm. Generally, the variation of thickness corresponding with significantly improving in composite section tension flange yielding (TFY), and the improving rates ranged between 1 to 2 as the thickness changed from 8mm to 30 mm which confirmed that the increasing of bottom flange thickness till 30 mm without turning failure to compression mode is allowed in this mode. Figure 4.19 clearly depicts the effect of bottom flange thickness on TFY moment capacity in composite Mode II

Table 4- 6 tension flange yielding (TFY) moment capacity -mode II

No.	Var.	Code	T	C	a	yf	Yw	M, kN.m	Rates
1	Cover steel plate	C-Is#-1	2328000	4410000	37.65	591.18	291.18	879.46	1.00
2		C-Is#-2	2496000	4410000	47.06	586.47	286.47	967.03	1.10
3		C-Is#-3	2664000	4410000	56.47	581.76	281.76	1053.02	1.20
4		C-Is#-4	2832000	4410000	65.88	577.06	277.06	1137.43	1.29
5		C-Is#-5	3000000	4410000	75.29	572.35	272.35	1220.26	1.39
6		C-Is#-6	3168000	4410000	84.71	567.65	267.65	1301.51	1.48
7		C-Is#-7	3336000	4410000	94.12	562.94	262.94	1381.17	1.57
8		C-Is#-8	3504000	4410000	103.53	558.24	258.24	1459.26	1.66
9		C-Is#-9	3672000	4410000	112.94	553.53	253.53	1535.76	1.75
10		C-Is#-10	3840000	4410000	122.35	548.82	248.82	1610.68	1.83
11		C-Is#-11	4008000	4410000	131.76	544.12	244.12	1684.02	1.91
12		C-Is#-12	4176000	4410000	141.18	539.41	239.41	1755.78	2.00

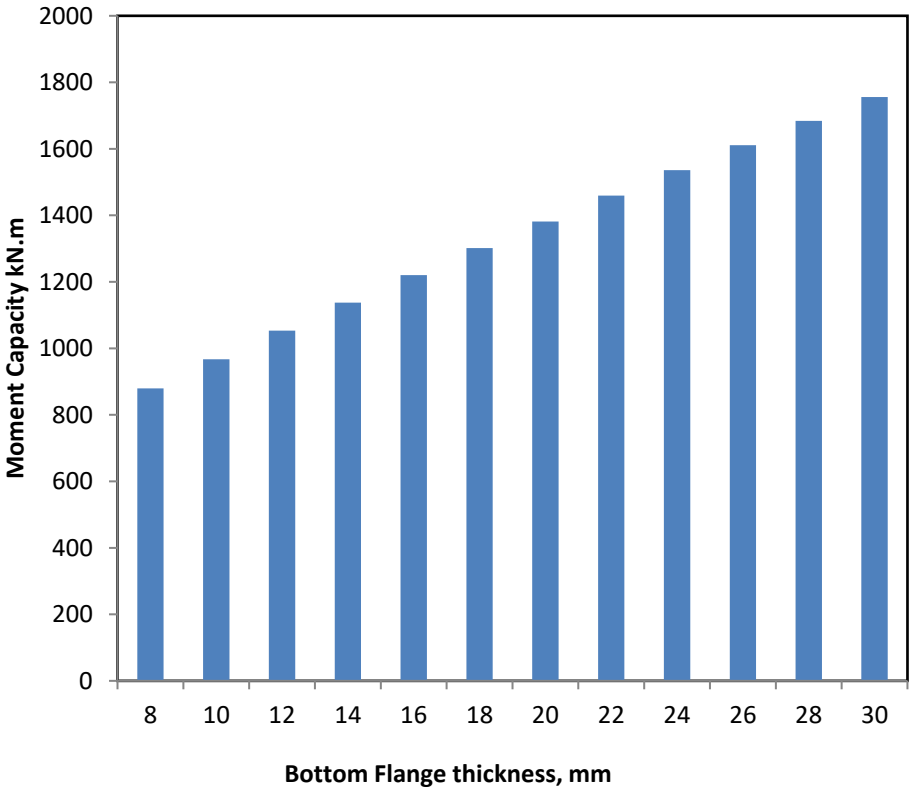

Figure 4- 19 Effect of bottom flange thickness on TFY moment capacity-Mode II

4.5.2. Compression Flange Yielding (CFY)

Table 4.7 lists the determined compression flange yielding (CFY) moment capacity of composite section of merged concrete-steel compressive region (Mode II). Likewise, TFY, the variation of the adopted cover plate thickness affects the CFY moment capacities with various rates. The best improving of 2.16 rate, is associated with the highly tension area of 30 mm. The comparative analysis between TFY and CFY shows that, the dominated failure mode is TFY where the rate of CFY moment capacities to TFY moment capacities more than 1 for all samples, the high rate is 1.1 and associated with highly cover plate thickness. Figure 4.20 depicts comparative analysis of TFY verse CFY moment capacities in scope of the full bottom flange thickness effectiveness.

Table 4- 7 Compression flange yielding (CFY) moment capacity -Mode II

No.	Var.	Code	T	C	a	yf	Yw	aw	Rpg	M, kN.m	Rates	CFY/TFY
1	Cover steel plate	C-Is#-1	2328000	4242000	37.65	591.18	291.18	0.8	0.989	902.81	1.00	1.03
2		C-Is#-2	2496000	4410000	47.06	586.47	286.47	0.8	0.989	1005.88	1.11	1.04
3		C-Is#-3	2664000	4578000	56.47	581.76	281.76	0.8	0.989	1107.37	1.23	1.05
4		C-Is#-4	2832000	4746000	65.88	577.06	277.06	0.8	0.989	1207.27	1.34	1.06
5		C-Is#-5	3000000	4914000	75.29	572.35	272.35	0.8	0.989	1305.60	1.45	1.07
6		C-Is#-6	3168000	5082000	84.71	567.65	267.65	0.8	0.989	1402.34	1.55	1.08
7		C-Is#-7	3336000	5250000	94.12	562.94	262.94	0.8	0.989	1497.50	1.66	1.08
8		C-Is#-8	3504000	5418000	103.53	558.24	258.24	0.8	0.989	1591.09	1.76	1.09
9		C-Is#-9	3672000	5586000	112.94	553.53	253.53	0.8	0.989	1683.09	1.86	1.10
10		C-Is#-10	3840000	5754000	122.35	548.82	248.82	0.8	0.989	1773.50	1.96	1.10
11		C-Is#-11	4008000	5922000	131.76	544.12	244.12	0.8	0.989	1862.34	2.06	1.11
12		C-Is#-12	4176000	6090000	141.18	539.41	239.41	0.8	0.989	1949.60	2.16	1.11

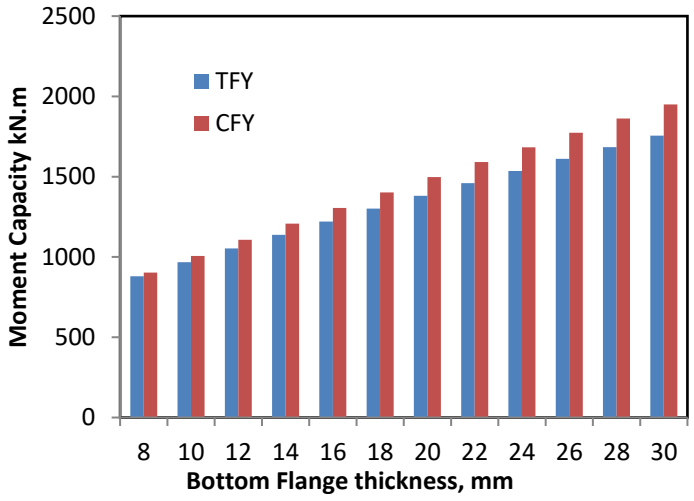

Figure 4- 20 Comparative analysis of bottom flange thickness effectiveness on moment capacity -TFY verse CFY

4.5.3. Lateral-Torsional Buckling (LTB)

Lateral-Torsional Buckling limit state is overall lateral buckling of the compression flange of the section and occurs when a compression flange of beam lacks lateral support. Table 4.8 lists the determined lateral-torsional buckling (LTB) moment capacity of composite section of merged concrete-steel compressive region: (Mode II). For various provided cover steel plate, the present constrain turned the assigned lateral-torsional buckling mode from elastic lateral-torsional buckling to plastic lateral – torsional buckling mode for a certain length domain, more than from (14 m to 20 m), the clearly strength different between two attainted modes are shown in Figure 4.21 illustrates the effect of mid span constraining on LTB moment capacity in Mode II, for various cover plate thickness.

Table 4- 8 Lateral-torsional buckling (LTB) moment capacity -Mode 2

No.	Var.	Code	cover plate, mm	r	Lr	LP	Lb	fcr	LTB-plastic	Lb	fcr	LTB-elastic
1	Unbraced length	C-Is#-1	0	6.41	13.32	3.91	7.00	418.73	445.90	14.00	39.95	101.80
2			0	6.41	13.32	3.91	8.00	405.36	430.14	16.00	35.12	89.48
3			0	6.41	13.32	3.91	9.00	391.98	414.39	18.00	31.11	79.26
4			0	6.41	13.32	3.91	10.00	378.60	398.63	20.00	27.75	70.70
5			0	6.41	13.32	3.91	11.00	365.23	382.88	22.00	24.90	63.45
6			0	6.41	13.32	3.91	12.00	351.85	367.12	24.00	22.47	57.26
7	Unbraced length	C-Is#-7	10	6.41	13.32	3.91	7.00	418.73	944.90	14.00	39.95	140.39
8			10	6.41	13.32	3.91	8.00	405.36	914.72	16.00	35.12	123.39
9			10	6.41	13.32	3.91	9.00	391.98	884.53	18.00	31.11	109.30
10			10	6.41	13.32	3.91	10.00	378.60	854.34	20.00	27.75	97.50
11			10	6.41	13.32	3.91	11.00	365.23	824.16	22.00	24.90	87.50
12			10	6.41	13.32	3.91	12.00	351.85	793.97	24.00	22.47	78.97
13	Unbraced length	C-Is#-12	20	6.41	13.32	3.91	7.00	418.73	1357.23	14.00	39.95	175.22
14			20	6.41	13.32	3.91	8.00	405.36	1313.87	16.00	35.12	154.01
15			20	6.41	13.32	3.91	9.00	391.98	1270.51	18.00	31.11	136.42
16			20	6.41	13.32	3.91	10.00	378.60	1227.16	20.00	27.75	121.68
17			20	6.41	13.32	3.91	11.00	365.23	1183.80	22.00	24.90	109.21
18			20	6.41	13.32	3.91	12.00	351.85	1140.44	24.00	22.47	98.56

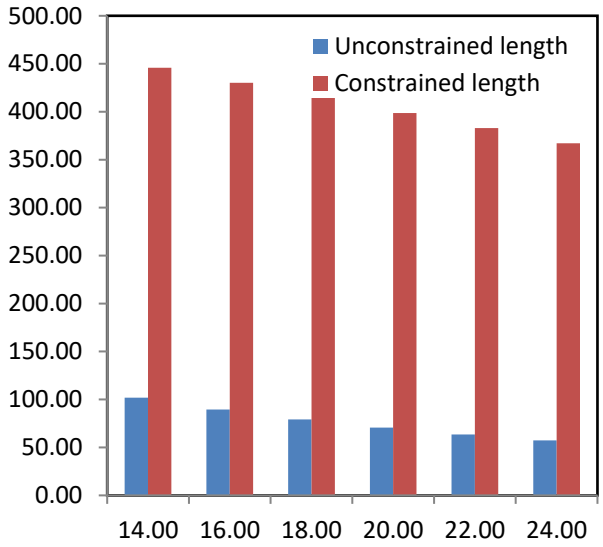

Without cover plate

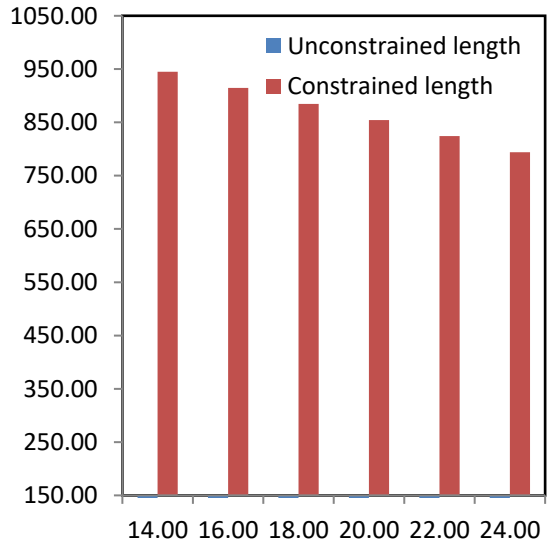

Cover plate thickness =10 mm

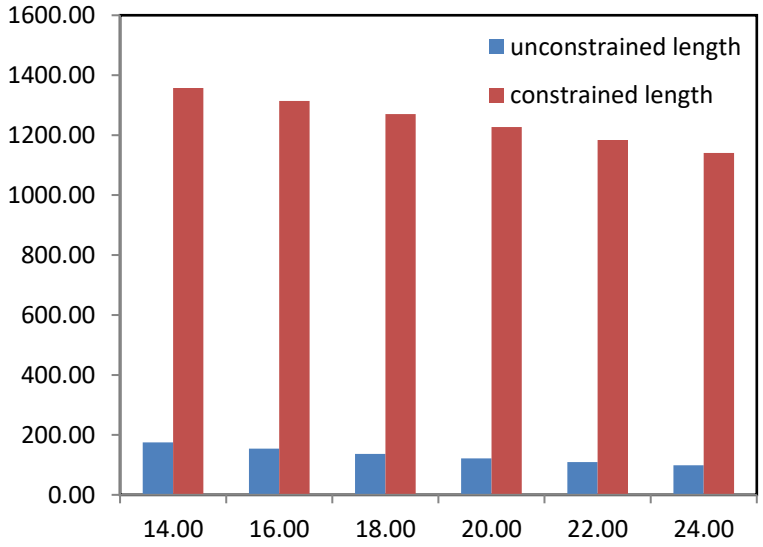

Cover plate thickness =20 mm

Figure 4- 21 Effect of mid span constraining on LTB moment capacity-Mode II for various cover plate thickness

4.6. Composite section of built up multi flanged U steel section: (Mode III)

Table 4.9 exhibits the specimen's matrix details of composite section of built up multi flanged U steel section (Mode III), wide spectrum of sample are considered,

the target variation is provided of various number (0-3) of multi intermediate flanges within web region, the samples are classified according to provided flange thickness. The providing intends constrained steel thin element within built up steel section and to turn the slender steel element to compacted or non-compacted, besides, providing additional tension area to contribute in enhancing flexural section capacity.

Table 4- 9 Specimens Details - ModeIII

No.	Var.	Designation	Nf	Fc'	fyf	fyw	ttf	tbf	tw	bc	hc	btf	bbf	hw	Asf	Asw
1	Intermediate flanges numbers, Nf	C-Us-1	1	35	420	345	10	10	4	600	200	200	200	600	2000	4800
2		C-Us-2	1	35	420	345	10	20	4	600	200	200	200	600	4000	4800
3		C-Us-3	1	35	420	345	10	30	4	600	200	200	200	600	6000	4800
4		C-Us-4	2	35	420	345	10	10	4	600	200	200	200	600	2000	4800
5		C-Us-5	2	35	420	345	10	20	4	600	200	200	200	600	4000	4800
6		C-Us-6	2	35	420	345	10	30	4	600	200	200	200	600	6000	4800
7		C-Us-7	3	35	420	345	10	10	4	600	200	200	200	600	2000	4800
8		C-Us-8	3	35	420	345	10	20	4	600	200	200	200	600	4000	4800
9		C-Us-9	3	35	420	345	10	30	4	600	200	200	200	600	6000	4800

4.6.1. Tension Flange Yielding (TFY)

Table 4.10 lists the determined tension flange yielding (TFY) moment capacity of composite section of multi flanges number (Mode III) for various presented flange number of various thicknesses. For specific flange number, the determined moment capacity increased as flange thickness increased, the assigned strength is extremely improved as flange number increase for a certain limit of provide the tension area where the provided tension force component more than the corresponding compressive force and so, the section could be turned to be over. In current case study, two flanges of various flange thickness are proper for compactable design (the improving rates are 2.16 and 2.73) while the three-flange conditioned by lower flange

thickness (10mm) (the improving rates is 1.82. Figure 4.22 shows the effect of intermediate flanges number on TFY moment capacity for various flange thickness.

Table 4- 10 Tension flange yielding (TFY) moment capacity- Mode III

No.	Var.	Code	Nf	tbf	T	C	a	yf	Yw	M, kN.m	Rates
1	Intermediate flanges numbers, Nf	C-Us-1	1	10	2496000	4410000	47.06	586.47	286.47	967.03	1.00
2		C-Us-2		20	3336000	4410000	94.12	562.94	262.94	1381.17	1.43
3		C-Us-3		30	4176000	4410000	141.18	539.41	239.41	1755.78	1.82
4		C-Us-4	2	10	3336000	4410000	94.12	562.94	262.94	1381.17	1.43
5		C-Us-5		20	5016000	4410000	188.24	515.88	215.88	2090.87	2.16
6		C-Us-6		30	6696000	4410000	282.35	468.82	168.82	2642.44	2.73
7		C-Us-7	3	10	4176000	4410000	141.18	539.41	239.41	1755.78	1.82
8		C-Us-8		20	6696000	4410000	282.35	468.82	168.82	2642.44	2.73
9		C-Us-9		30	9216000	4410000	423.53	398.24	98.24	3173.34	3.28

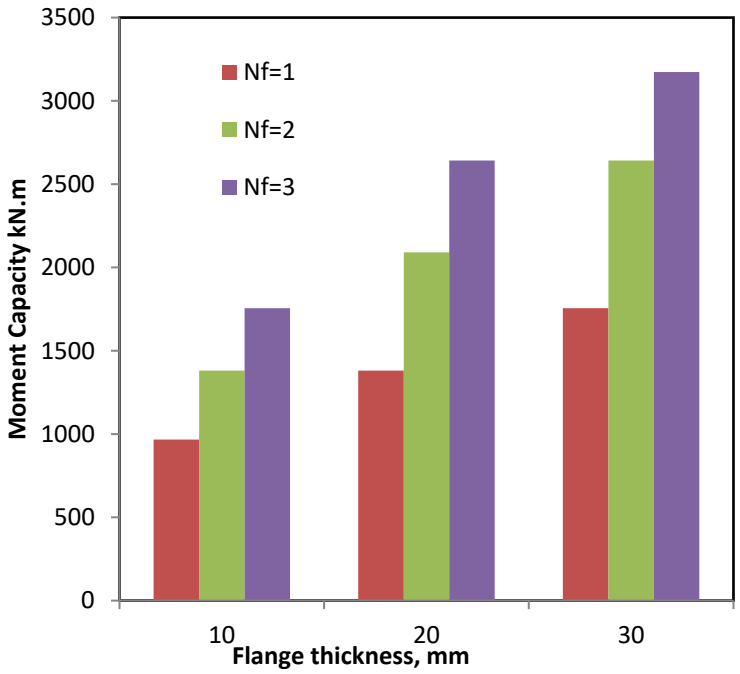

Figure 4- 22 Effect of intermediate flanges number on TFY moment capacity for various flange thickness

4.6.2. Compression Flange Yielding (CFY)

Table 4.11 lists the determined compression flange yielding (CFY) moment capacity of composite section of multi flanges (Mode III). The compression flange yielding (CFY) significantly affected by mode configuration, for specific geometry characteristic, CFY tends to be dominated failure mode where MCFY/MTFY less than 1 as shown in Table 4.11. Generally, for specific flange number, the determined moment capacity increased as flange thickness increased, the assigned strength is extremely improved as flange number increase for a certain limit of provides the tension area. In current case study, two flanges of various flange thickness are proper for compactable design (the improving rates are 2.73 and 3.63) where the rate of CFY to TFY approximately and likewise TFY, the three-flange conditioned by lower flange thickness (10mm) (the improving rates is 2.21. Figure 4.22 shows the effect of intermediate flanges number on TFY moment capacity for various flange thickness. Figure 4.23 is clearly depicting the effect of intermediate flanges number on CFY moment capacity for various flange thickness while Figure 4.24 exhibits comparative view of CFY verse TFY modes that depicts the effect of intermediate flanges number on moment capacity for various flanges thickness.

Table 4- 11 Compression flange yielding (CFY) moment capacity Mode III

No.	Var.	Code	Nf	tbf	T	C	a	yf	Yw	aw	Rpg	M, kN.m	Rates	CFY/TFY
1	Intermediate flanges numbers, Nf	C-Us-1	1	10	1668000	4410000	47.059	586.471	286.471	0.4	0.986	748.65	1.00	0.77
2		C-Us-2	1	20	2508000	5250000	94.118	562.941	262.941	0.4	0.986	1220.96	1.63	0.88
3		C-Us-3	1	30	3348000	6090000	141.176	539.412	239.412	0.4	0.986	1653.75	2.21	0.94
4		C-Us-4	2	10	2508000	4410000	94.118	562.941	262.941	0.4	0.986	1220.96	1.63	0.88
5		C-Us-5	2	20	4188000	5250000	188.235	515.882	215.882	0.4	0.986	2047.01	2.73	0.98
6		C-Us-6	2	30	5868000	6090000	282.353	468.824	168.824	0.4	0.986	2714.94	3.63	1.03
7		C-Us-7	3	10	3348000	4410000	141.176	539.412	239.412	0.4	0.986	1653.75	2.21	0.94
8		C-Us-8	3	20	5868000	5250000	282.353	468.824	168.824	0.4	0.986	2714.94	3.63	1.03
9		C-Us-9	3	30	8388000	6090000	423.529	398.235	98.235	0.4	0.986	3420.37	4.57	1.08

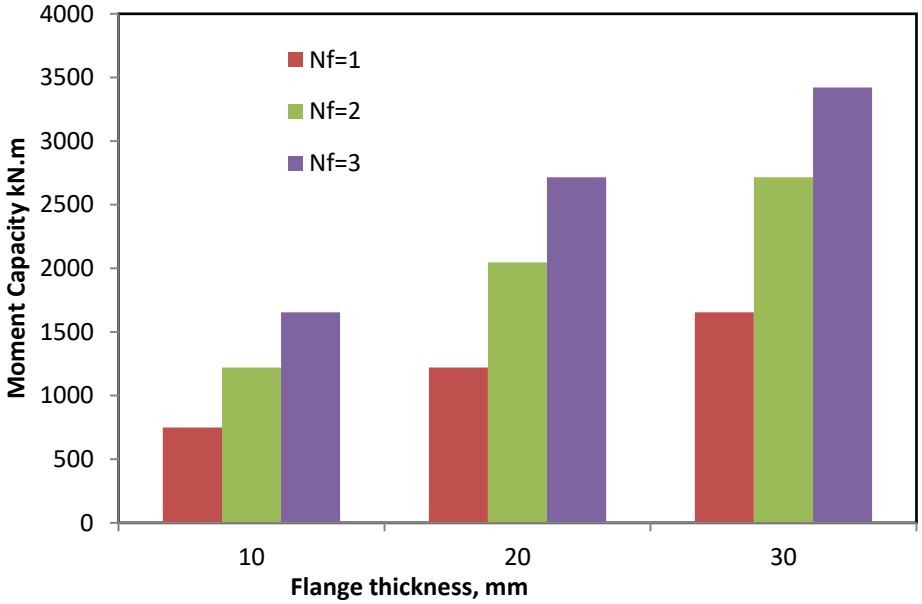

Figure 4- 23 Effect of intermediate flanges number on CFY moment capacity for various flange thickness

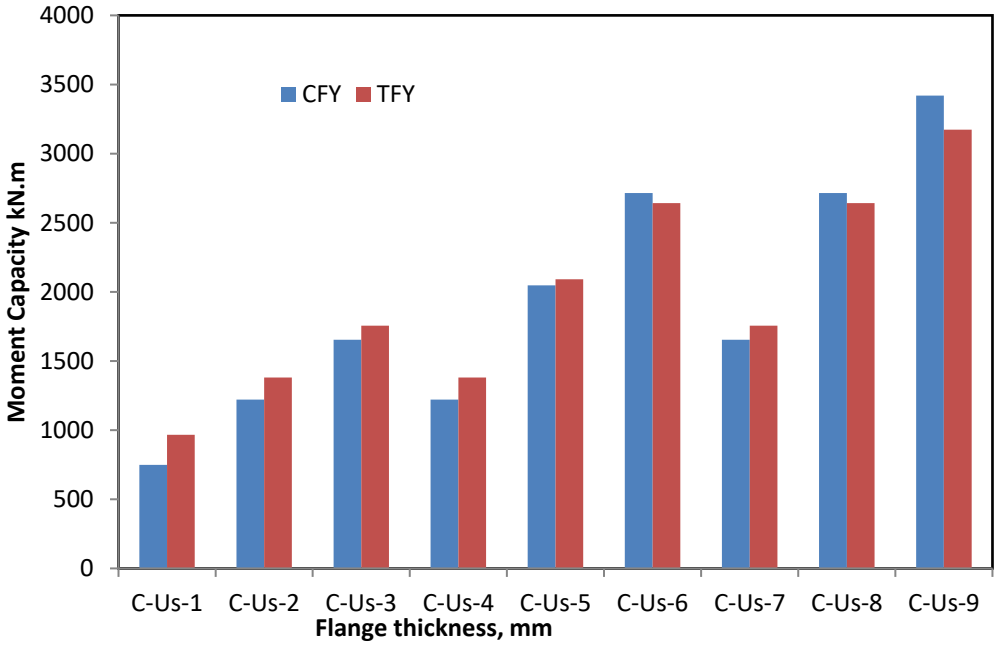

Figure 4- 24 Effect of intermediate flanges number on moment capacity for various flanges thickness CFY verse TFY modes

4.6.3. Lateral-Torsional Buckling (LTB)

Table 4.12 lists the determined lateral-torsional buckling (LTB) moment capacity of composite section of multi flanges (Mode III). Likewise previous modes, for various provided flanges, the present constrain turned the assigned lateral-torsional buckling mode from elastic lateral-torsional buckling to plastic lateral – torsional buckling mode for a certain length domain, more than from (14 m to 20 m), the clearly strength different between two attainted modes are shown in Figure 4.21 illustrates the effect of mid span constraining on LTB moment capacity in Mode III, for various intermediate flanges. Figure 4.25 illustrates the effect of intermediate multi flanges number on LTB moment capacity in proposed composite mode III

Table 4- 12 lateral-torsional buckling (LTB) moment capacity - Mode III

No.	Var.	Code	Nf	r	Lr	LP	Lb	fcr	LTB-plastic	Lb	fcr	LTB-elastic
1	Unbraced length	C-Us-2	1	6.41	13.32	3.91	7.00	418.73	854.34	14.00	39.95	161.17
2			1	6.41	13.32	3.91	8.00	405.36	824.16	16.00	35.12	123.39
3			1	6.41	13.32	3.91	9.00	391.98	793.97	18.00	31.11	97.50
4			1	6.41	13.32	3.91	10.00	378.60	763.79	20.00	27.75	78.97
5			1	6.41	13.32	3.91	11.00	365.23	733.60	22.00	24.90	65.27
6			1	6.41	13.32	3.91	12.00	351.85	703.41	24.00	22.47	54.84
7	Unbraced length	C-Us-5	2	6.41	13.32	3.91	7.00	418.73	783.08	14.00	39.95	142.17
8			2	6.41	13.32	3.91	8.00	405.36	755.41	16.00	35.12	108.85
9			2	6.41	13.32	3.91	9.00	391.98	727.74	18.00	31.11	86.01
10			2	6.41	13.32	3.91	10.00	378.60	700.07	20.00	27.75	69.66
11			2	6.41	13.32	3.91	11.00	365.23	672.40	22.00	24.90	57.57
12			2	6.41	13.32	3.91	12.00	351.85	644.74	24.00	22.47	48.38
13	Unbraced length	C-Us-8	3	6.41	13.32	3.91	7.00	418.73	711.81	14.00	39.95	123.18
14			3	6.41	13.32	3.91	8.00	405.36	686.66	16.00	35.12	94.31
15			3	6.41	13.32	3.91	9.00	391.98	661.51	18.00	31.11	74.52
16			3	6.41	13.32	3.91	10.00	378.60	636.36	20.00	27.75	60.36
17			3	6.41	13.32	3.91	11.00	365.23	611.21	22.00	24.90	49.88
18			3	6.41	13.32	3.91	12.00	351.85	586.06	24.00	22.47	41.91

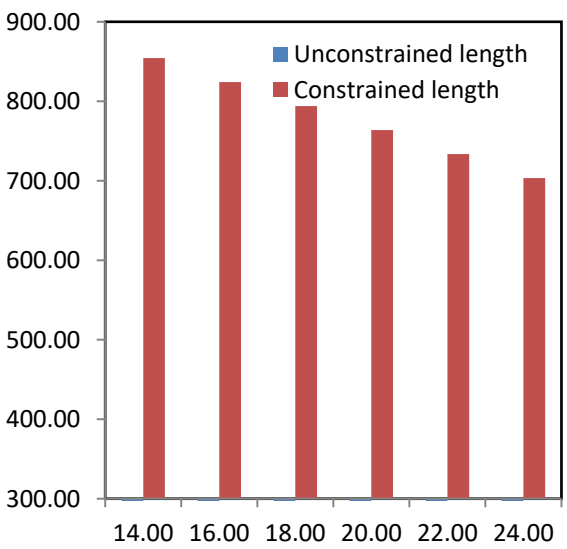

Nf=1

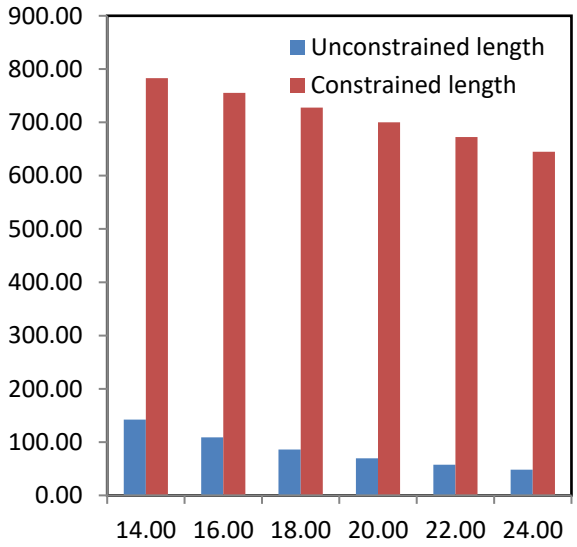

Nf=2

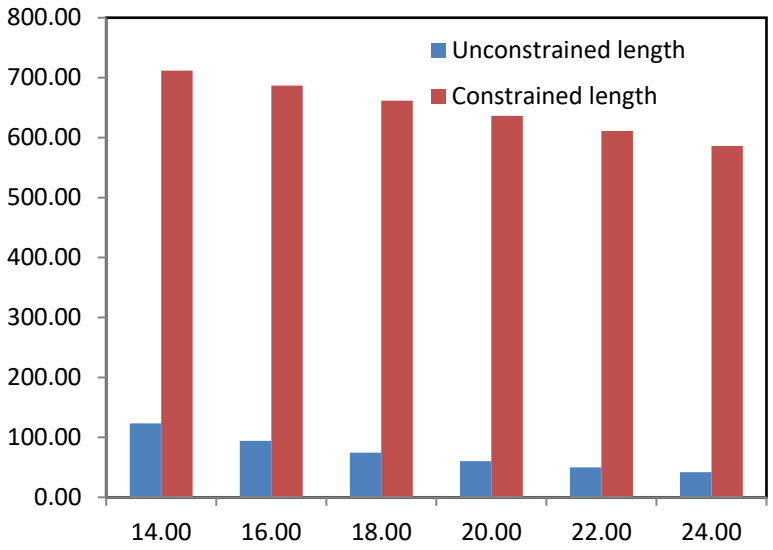

Nf=3

Figure 4- 25 Effect of intermediate multi flanges number on LTB moment capacity

4.7 Finite Element Modeling

In this study, a non-linear analysis is carried out using the technique of the theory of the finite element and by employing the ANSYS program that works with this theory. During the analysis, the geometry and material nonlinearities are taken into consideration to simulate the behavior of the beam-column joints. In the stage of preprocessing, selecting the suitable elements for the materials, and input the real behavior reaching to the loading and boundary conditions were performed to simulate the experimental test with the same condition. Defining the behavior of the material can be performed by the use of constitutive models. To define concrete nonlinearity as a quasi-brittle material, smeared and brittle cracking models, the concrete damage Plasticity (CDP) is selected. A verification process was performed on two joints by finite element analysis with ANSYS APDL. The verification has been carried out with the experimental work that previously implemented by group of researchers [59] through the load-displacement relationship, ultimate load, and displacement, and cracks pattern. The validation revealed with the experiemental specimens that presented by Sangeetha et al. [59] showed a good agreement with the experimental results as revealed in Table 4.13. The finite element model has 12684 elements. A convergence criterion was utilized about the refine mesh and input values, which showed non-convergence occur below 0.2 of the open and close shear transfer coefficients and very good matching occurred in the number of the elements over 8000 elements.

Table 4.13: Verification results.

Beam ID	$P_{u, Exp}$	$P_{u, ANSYS}$	P_u%	$\Delta_{Exp.}$	Δ_{ANSYS}	Δ%
CB-2SC	50	51.67	96.76%	1.76	1.59	90.34%
CB-4SC	75	73.41	97.88%	2.61	2.51	96.17%

4.7.1 Load-displacement relationship

In order to investigate the different variables on the load carrying capacity and maximum displacement of the composite beams, numerical simulation of composite beams were performed in ANSYS software. The parameters of the beams were the location of the steel section which placed under the concrete section and inside the concrete section as seen in Figure (4-26 a & b). The third model included use of steel plate in form of U-shape grooved inside the concrete section as seen in Figure (4-26 c). the load carrying capacity reached to (2568.5 kN) and displacement by (42.17) mm as revealed in Figure (4-27). The load capacity reduced to (2510.8) kN and the displacement increased to (59.17) mm when the steel section moved inside the concrete section (Figure 26 b) which equal to reduction in strength by (3%) and increment in the displacement by (40%) as revealed in Figure (4-28). It should be noted that the beam with mode II depicts a slight strain hardening. The third model with steel plates showed decrement in the ultimate strength by (19.5%) and slight increment in the displacement as revealed in Figure (4-29).

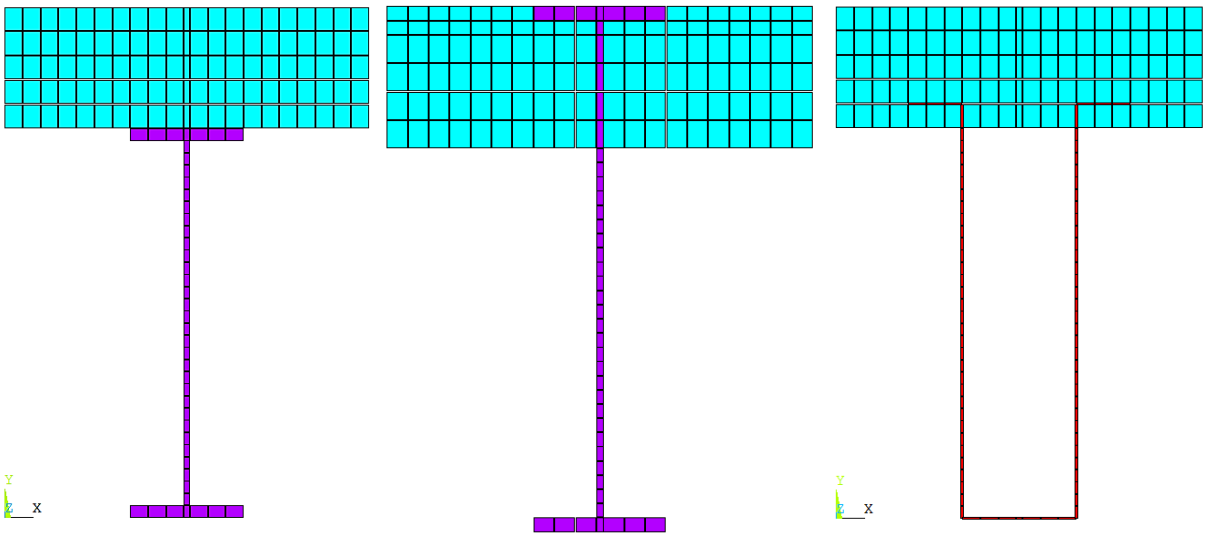

(a) (b) (c)

Figure 4- 26 Numerical models simulation.

Table 4- 13 Details of specimens.

ID	*f*'c	Parameters	Pcr (kN)	Defl. cr (mm)	Pu (kN)	Linearity (%)	Pw (kN)	Defl. (mm)
Mode 1	35	-	392	4.05	2568.5	15.26%	1712.33	43
Mode 1-45	45	*f*'c	477	4.35	2788.5	17.11%	1859.00	52.77
Mode 1-55	55	*f*'c	540	5.23	2880	18.75%	1920.00	55.41
Mode 2	35	-	364	4.94	2510	14.50%	1673.33	12.1
Mode 2 -DF	35	Double flange	441	7.44	3254.6	13.55%	2169.76	36.24
Mode 2-TF	35	Triple flange	458	10.36	3877.9	11.81%	2585.30	54.42
Mode 3	35	-	284	4.21	2066.7	13.74%	1377.80	50.89
Mode 3- DP	35	Double Plate	354	12.46	3238.2	10.93%	2158.82	64.12
Mode 3- TP	35	Triple Plate	410	13.25	3489.3	11.75%	2326.23	68.45

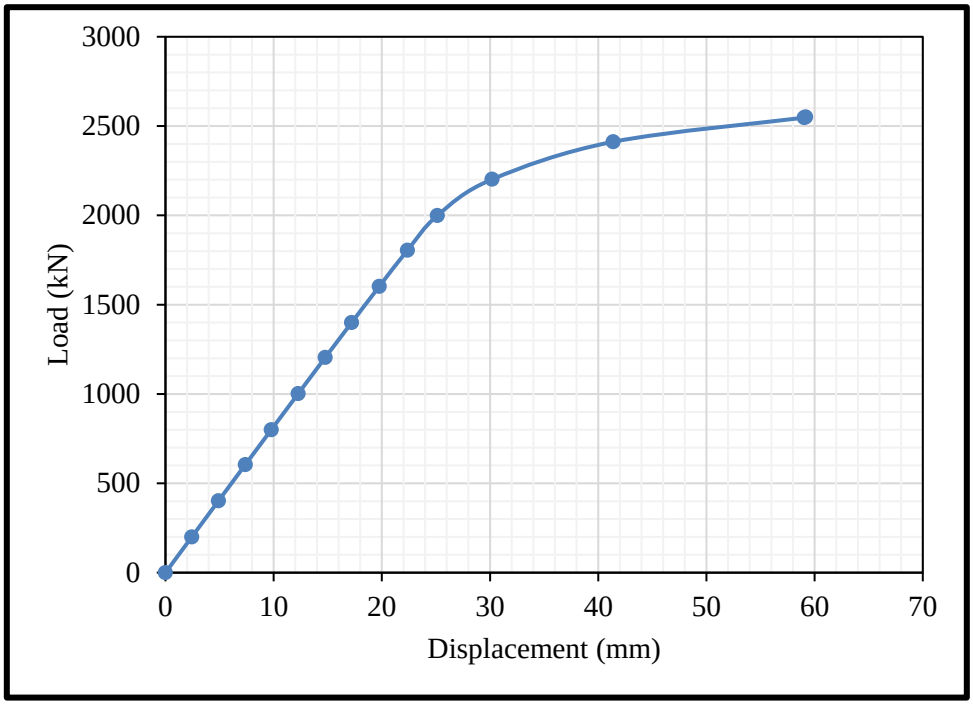

Figure 4- 27 Load displacement relationship of composite beam (Mode 1)

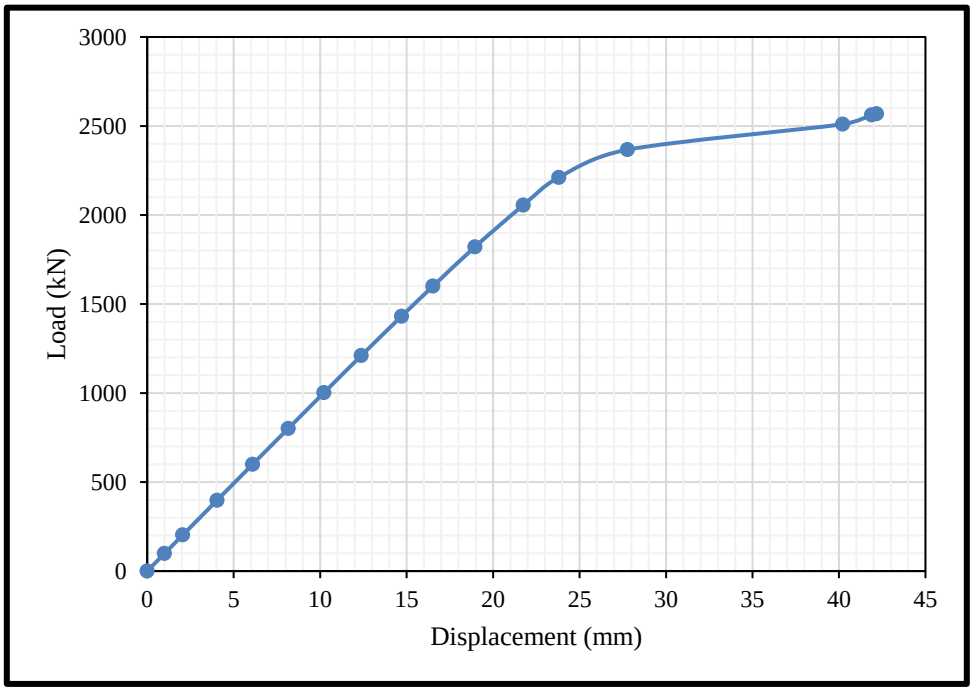

Figure 4- 28 Load displacement relationship of composite beam (Mode 2)

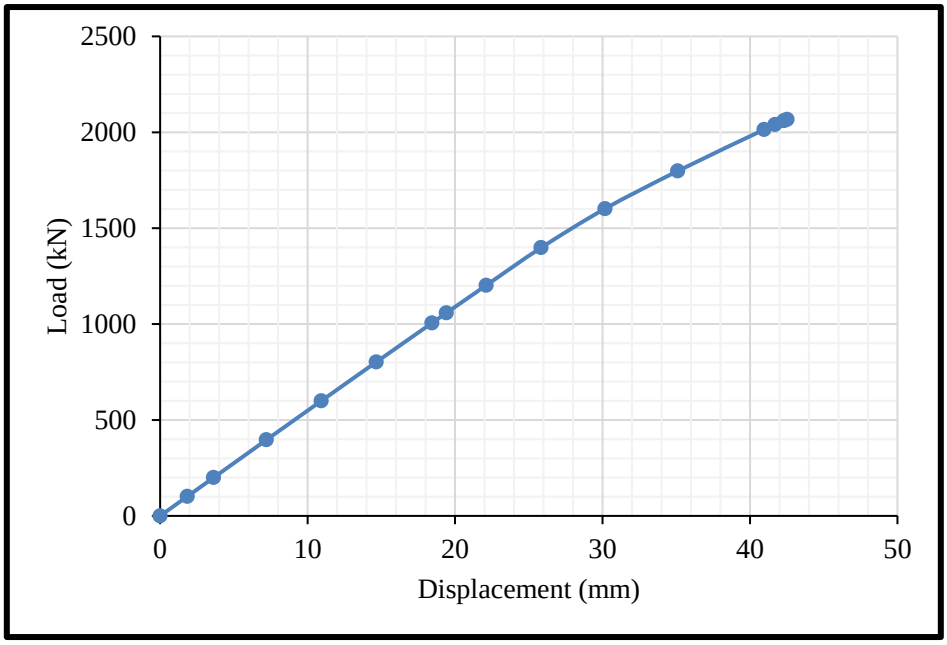

Figure 4- 29 Load displacement relationship of composite beam (Mode 2)

The additional parameters of the beams were the thickness of flanges in the merged composite beam, in addition to the number of intermediate plates (two and three plates). The composite beam behaves as a linear material until reaching the yield point of the concrete. Overhead this point, the load increases gradually up and reaches the maximum load capacity. The load carrying capacity reached to (2568.5 kN) and displacement by (42.17) mm as revealed Table (4-13). Concerning the effect on the of the variables on the cracking load, the increase of the compressive strength of the traditional composite beams to 45 and 55 MPa enhanced the cracking load by 21.7% and 37.8% respectively in comparison with the Mode I beam as revealed in Figure (4-29 a). Increase the flange thickness for the mode II beams to double and trible thickness enhanced the cracking load by (21%) and (25.8%) respectively when compared with the MODE II beam as revealed in Figure (4-29 b). Doubling the thickness into two and three times for

beams (Mode 3-DP and Mode 3-TP) upgraded the cracking load by (24.7% and 44.4%) respectively when compared with Mode 3 beam as depicted in Figure (4-29 c). Concerning the ultimate load and maximum displacement, the results showed that the increase of the compressive strength to 45 and 55 MPa enhanced the ultimate load carrying capacity by 8.56% and 12.1% respectively as revealed in Figure (4-30 a). The increase of flange thickness to (40 and 60 mm) for merged composite beams enhanced the ultimate load carrying capacity by 29.66% and 54.4% respectively as revealed in Figure (4-30 b). The increase of intermediate plates for the multi-flange composite beam to two and three plates enhanced the ultimate load by 56.7% and 68.8% respectively as seen in Figure (4-30 c). Regarding the deflection, the results showed that the increase of the compressive strength to 45 and 55 MPa enhanced the maximum deflection by 7.4% and 29% respectively as revealed in Figure (4-31 a). The increase of flange thickness to (40 and 60 mm) for merged composite beams upgraded the maximum deflection too much which were by 50.6% and 101% respectively as revealed in Figure (4-31 b). The increase of intermediate plates for the multi-flange composite beam to two and three plates led to huge upgrade in the maximum deflection by 195.9% and 214.7% respectively as seen in Figure (4-31 c).

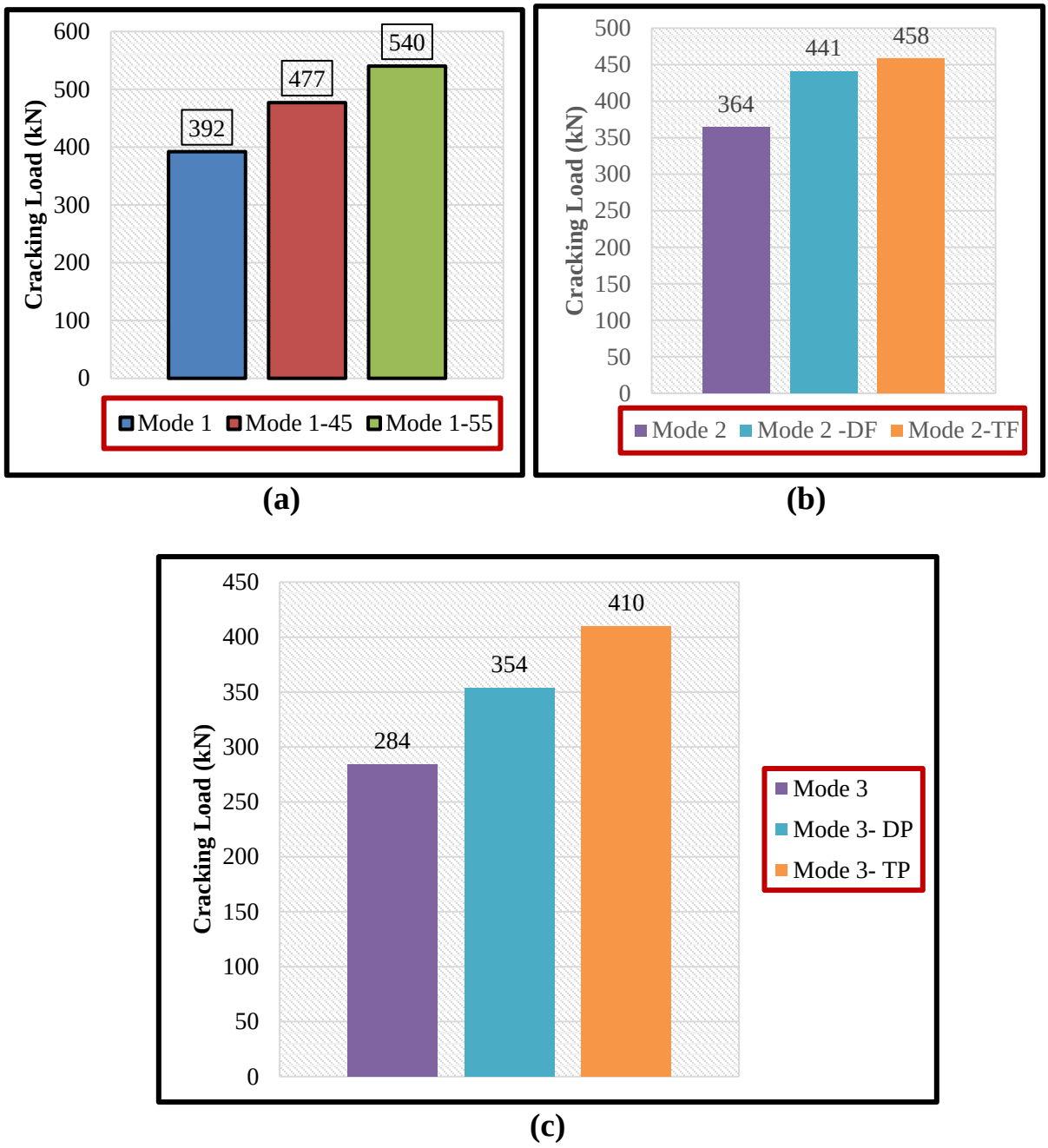

Figure 4- 30 Cracking load of the composite beam.

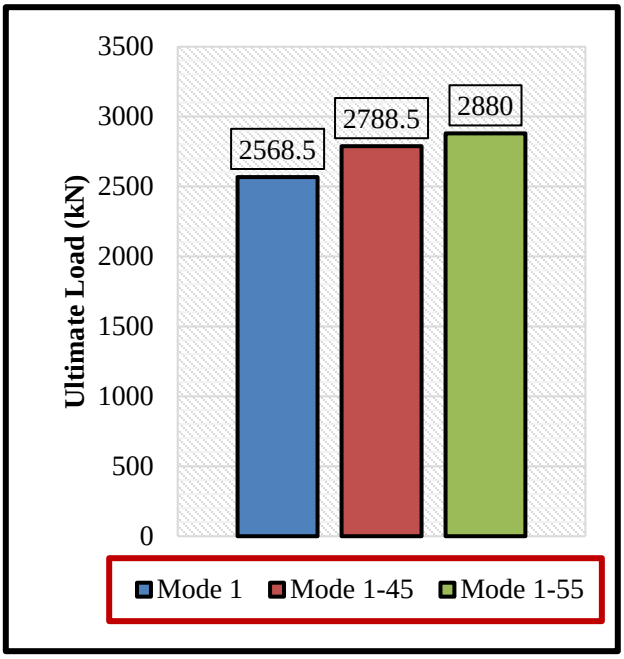

(a)

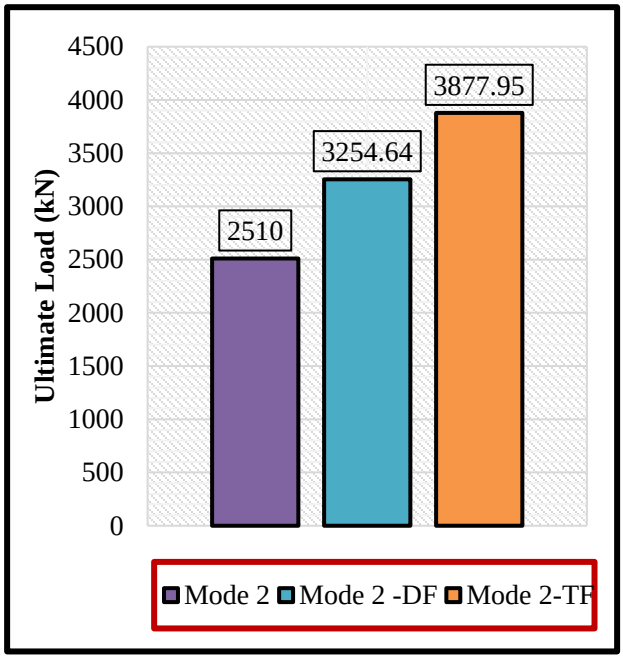

(b)

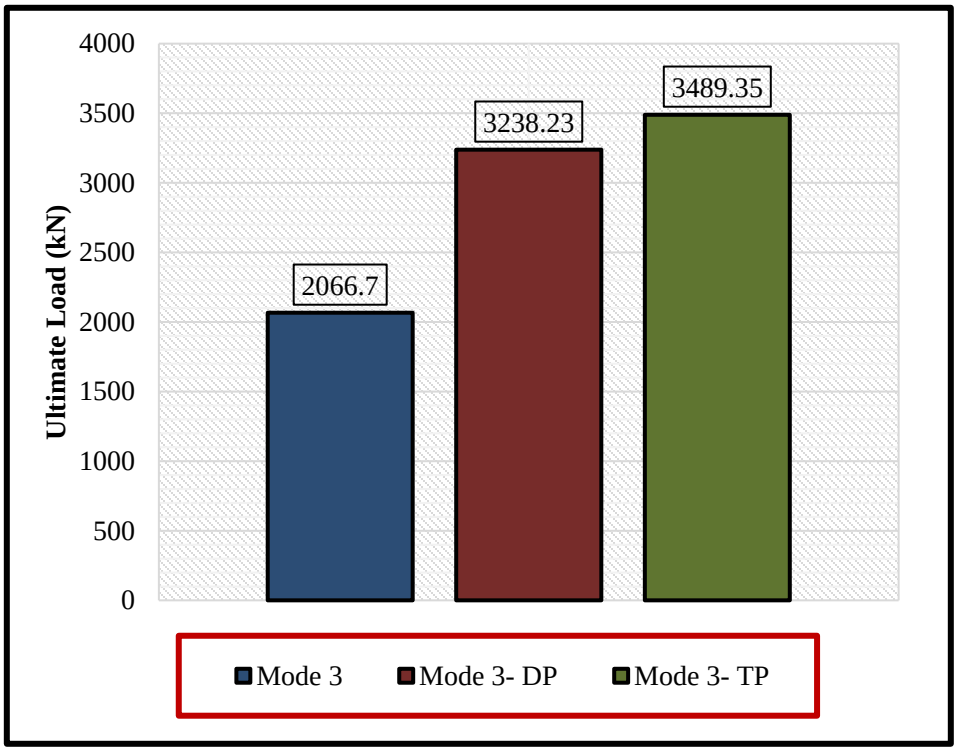

(c)

Figure 4- 31 Ultimate load of the composite beam.

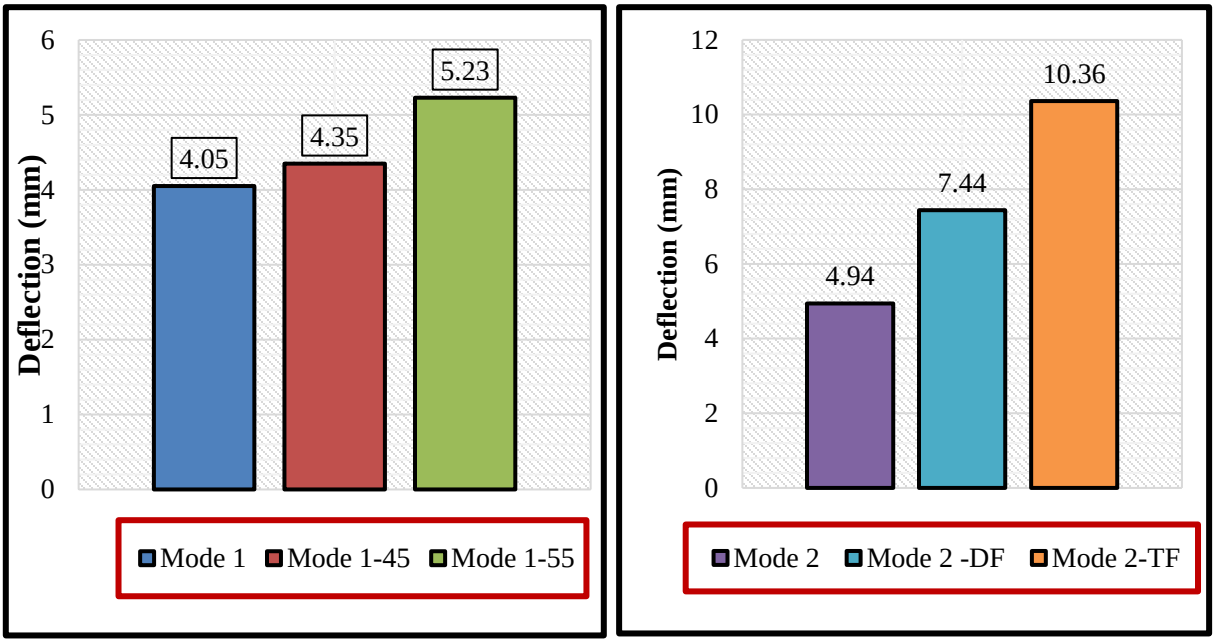

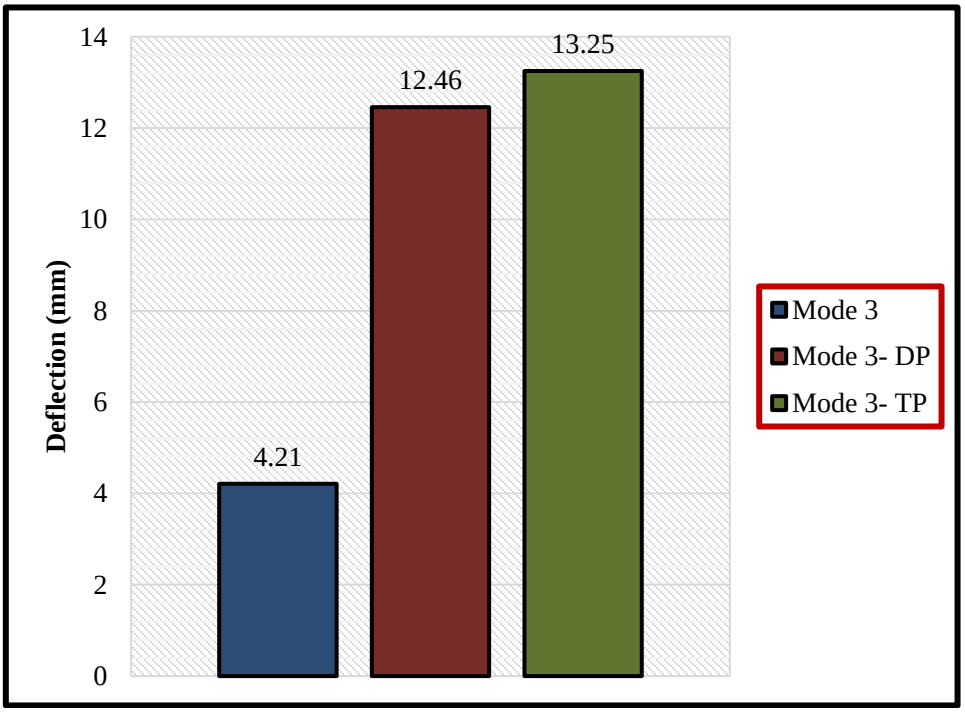

Figure 4- 32 Maximum displacement of the composite beam.

4.7.2 Crack Pattern

The crack pattern showed that the composite beams failed in concrete which the stresses concentrated at the concrete section more that the steel section beside that the concrete section has the minimum requirement of steel reinforcement for shrinkage as revealed in Figure (4-31). Huge spread of cracks appeared at the mode 1 beam which the crack propagated along the beam. Shifting the steel section inside the concrete beam reduced the cracks spread and concentrated the cracks at the mid span region. Use of steel plate showed higher stresses along the concrete and less stresses in the steel plate.

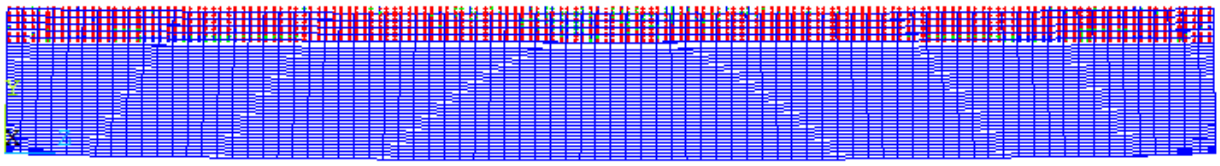

(a) Mode 1

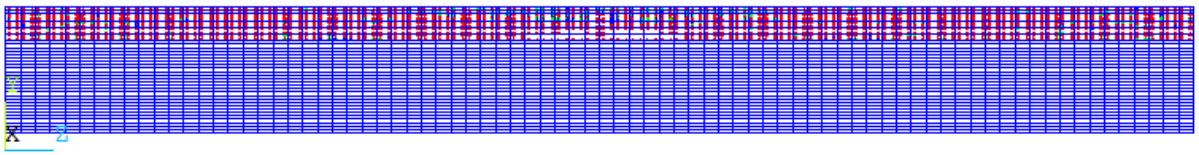

(b) Mode 2

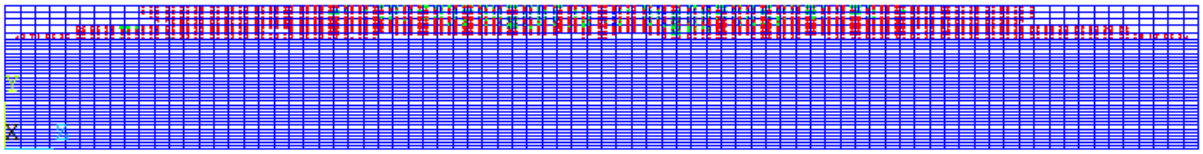

(c) Mode 3

Figure 4- 33 Crack pattern of composite beams side view

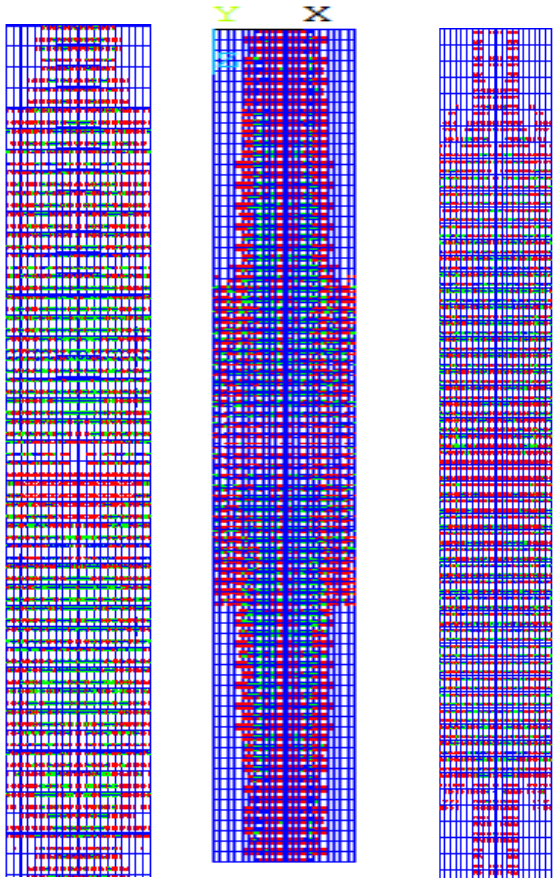

(a) Mode 1 (b) Mode 2 (c) Mode 2

Figure 4- 34 Crack pattern of composite beams top view

4.7.3 Stress Distribution

Figure (4-34) to (4-36) exhibited the stresses distribution within composite section of various mode, the stress distribution confirmed that the results were related to the ductility improvement of mode II with slightly strength hardening while the absence of the multi-flanges affected the behavior of the section that have the mode III. Stress distribution in all beams showed different distribution. Level of intensity ranged from colors (blue-green- yellow-brown-red) respectively in concentration, the minimum intensity is blue while maximum intensity referred in red color. It must

be noticed that these figures explained the path of stresses and the zones of its concentration

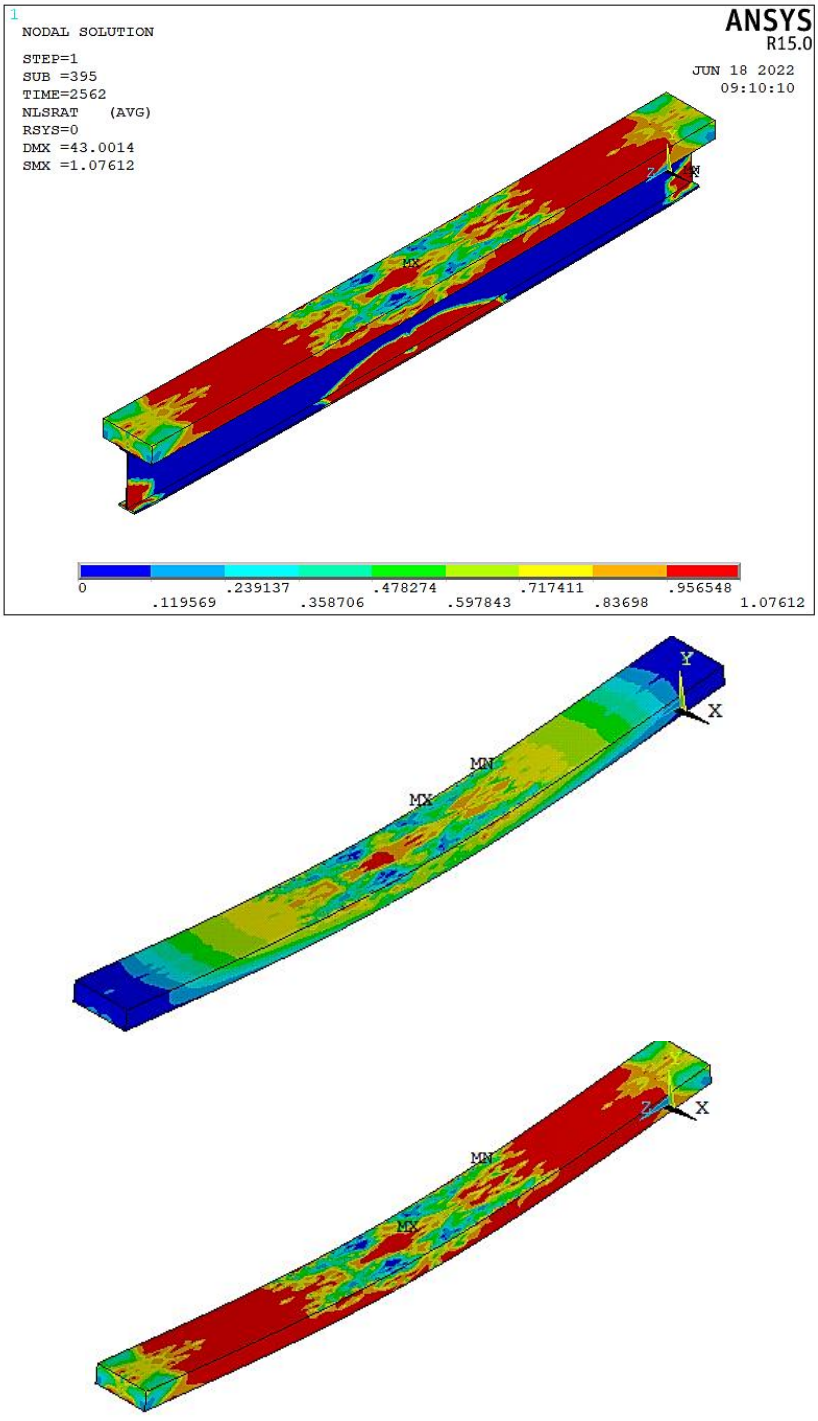

Figure 4- 35 Stress distribution of concrete, steel, and composite parts of beam Mode 1.

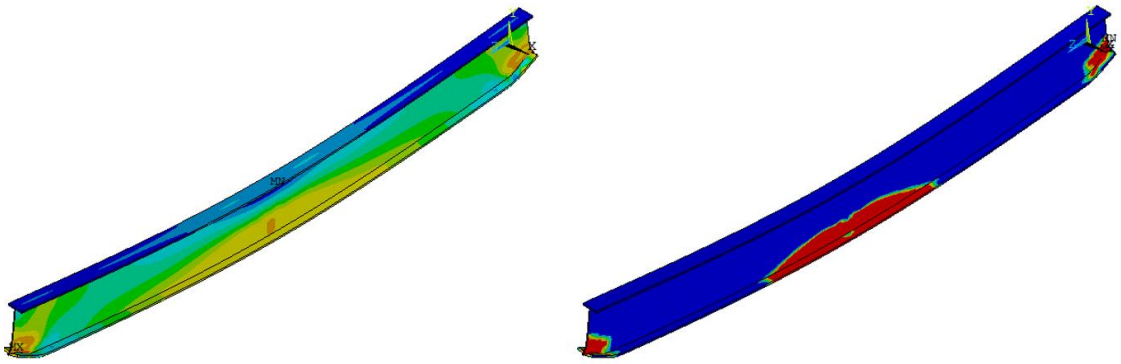

Figure 4- 36: Stress distribution of steel parts of beam Mode 1..

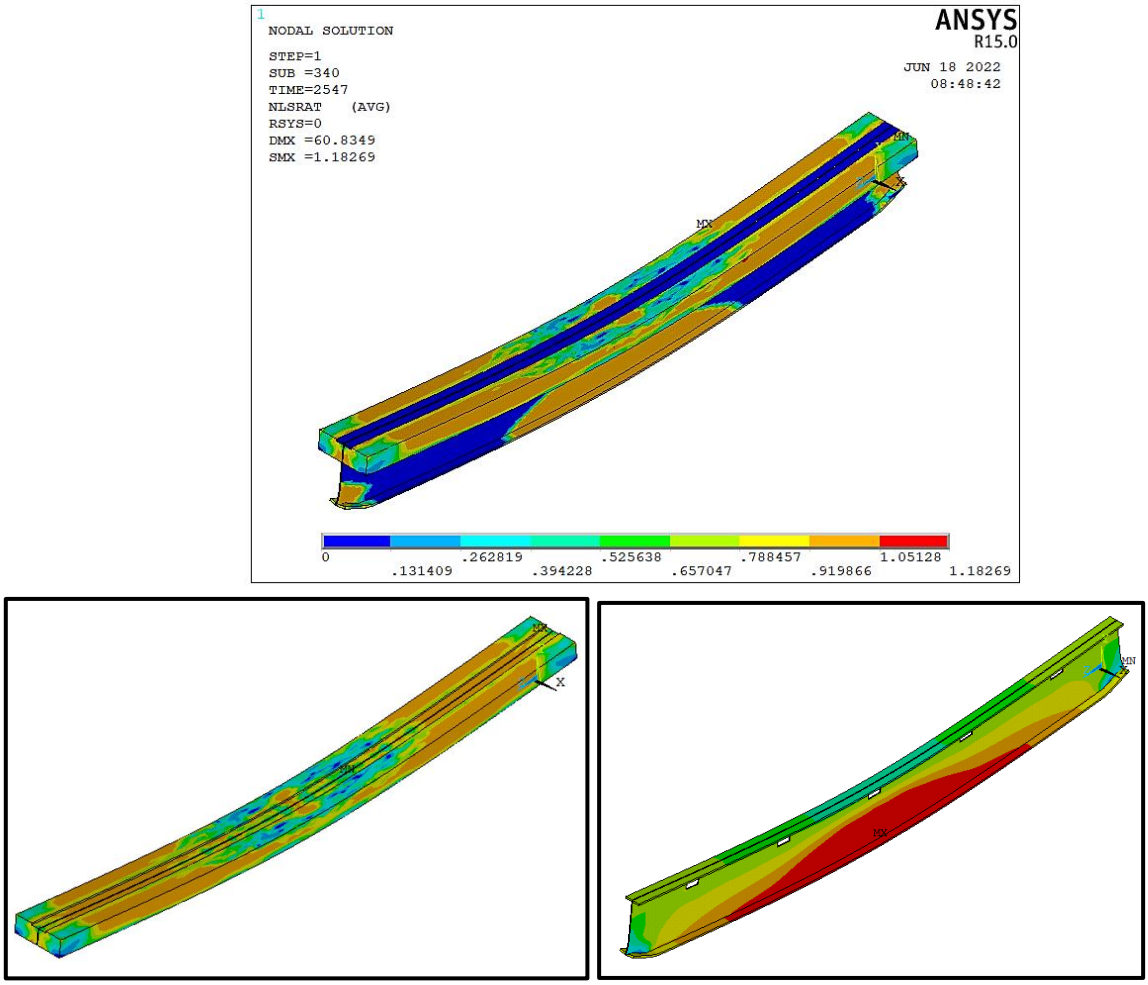

Figure 4- 37 Stress distribution of concrete, steel, and composite parts of beam Mode 2.

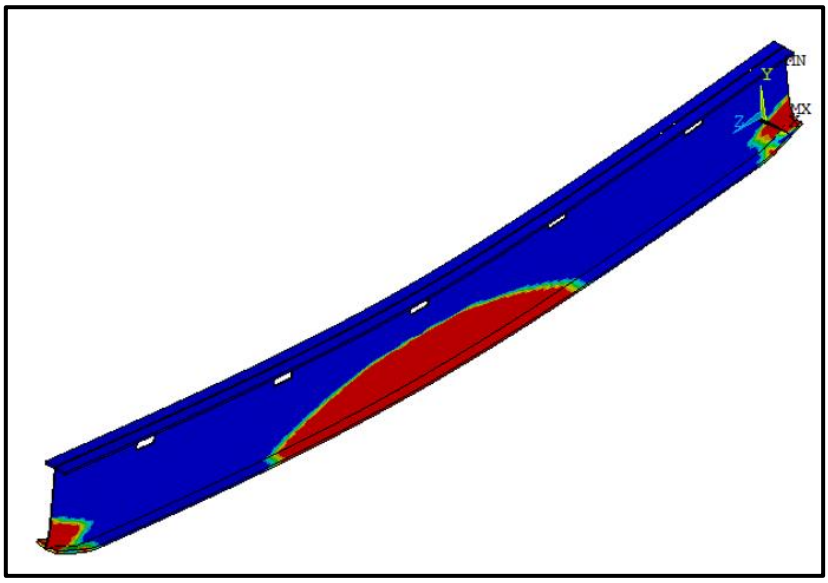

Figure 4- 38 Stress distribution of steel parts of beam Mode 2.

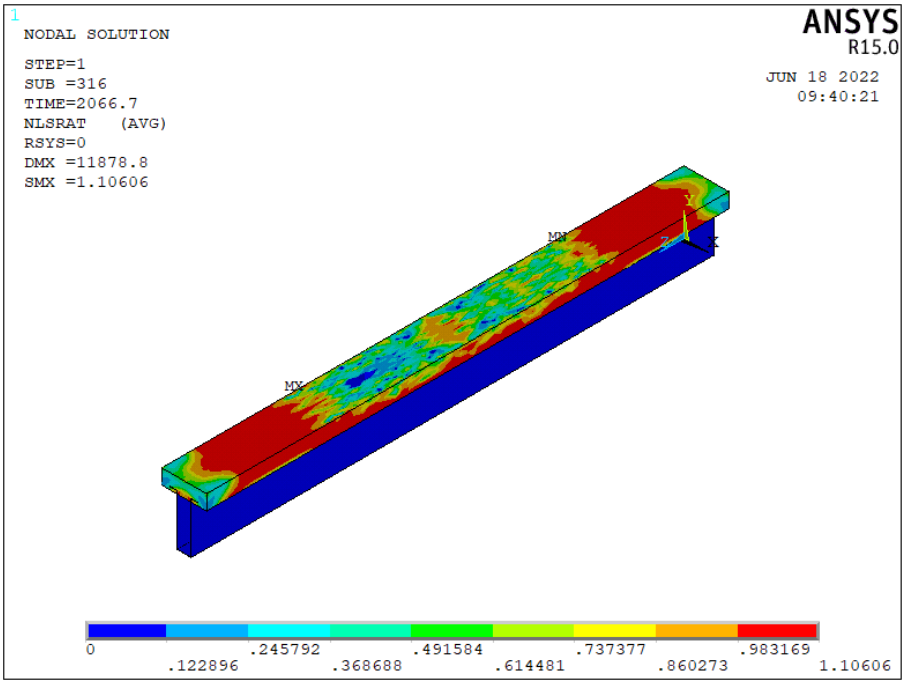

Figure 4- 39 Stress distribution of concrete, steel, and composite parts of beam Mode 3.

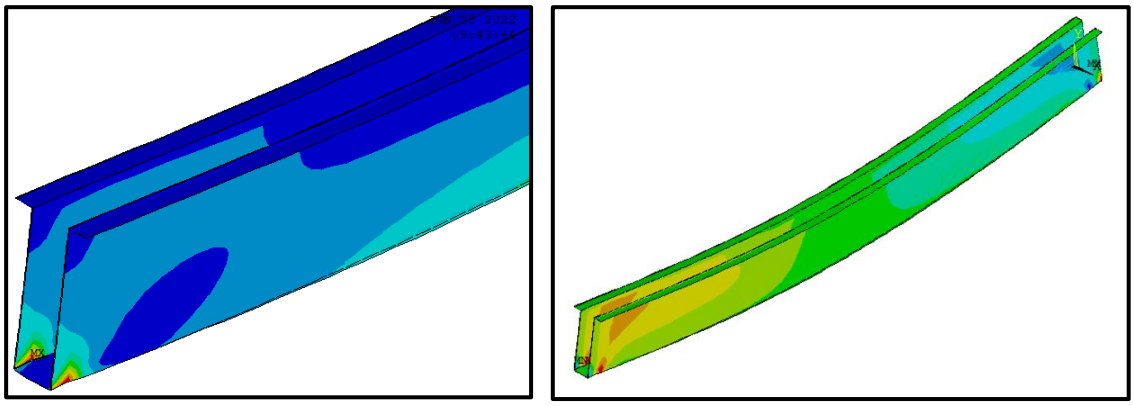

Figure 4- 40 Stress distribution of steel parts of beam Mode 3.

4.7.4 Analyzed Beam Ductility

The ratio between the displacement corresponding to the ultimate load and the displacement corresponding to the first yielding of the flexure reinforcement was described by Marzouk and Hussein and used in this study to calculate the ductility index. The measured beam ductility was determined using a method suggested the researchers by Priestley and Park and also proposed by Robertson and Durrani (1991). The concept of yield displacement makes it difficult to calculate ductility factors from experimental data since the load-displacement relationship does not have a well-defined yield point. E.g., because of the material's non-linear behavior or the yield in a particular section of the system, the model (Mode 1) showed a ductility index reached to (10.52) which increased to (12.1) when the steel section moved inside the concrete section which equal to (20%) enhancement. The ductility of the third model (mode 3) showed less ductility which was (5.89) and less than the mode 1 model by (44%) and mode 2 by (52%) as revealed in Figure (4-37).

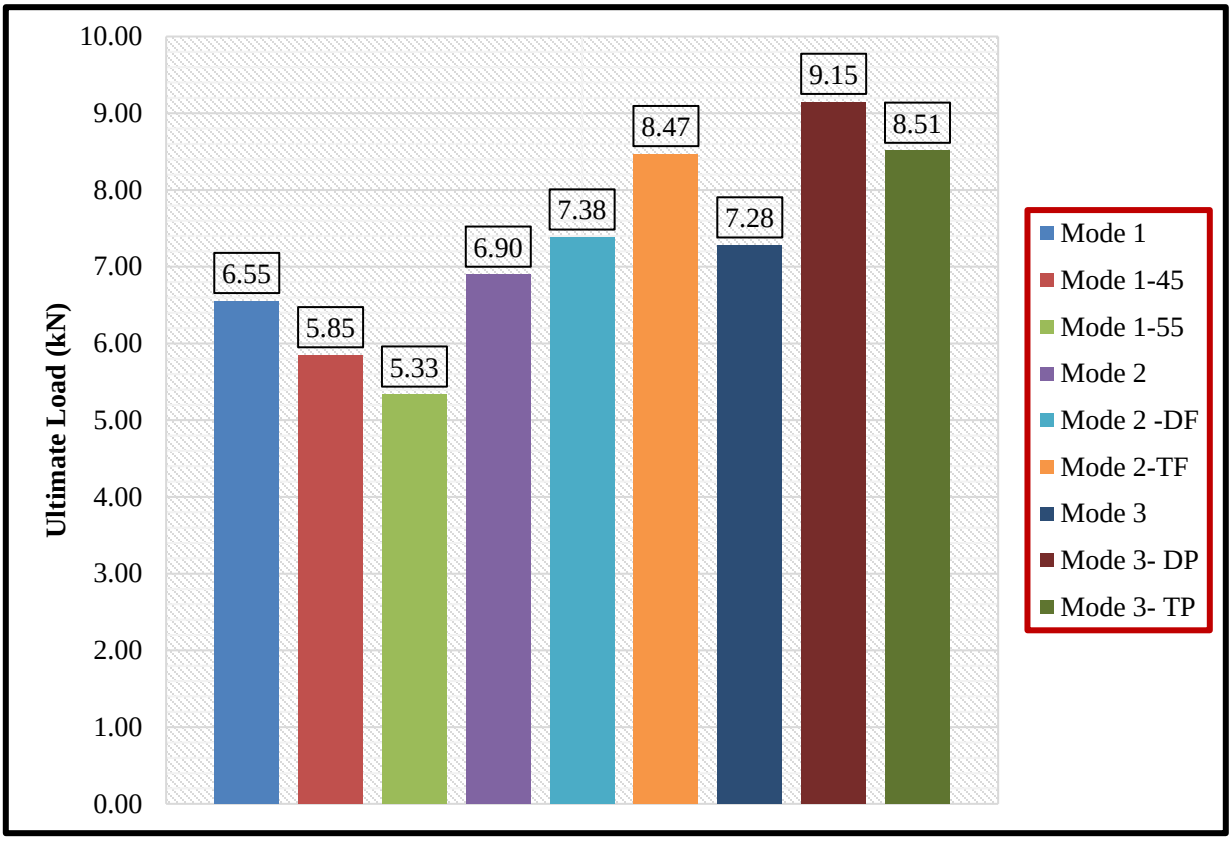

Figure 4- 41 ductility index of the analyzed beams.

CHAPTER FIVE: CONCLUSIONS AND RECOMMENDATIONS

5.1. Conclusions

The present study is focused on the behavior on the flexural behavior of composite steel concrete beams with various composite mode of concrete-built up steel section composite beams using proposed composite configuration modes. Based on the results obtained numerically and from the FEM, it is concluded that the manner in which flexure failure occurs varies widely. Many factors have significant effect on the flexural behavior of such beams, and these effects can be summarized as follows:

1. The selection of optimum material distribution within composite section depends on the adopted shape configuration of used built up steel section.
2. For intermediate length, where the compression force in deck could be contributed significantly in resistance forces, proper dimension selection and section configuration could be effect section moment capacity and the dominated failure mode.
3. The best improving associated with yield parameters that relate to bottom flange likewise strength, thickness and widths while the effect of concrete deck limited to effected width, besides; the webs' geometrical and material characteristics have slightly effect on the obtained TFY moment capacities.
4. Always there is a certain limit of improving in scope of geometry and material adopted properties.
5. For the traditional composite mode, the comparative analysis between TFY and CFY shows that, the dominated failure mode is TFY where the rate of CFY moment capacities to TFY moment capacities more than 1 for all samples.

6. For all considered composite modes, the present mid span constrain length is turned the assigned lateral-torsional buckling mode from elastic lateral-torsional buckling to plastic lateral – torsional buckling mode for a certain length domain (14 m to 20 m).
7. For merged compressive region introduced composite mode, always there are a domain of cover plate thickness that compatible with main design criteria which maintain optimum section of compatible tension and compression forces.
8. For merged compressive region introduced composite mode, the variation of thickness corresponding with significantly improving in composite section tension flange yielding (TFY), and the improving rates ranged between 1 to 2 as the thickness changed from 8mm to 30 mm.
9. For composite section of multi flanges number (Mode III), for specific flange number, the determined moment capacity increased as flange thickness increased, the assigned strength is extremely improved as flange number increase for a certain limit of provide the tension area
10. In current case study, two flanges of various flange thickness are proper for compactable design (the improving rates are 2.16 and 2.73) while the three-flange conditioned by lower flange thickness (10mm) (the improving rates is 1.82. Figure 4.22 shows the effect of intermediate flanges number on TFY moment capacity for various flange thickness.
11. The numerical side involved verification of the three beams with multi configuration which the load carrying capacity of the traditional composite beam reached to (2568.5 kN) and displacement by (42.17) mm. The load capacity reduced to (2510.8) kN and the displacement increased to (59.17) mm when the steel section moved inside the concrete section (Figure 26 b) which equal to reduction in strength by (3%) and increment in the displacement by (40%). It

should be noted that the beam with mode II depicts a slight strain hardening. The third model with steel plates showed decrement in the ultimate strength by (19.5%) and slight increment in the displacement.

12. The numerical study included additional parameters of the beams which were the thickness of flanges in the merged composite beam, in addition to the number of intermediate plates (two and three plates). The increase of the compressive strength of the traditional composite beams to 45 and 55 MPa enhanced the cracking load by 21.7% and 37.8% respectively in comparison with the Mode I beam. Increase the flange thickness for the mode II beams to double and trible thickness enhanced the cracking load by (21%) and (25.8%) respectively when compared with the MODE II beam. Doubling the thickness into two and three times for beams (Mode 3-DP and Mode 3-TP) upgraded the cracking load by (24.7% and 44.4%) respectively when compared with Mode 3 beam.
13. Concerning the ultimate load, the results showed that the increase of the compressive strength to 45 and 55 MPa enhanced the ultimate load carrying capacity by 8.56% and 12.1% respectively. The increase of flange thickness to (40 and 60 mm) for merged composite beams enhanced the ultimate load carrying capacity by 29.66% and 54.4% respectively. The increase of intermediate plates for the multi-flange composite beam to two and three plates enhanced the ultimate load by 56.7% and 68.8% respectively.
14. Regarding the deflection, the results showed that the increase of the compressive strength to 45 and 55 MPa enhanced the maximum deflection by 7.4% and 29% respectively. The increase of flange thickness to (40 and 60 mm) for merged composite beams upgraded the maximum deflection too much which were by 50.6% and 101% respectively. The increase of

intermediate plates for the multi-flange composite beam to two and three plates led to huge upgrade in the maximum deflection by 195.9% and 214.7% respectively.

5.2. Recommendations for Future works

The following recommendations could be considered in the future works relate to the current proposed composite modes of concrete-built up steel section beams:

1. More shape configuration of composite concrete built up steel section could be proposed.
2. Deep beam composite concrete-built up steel section could be studied in scope of shear.
3. Experimental and numerical models could be considered in future studies.

REFERENCE

[1] S. W. Pathirana, U. Brian, M. Olivia, and Z. Xinqun, "Flexural Behaviour Of Composite Steel–Concrete Beams Utilizing Blind Bolt Shear Connectors." Engineering Structures Vol. 114, pp. 181-194, 2016.

[2] K. Brendan. "Behaviour and design of composite steel-concrete beams subjected to flexure and axial load", 2014.

[3] Yam, Lloyd C. P. "Design of composite steel-concrete structures", Surrey University press, London, pp. 168, 1981.

[4] C. Caprani, "Composite Construction and Design" November, 2014.

[5] J. McCall, "Genetic Algorithms for Modelling and Optimization" Journal of Computational and Applied Mathematics Vol. 184, No. 1, pp. 205-222, 2005.

[6] S. Ádány, "Buckling Mode Classification of Members with open Thin-walled Cross Sections by using the finite strip method" Johns Hopkins University, 2004.

[7] G. W. Owens and P. Knowles: Steel Designer's Manual (Fifth edition), The steel construction Institute (U.K), Oxford Blackwell Scientific Publication, 1992.

[8] C.G. Salmon, J. Johnson, and F.A. Malhas, "Steel Structures Design and Behavior", Pearson Education, Inc., Fifth Edition, ISBN: 0-13-188556-1, 2009.

[9] B. Davison, and G.Owens, "Steel Designers' Manual", The Steel Construction Institute, Sixth Edition, ISBN: 978-1-4051-4818-4, 2007.

[10] H. Adeli, H. Kim, "Cost Optimization of Welded of Composite Floors Using Neural Dynamics Model", 2001.

[11] M. Kripka, "Stochastic Optimization Applied to RC Building Grillages", pp. 763-775, 2005.

[12] Degertekin and Hayalioglu, "Optimum Design of Steel Space Frames: Tabu Search vs. Simulated Annealing and Genetic Algorithms" (2009)

[13] O. Ğ. U. Z. H. A. N. Hasançebi, and E. Dogan. "Optimizing Single-Span Steel Truss Bridges with Simulated Annealing." pp. 763-775, 2010.

[14] V. E. Rosca, A. Elena, and E. T. Carmen, "Practical optimization of composite steel and concrete girders." Buletinul Institutului Politehnic din lasi. Sectia Constructii, Arhitectura, Vol. 58, No. 1, pp. 85, 2012.

[15] R. P. Johnson, and I. M. May, "Partial-interaction design of composite beams", The Structural Engineer, Vol. 53, No. 8, pp. 305-311, 1975.

[16] M. J. S. Hirst, and M. F. Yeo, "The analysis of composite beams using standard finite element programs", Computers and Structures, Vol. 11, pp. 233-237, 1980.

[17] Y. Arizumi, and S. Hamada, "Elastic-plastic analysis of composite beams with incomplete interaction by finite element method" Computers and Structures, Vol. 14, No. 5, pp. 453-462, 1981.

[18] G. Manfredi, and G. Fabbrocino, "Modeling of Steel-Concrete Composite Beams Under Negative Bending", Journal of Engineering Mechanics, Vol. 125, No. 6, pp.654-662, 1999.

[19] Maiorana, Emanuele, Carlo Pellegrino, and Claudio Modena. "Influence of longitudinal stiffeners on elastic stability of girder webs." Journal of Constructional Steel Research, Vol. 67, No. 1 pp.51-64, 2011.

[20] J. Nie, and Y.Xiao " Experimental Studies on Shear Strength of Steel–Concrete Composite Beams" Journal of Structural Engineering, Vol. 130, No. 8 pp. 1206-1213, 2004.

[21] Q. Q. Liang, and H. R. Ronagh, " Strength Analysis of Steel–Concrete Composite Beams in Combined Bending and Shear “Journal of Structural Engineering, Vol. 131, No. 10, pp. 1593-1600, 2005.

[22] I. N. Korkess, and A. H. Yousifany, "Behavior of Composite Steel-Concrete Beam Subjected to Negative Bending" September, 2007.

[23] A.A. Mohammed, "Experimental and numerical investigation of simply supported steel - concrete composite beams", Ph.D. ’s Thesis, University of Basrah, 2008.

[24] M. A. Neto, Y. Wenbin, and P.L. Rogério, "Generalized Timoshenko modelling of composite beam structures: sensitivity analysis and optimal design." Engineering Optimization, Vol 40, No. 10, pp. 891-906, 2008.

[25] M.M. Alinia, S. Maryam, and H. R. Habashi. "Shear failure characteristics of steel plate girders." Thin-Walled Structures Vol. 47, No. 12, pp. 1498-1506, 2009.

[26] E. Y. Cho, and K. S. Dong "Elastic web bend-buckling analysis of longitudinally stiffened I-section girders." International Journal of Steel Structures, Vol. 11, No. 3, pp. 297-313, 2011.

[27] F. Faluyi, and C. Arum, "Design optimization of plate girder using generalized reduced gradient and constrained artificial bee colony algorithms" International Journal of Emerging Technology and Advanced Engineering Vol. 2, No. 7, pp. 304-312, 2012.

[28] A. Khalaf, "Nonlinear Finite Element Analysis of Simply Supported Composite Beams Stiffened with a Steel Channel", Vol.16, no. 1, 2016.

[29] Lee et al., "Mechanics of Web Panel Post buckling Behavior in Shear", 2014.

[30] M. Hamdaoui, G. Robin, M. Jrad, and E. M. Daya, "Optimal design of frequency dependent three-layered rectangular composite beams for low mass and high damping", Composite Structures, 120, pp. 174-182, 2015.

[31] F. Erdal, O. Tunca, and E. Doğan, "Optimum design of composite corrugated web beams using hunting search algorithm", International Journal of Engineering and Applied Sciences, Vol. 9, pp. 156-168, 2017.

[32] Yossef, N. M., and S. Taher. "Cost optimization of composite floor systems with castellated steel beams." Practice Periodical on Structural Design and Construction Vol. 24, 2019.

[33] M. AEl-Aghoury, A. M. Ebid, and K. C. Onyelowe, "Optimum Design of Fully Composite, Unstiffened, Built-Up, Hybrid Steel Girder Using GRG, NLR, and ANN Techniques", Journal of Engineering, 2022.

[34] ACI 318, Building Code Requirements for Structural Concrete, 2014

[35] AISC, American institute of steel construction, 2016

[36] E. Madenci, and I. Guven, "the Finite Element Method and Application in Engineering Using ANSYS", Springer New York Heidelberg Dordrecht London, 2nd Edition, ISBN:978-1-4899-7550-8, 2015.

[37] S. Moaveni, "Finite Element Analysis Theory and Application with ANSYS", Prentice Hall, Upper Saddle River, New Jersey 07458, 1999.

[38] O.C. Zienkiewicz, "The Finite Element Method", 3rd Ed., McGraw-Hill Book Company, New York, 1977.

[39] P. Fanning, "Nonlinear Model of Reinforced and Post-Tensioned Concrete Beams", Electronic Journal of Structural Engineering, Vol.2, pp.111-119, 2001.

[40] H. Kwak, and F.C. Filippou, "Finite Element Analysis of Reinforced Concrete Structures Under Monotonic Load", Department of Civil Engineering / University of California / Berkeley / California, USA, Report No. UCB SEMM-90/14, November, 1990.

[41] G. Wischers, "Application of Effects of Compressive Loads on Concrete", Betontechnische Berichte, No.2 and 3, Duesseldorf, Germany, 1978.

[42] L.S. Hsu, and C.T.T. Hsu, "Complete Stress-Strain Behaviour of High-Strength Concrete under Compression", Magazine of Concrete Research (ASCE Journal), Vol.46, No.169, pp.301-312, 1994.

[43] W.F. Chen, "Plasticity in Reinforced Concrete", McGraw-Hill, 1982.

[44] Guide to Quality Control and Testing of High-Strength Concrete Reported by ACI Committee 363.2R-92.

[45] ASCE Committee on Concrete and Masonry Structures, "A State-of-the-Art Report on the Finite Element Analysis of Reinforced Concrete structures", ASCE Special Publication, 1981.

[46] P. Desayi, and S. Krishnan, "Equation for the Stress-Strain Curve of Concrete", Journal of the American Concrete Institute, Vol.61, No.3, pp.345-350, March, 1964.

[47] W.F. Chen, and A.F. Saleeb, "Constitutive Equations for Engineering Materials", West Lafayette, Indiana, December 1981.

[48] Z.P. Banzant, "Comment on Orthotropic Models for Concrete and Geomaterials", Journal of Engineering Mechanics Division, ASCE, Vol.106, No. 3, pp. 849-865, 1983.

[49] K. Willam, and E. Warnke, "Constitutive Model for the Triaxial Behavior of Concrete", Proceedings International Association for Bridge and Structural Engineering, Vol.19, pp. 1-30, 1975.

[50] ANSYS, "Analysis Guide", Version 11, Swanson Analysis System Inc., 2007.

[51] Y.R. Rashid, "Analysis of Prestress Concrete Pressure Vessels", Nuclear Engineering and Design, Vol.7, No.4, pp.334-344, 1968.

[52] R.A. Hawileh, A. Rahman, and H. Tabatabai, "Nonlinear Finite Element Analysis and Modeling of Precast Hybrid Beam–Column Connection Subjected to Cyclic Loads", Applied Mathematical Modelling, Vol. 34, pp. 2562-2583, 2010.

[53] R.A. Hawileh, J.A. Abdalla, and M.H. Tanarslan, "Modeling of Nonlinear Response of RC Shear Deficient T-Beam Subjected to Cyclic Loading", Computers and Concrete, Vol.10, No.4, pp. 413–428, 2012.

[54] S.K. Padmarajaiah, and A.A Ramaswamy, "Finite Element Assessment of Flexural Strength of Prestressed Concrete Beams with Fiber Reinforcement", Cement Concrete Composite, Vol.41, pp.24-229, 2002.

[55] European Committee for Standardization (CEN), Eurocode 3, "Design of Steel Structures", Part 1.1: General Rules and Rules for Building, DD ENV, EC3, 1993.

[56] Y.M.Y. Al-Sahlawi, "Strengthening of Self Compacting Reinforced Concrete T-Deep Beams with Opening by CFRP Sheet", M.Sc. Thesis , College of Engineering, University of Kufa, Iraq, 2018.

[57] A.J. Wolanski, "Flexural Behavior of Reinforced and Prestressed Concrete Beams Using Finite Element Analysis", M.Sc. Thesis, University of Marquette, 2004.

[58] D. Kachlakev, T. Miller, S. Yim, K. Chansawat, T. Potisuk, "Finite Element Modeling of Reinforced Concrete Structures Strengthened with FRP Laminates", Report SPR 316, California Polytechnic State University, San Luis Obispo, 2001.

[59] P. Sangeetha, G. S. Ramana, J. A. Vigneshwar, K. Vaishnavi, and A. Srinidhi, “Flexural Strength of Steel-Concrete Composite Beams Under Two-Point Loading” Civil and Environmental Engineering Reports, Vol. 30, 2020.

الخلاصة

يتناول البحث تحريا نظريا للعتبات المركبة المكونة من مقاطع الحديد والخرسانة باستخدام عدة اشكال. تضمن الجانب الأول من الدراسة التحقيق في العتبات المركبة عدديا. تم اقتراح ثلاثة اشكال مع التوزيع المتنوع للمواد إلى جانب التحقيق في تأثير تباين الأبعاد والخصائص على المقاومة النهائية لهذه العتبات لتلبية متطلبات التصميم وفقا لأحكام الكود الأمريكي (ACI و AISC للخرسانة والحديد على التوالي). يتم ترتيب المواد المختلفة في تكوين متعدد وفقا لإجراء التصميم الأمثل ، والذي يميل التحسين إلى استخدامه وتوظيف المواد في وضع مثالي. المتغير الرئيسي في هذه الدراسة هو أداء ثلاثة اشكال كانت المركب التقليدي ، ودمج كل من الخرسانة والصلب في منطقة الضغط ، واستخدام قسم فولاذي على شكل حرف U بدلا من القسم الفولاذي على شكل (I).

وكشفت النتائج أن اختيار التوزيع الأمثل للمواد داخل المقطع المركب يعتمد على الشكل المعتمد للمقطع الفولاذي المبني. اختيار الابعاد المناسبة والشكل اثر على المقاومة النهائية للمقطع. من اهم المتغيرات اليت أثرت بشكل كامل على السلوك هو ابعاد وسمك المقطع الفولاذي وبالأخص ابعاد الفلنج في حين أن تأثير الجزء الخرساني يقتصر على العرض ، إلى جانب ذلك ؛ الخصائص الهندسية من خلال النتائج المستحصلة اظهرت ان هناك حد معين للتحسينات في نطاق السلوك والمقاومة القصوى للعتبة. بالنسبة للعتبة المركبة ذات الشكل التقليدي ، اظهر التحليل بين سمك الفلنج كان له تأثيرا كبيرا على الفشل حيث زيادة سمك الفلنج قد حسنت كثيرا من مقاومة العتبة . بالنسبة للنمط الثاني من العتبات وهو وجود الخرسانة والحديد في جزء واحد في منطقة الانضغاط اظهرت ان السلوك العام للعتبة اظهر مقاومة انضغاط عالية لكن هذا المقاومة لن تنعكس على سلوك المقاومة للعتبة بشكل كامل ما لم يتم تقوية جزء الشد من خلال زيادة سمك الفلنج السفلي للعتبة والتي اظهرت تحسيانت في المقاومة القصوى للعتبة.

وشمل الجانب الثاني تحليل العتبات المركبة باستخدام تحليل العناصر المحدودة باستخدام برنامج ANSYS. كانت متغيرات التحليل بالعناصر المحدودة هي موقع الجزء الفولاذي بشكل تقليدي وبشكل مدمج مع الخرسانة بينما تضمن النموذج الثالث استخدام لوحة فولاذية على شكل حرف. كشف النموذج ذو الوضع المنفصل (الفولاذ الموجود أسفل القسم الخرساني) عن قدرة حمل قصوى أعلى من النماذج الأخرى.

جمهورية العراق
وزارة التعليم العالي والبحث العلمي
جامعة ميسان / كلية الهندسة
قسم الهندسة المدنية

التحليل اللاخطي للعتبات المركبة بسيطة الاسناد والمتكونة من الخرسانة والفولاذ بمختلف الابعاد

رسالة
مقدمة الى كلية الهندسة جامعة ميسان
كجزء من متطلبات نيل درجة الماجستير في الهندسة المدنية
(انشاءات)

من قبل
برير محمد عبد الواحد
بكلوريوس هندسة مدنية

اشراف
الأستاذ الدكتور سعد فهد رسن

1443 2022